On a PGD model order reduction technique for mid-frequency acoustic

Andrea Barbarulo

ENSC-20XX/XXX

THÈSE DE DOCTORAT
DE L' ÉCOLE NORMALE SUPÉRIEURE DE CACHAN

Présentée par

Andrea Barbarulo

pour obtenir le grade de

DOCTEUR DE L' ÉCOLE NORMALE SUPÉRIEURE DE CACHAN

Domaine

MÉCANIQUE - GÉNIE MÉCANIQUE - GÉNIE CIVIL

Sujet de la thèse

On a PGD model order reduction technique for mid-frequency acoustic

Soutenue à Cachan le 30 Novembre 2012 devant le jury composé de :

Francisco Chinesta	École Centrale de Nantes	Président
Mohamed Ichchou	École Centrale de Lyon	Rapporteur
Sergio De Rosa	Professeur, Università di Napoli "Federico II"	Rapporteur
Robin S. Langley	Professeur, University of Cambridge	Examinateur
Bernard Troclet	Professeur, ENS de Cachan, EADS-Astrium	Examinateur
Pierre Ladevèze	Professeur, ENS de Cachan	Directeur de thèse
Hervé Riou	Professeur, ENS de Cachan	Co-encadrant

LMT-Cachan
ENS Cachan / CNRS / UPMC / PRES UniverSud Paris
61 avenue du Président Wilson, F-94235 Cachan cedex, France

Contents

Contents i

List of Figures v

Introduction 1

1 The Mid-Frequency problem in acoustic 7

1 Reference problem and notation 9

2 Low-Frequency approaches extended to Mid-Frequency 10

2.1 The finite element method and its improvements to tackle mid-frequency 10

2.2 The Boundary Element Method 15

2.3 The enrichment methods 16

2.4 The meshless methods 17

3 High-Frequency approaches extended to Mid-Frequency 18

3.1 The Statistical Energy Analysis 18

3.2 Energy Flow Analysis 19

3.3 Wave Intensity Analysis 20

3.4 Statistical modal Energy distribution Analysis 20

3.5 Ray Tracing Method 20

3.6 Quasi-SEA method 21

3.7 Asymptotical Scaled Modal Analysis 21

4 A Trefftz methods category in order to solve Mid-Frequency problems . . 21

4.1 Ultra Weak Variational Formulation 22

4.2 T-elements 22

4.3 The Discontinuous Enrichment Method 23

4.4 Wave Boundary Element Method 23

4.5 Wave Based Method 24

5 Hybrid methods for Mid-Frequency 25

5.1 The Hybrid Finite Element/Statistical Energy Analysis method . . 26

6 Conclusion 26

2 The Variational Theory of Complex Rays to solve Mid-Frequency acoustical problem **29**
1 An introduction to VTCR . . . 31
2 The basic concepts of the VTCR . . . 31
3 Properties of the VTCR . . . 33
4 Illustration of the performance of the VTCR in acoustical and structural applications . . . 34
4.1 Two-dimensional Helmholtz problems in acoustics . . . 34
4.2 Structural vibration problems . . . 43
4.3 Structures containing holes . . . 49
4.4 Structural vibrations of shells . . . 49
4.5 The Fourier Version of the VTCR . . . 54
4.6 Error estimator . . . 56
4.7 3D acoustics . . . 61
5 VTCR, still an open question? . . . 68

3 The Reduced Order Model techniques **71**
1 Reduced Order Model techniques . . . 72
2 The Proper Orthogonal Decomposition . . . 72
2.1 Reduced Order Model based on POD . . . 72
3 The Proper Generalized Decomposition . . . 73

4 PGD-VTCR, an alliance to tackle mid-frequency broad band **75**
1 Proper Generalized Decomposition and VTCR: a ROM technique to perform efficient frequency band calculations . . . 77
1.1 The reference problem and the choice of the approximation . . . 77
2 A simple algorithm to introduce PGD-VTCR . . . 79
2.1 A numerical example . . . 80
2.2 A surprising numerical problem . . . 82
3 A Petrov-Galerkin algorithm . . . 85
3.1 A numerical example . . . 87
3.2 How to proper dimension matrices . . . 93
3.3 Petrov-Galerkin algorithm's limitations . . . 96
4 Conclusion . . . 97

5 A new class of algorithms **99**
1 A dedicated pre-conditioner for VTCR . . . 100
2 An improved algorithm for PGD-VTCR . . . 102
3 Minimal residue direction algorithm: the state of the art for PGD-VTCR on frequency bands . . . 104
3.1 A numerical example . . . 106
4 Conclusion . . . 109

6 PGD applied to acoustic with uncertainty parameters 111
1 Uncertainty in Mid-Frequency acoustic 112
2 A PGD technique to take account for uncertainty in VTCR for Mid-Frequency analysis 113
2.1 1D validation example 114
2.2 A low cost solution towards high-frequency 121
2.3 2D preliminary results 121
3 Conclusion 123

Conclusion 125

Bibliography 127

List of Figures

1 Qualitative frequency response of a system 2

1.1 Reference problem 9

2.1 Acoustic problem: definition of the geometry 35
2.2 An example of a function satisfying (2.6), in this case a propagative wave 35
2.3 Convergence rates for a square acoustic cavity (size $a \times a$, $ka = 30$), using a single acoustic cavity for the VTCR and an $n \times n$ uniform mesh for the FEM 36
2.4 An acoustic cavity divided into subdomains 37
2.5 The VTCR solution with 60 DOFs (left) and the FEM solution with 2,121 DOFs (right) at $\omega = 2\pi \times 400$ Hz (top) and $\omega = 2\pi \times 650$ Hz 38
2.6 The convergence curves at the reference point for the acoustic cavity divided into subdomains (see Figure 2.4) 39
2.7 Example of the acoustic cavity of a car 39
2.8 The imaginary part of the VTCR pressure in the car cavity (see Figure 2.7) 40
2.9 The VTCR velocity at the boundary where the velocity was prescribed (see Figure 2.7) 41
2.10 The imaginary part of the pressure in the car cavity (see Figure 2.7) using three FEM models: 750 DOFs (top), 1,417 DOFs (middle) and 3,305 DOFs (bottom) 42
2.11 The reference problem for plates 43
2.12 Interior, edge and corner modes for a homogeneous plate 44
2.13 The reference problem and the action of the environment 45
2.14 The NASTRAN solution with $24,000$ DOFs (left) and the VTCR solution with 88 DOFs (right) 45
2.15 The reference problem and the action of the environment (free structure) . 46
2.16 Evolution of the number of DOFs *vs.* the frequency for the problem of Figure 2.15 47
2.17 The reference problem and the action of the environment 47
2.18 The deformed shape for the problem of Figure 2.17 obtained with the VTCR at 630 Hz (left) and 600 Hz (right) 48
2.19 Comparison of the energy densities at 630 Hz given by AutoSEA (left) and by the VTCR (right) 48

2.20 The VTCR solution for a holed plate 49
2.21 The FEM solution for a holed plate 50
2.22 Sample waves for the interior zone of a cylinder 50
2.23 Sample waves for the edge zones of a cylinder 51
2.24 Sample waves for the corner zones of a cylinder 51
2.25 The geometric model of a half-cylinder; the cylinder is fixed along one end and a force density F_d is applied along the other 51
2.26 The solutions of the half-cylinder problem of Figure 2.25 obtained with the VTCR (left) and with NASTRAN (right) 52
2.27 The geometry of the 3D assembly. A force density Fd is applied along one side of Shell 1, all the other boundaries being fixed. 52
2.28 The results for the 3D assembly of Figure 2.27 obtained with the VTCR (left) and with NASTRAN (right) 53
2.29 Examples of real parts of complex pressure fields associated with Fourier-based functions from (2.14). $\Omega_E = 0.5$ m $\times$ 0.5 m; $k = 120\,\mathrm{m}^{-1}$; $N_E = 30$; $n = 0$ (left), $n = 12$ (center) and $n = 23$ (right) 54
2.30 Validation using the example of a square domain with homogeneous boundary conditions and a Dirac loading force: comparison of the VTCR solution (continuous line) and the reference solution (dotted line) along the line $y = 0.190625$ with $kL = 8$ 55
2.31 Validation using the example of a square domain with homogeneous boundary conditions and a Dirac loading force: convergence curves for nondimensional wave numbers $kL = 8, 24, 40, 56, 72$ and 88 55
2.32 Validation using an L-shaped domain with mixed boundary conditions: problem definition (left) and the real part of the VTCR solution for $kL = 8$ with 54 DOFs (right) 56
2.33 Definition of the car acoustic cavity (boundary conditions and internal mesh) 57
2.34 Contour plots of the real part of the pressure field in the car acoustic cavity of Figure 2.33 at $\omega = 2\pi \times 2,500$ rad.s^{-1} (left) , $\omega = 2\pi \times 4,000$ rad.s^{-1} (center) and $\omega = 2\pi \times 8,000$ rad.s^{-1} (right) 57
2.35 Top: description of the example. Bottom: the real part of the exact pressure field for $k = 30\,\mathrm{m}^{-1}$ (left) and for $k = 90\,\mathrm{m}^{-1}$ (right) 59
2.36 Comparison of the true local error (2.15), the local error estimator (2.17) and the H^1 relative error for the example of Figure 2.35 in the case of a Fourier-based approximation (2.14) 60
2.37 Representation of the functions $Y_l^m(\theta, \varphi)$ used in (2.19). Line (a) corresponds to $l = 0$ and $m = 0$. Line (b) corresponds to $l = 1$ and $m = -1, ..., 1$. Line (c) corresponds to $l = 2$ and $m = -2, ..., 2$. Line (d) corresponds to $l = 3$ and $m = -3, ..., 3$ *(courtesy of Wikipedia)* 62
2.38 The convergence curves of the pressure field given by the 3D VTCR for a cubic wave guide problem with Robin boundary conditions: $kL = 5$, $kL = 10$ and $kL = 15$ 62

2.39 Scattering by a sphere: the discretized computational domain 63
2.40 The scattering pressure fields for $2kR_1 = 7$ (left), $2kR_1 = 12$ (middle) and $2kR_1 = 17$(right) 63
2.41 Convergence curves of the sound-hard scattering by a sphere, in relative L^2 norm, as a function of the number of DOFs for $2kR_1 = 7$, $2kR_1 = 12$ and $2kR_1 = 17$ 64
2.42 The regularized amplitude profiles calculated at points A (left) and B (right) of Figure 2.40 with $2kR_1 = 12$ 64
2.43 Definition of the acoustic car cavity 65
2.44 The real part of the pressure field obtained with the 3D Fourier VTCR for the problem of Figure 2.43 at 700 Hz 66
2.45 The real part of the pressure field obtained with the 3D Fourier VTCR for the problem of Figure 2.43 at 1,200 Hz 66
2.46 The real part of the pressure field obtained with the 3D Fourier VTCR for the problem of Figure 2.43 at 1,700 Hz 67

4.1 Square cavity under different boundary conditions 80
4.2 PGD with 40 modes vs. Regular VTCR 81
4.3 VTCR reference real pressure field (left) compared to PGD real pressure field (right) at resonance frequency $\omega = 2\pi 1959[Hz]$ 82
4.4 L-shaped cavity 82
4.5 VTCR reference real pressure field (left) compared to PGD real pressure field (right) at $\omega = 2\pi 1900[Hz]$ 83
4.6 Sub-discretized square cavity 83
4.7 VTCR reference real pressure field (left) compared to PGD real pressure field (right) for a sub-discretized square cavity 84
4.8 Comparison between first eigenvalues of $\mathbf{K}^*\mathbf{K}$ for the sub-discretized problem (in blue) and the the non sub-discretized one (in red), as we can see eigenvalues are completely difference in the two cases. 85
4.9 L-shaped acoustic cavity (with a prescribed pressure $P = 0$ $[Pa]$ and a prescribed velocity $V = 1$ $[m/s]$) to test the efficiency of Algorithm (3) . 88
4.10 The relative error $\varepsilon(\mathbf{X}^M)$ (4.18) for different δ_q with $q_{\max} = \infty$ (a) and for different $q_{\max}$ with $\delta_q = 0$ (b). $\Delta\omega_1 = 2\pi 100$ $[Hz]$. 89
4.11 The relative error $\varepsilon(\mathbf{X}^M)$ (4.18) for different δ_q with $q_{\max} = \infty$ (a) and for different $q_{\max}$ with $\delta_q = 0$ (b). $\Delta\omega_2 = 2\pi 200$ $[Hz]$. 90
4.12 The relative error $\varepsilon(\mathbf{X}^M)$ (4.18) for different δ_q with $q_{\max} = \infty$ (a) and for different $q_{\max}$ with $\delta_q = 0$ (b). $\Delta\omega_3 = 2\pi 400$ $[Hz]$. 91
4.13 The relative error $\varepsilon(\mathbf{X}^M)$ (4.18) for $\delta_q = 0.0001$ and $q_{\max} = 8$. $\Delta\omega_1 = 2\pi 400$ $[Hz]$. 92
4.14 The frequency response functions of the various approximations of the reference problem for different expansion orders M 93
4.15 Comparison of the approximate and reference real pressure fields for $\omega = \omega_0 - \frac{\Delta\omega_3}{2}$, $\omega = \omega_0$ and $\omega = \omega_0 + \frac{\Delta\omega_3}{2}$ 93

4.16 **K** size increasing with frequency 94
4.17 **K** resizing according to ϕ bases 94
4.18 L-shaped acoustic cavity to test sizing effect 95
4.19 Energy response for non-expanded matrices 95
4.20 Not converged real pressure field for $\omega = 2\pi 1200\ [Hz]$ 96

5.1 **K** matrix shape for a generic three subdomain problem 100
5.2 SVD application subdomains (in blue) 101
5.3 Comparison between SVD based pre-conditioner and old energy based pre-conditioner 102
5.4 L-shaped acoustic cavity 107
5.5 Convergence curve for an L-shaped cavity. 108
5.6 Convergence curve for an L-shaped cavity, with a preconditioned matrix system. 108
5.7 Global energy of the L-shaped acoustic cavity for 2, 3, 4 or 5 PGD couples. The reference solution is computed with the VTCR, frequency by frequency. 109
5.8 Compared real pressure field for $\omega = 2\pi 1500[Hz]$ 109

6.1 Frequency response of 98 "identical" cars from the same production line (courtesy of Toyota) 112
6.2 1D problem to assest stochastic PGD-VTCR 114
6.3 PGD-VTCR mean pressure compared to mean reference 116
6.4 Residual error (5.23) 117
6.5 Evolution of sub-iteration number necessary to reach a stationarity criteria 118
6.6 Exemples of frequency functions on Example 6.2 118
6.7 Exemples of stochastic functions on Example 6.2 119
6.8 Ratio between real error and PGD residue 119
6.9 Real pressure evolution (middle point) with PGD approximation 120
6.10 PDF of pressure on middle point for a normal gaussian distribution 120
6.11 "Low-cost" PGD-VTCR mean pressure compared to mean reference . . . 121
6.12 Convergency for 2D case 122
6.13 VTCR real pressure field compared to PGD-VTCR pressure field ($\omega = 2.\pi.1300$ and $Z = 845 + i50$) 122

List of Algorithms

1 Galerkin approach PGD for brad band problems 80
2 Approximation building algorithm 81
3 Petrov-Galerkin approach PGD for brad band problems 87

4 Rayleigh quotient based PGD algorithm for brad band problems 104
5 Minimal residue direction PGD algorithm for brad band problems 106
6 Approximation building algorithm with pre-conditioner 107

7 PGD for stochastic broad band problems 114
8 1D stochastic PGD algorithm 116

Introduction

In many industrial contexts, such as aerospace applications or cars design, numerical prediction techniques become more and more useful. They restrict the use of real prototypes to a minimum and make easier the design phase. In such industries and in the specific case of acoustic vibration, engineers are interested in computing the responses of systems on frequency bands. This is particularly true in mid-frequency where the sensibility to any design modification is extremely high.

A classical example of this need is automotive industries. Acoustical comfort is a strong market request but tendency to make lighter vehicles (to reduce fuel consumption) makes this task difficult to accomplish. In such a competitive business makes fast improvement in design is an important characteristic and in this contest a reliable and effective numerical tool is vital. Similar needs are present in aerospace industry. Lightness of structure is a key characteristic of aircraft and spacecrafts, every unneeded weight means more structural components to achieve a required payload and, therefore, increasing fuel consumption. On the other hand a very good control of internal noise is needed both to passenger comfort on aircraft and to guarante safety of payload and onboard electronic systems in spacecrafts. In this case numerical simulations are even more vital than automotive. In aeronautic industry an experimental campaign could be extremely costly or even impossible in space industry due to the unicity of every rocket or spacecraft.

In order to predict the vibration behavior of systems over frequency bands, standard numerical techniques usually involve many frequency-fixed computations, at many different frequencies. Although it is a straightforward and natural mean to answer to the posed problem when one has an efficient numerical tool at a fixed frequency, such a strategy can easily lead to huge computations, and the amount of data to store often increases significantly. This is particularly true in the context of medium frequency bands, where these responses have a strong sensitivity to the frequency. Indeed in such bands, a very fine frequency resolution of computation must be done, which accentuate the cited drawbacks. Then, for medium frequency vibrations, there is a clear need for improving the efficiency of prediction techniques on frequency bands.

A system acoustical response can be classified in three frequency range. Let's consider the size of the acoustic component to be smaller than the size of the acoustical response. On this case few mode resonate in the system and this range can be defined as low frequency (LF) (see Figure 1). This range is characterized by a strongly local response. This

range is solved thanks to classical finite element methods (FEM) which uses a large but finite number of small elements to discretize the problem. The dynamic field variables are described in terms of polynomial shape functions. However, since these shape functions are no exact solutions of the governing differential equations, a fine discretization is required to suppress the associated pollution error and to obtain reasonable prediction accuracy at higher frequencies.

If the the size of the acoustic component is significantly larger than the wave length, many modes resonate in the system and the range can be defined of high frequency (HF) (see Figure 1). In this frequency range the local response lose its importance and a global energetic estimation is sufficient to represent the system, moreover the response is strongly influenced by uncertain parameters. Statistical Energy Analysis (SEA) is the most established tool to have such a kind of prevision. It's based on a simple balance of energy in sub-systems of a structure, provides a global energy information and it's inherently extendible to keep in account uncertainty. Its global nature limits this approach to high frequency.

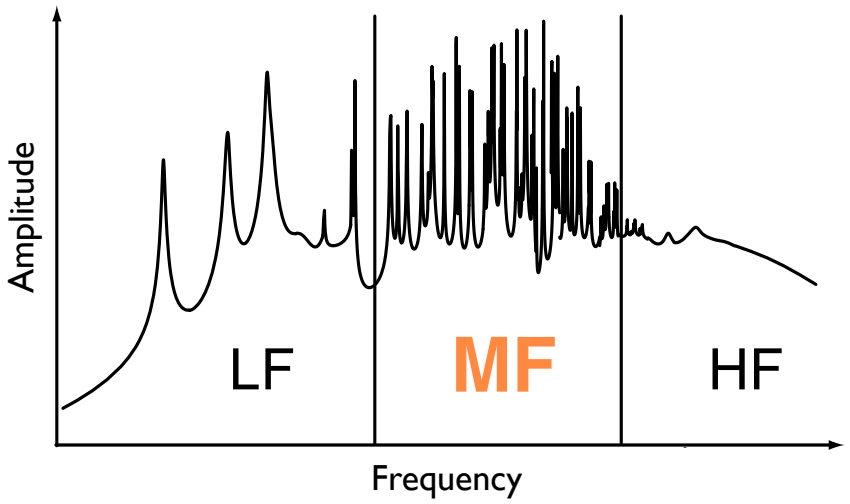

Figure 1: Qualitative frequency response of a system

Between the LF and the HF lies a peculiar frequency range called Mid-Frequency (MF) (see Figure 1). It's characteristics are hybrid between high and low frequency. The behavior stills modal and local so classical high frequency techniques fail in making good previsions, on the other hand FEM methods fail due to the computational cost. An other important characteristics is an important sensibility to uncertainty.

Various approaches, including Trefftz methods [Trefftz, 1926], have been proposed to overcome this problem. These methods differ from the FEM in the shape functions used for the expansion of the field variables, which are exact solutions of the governing differential equations. In many cases, these functions lead to a considerable reduction in model size and computational effort compared to element-based methods. These methods include, among others, a special version of the Partition of Unity Method (PUM)

[Strouboulis and Hidajat, 2006], the ultra-weak variational method [Cessenat and Despres, 1998], the least-squares method [Monk and Wang, 1999a], the Discontinuous Enrichment Method (DEM) [Farhat et al., 2001], the element-free Galerkin method [Bouillard and Suleau, 1998], the wave boundary element method [Perrey-Debain et al., 2004] and the wave-based method [Desmet et al., 2002a]. The Variational Theory of Complex Rays (VTCR), which was first introduced in [Ladevèze, 1996], belong in the same category. The main differences among all these methods lie in the treatment of the transmission conditions. Different types of discretizations can also be used: waveband, discrete wave direction, ...

The first characteristic of the VTCR is the use of a specific weak formulation of the problem which enables the approximations within the substructures to be *a priori* independent of one another. Thus, in each substructure, any type of shape function can be used, provided that it satisfies the governing equation. This gives the approach great flexibility and, consequently, makes it very efficient because any type of approximation function can be easily introduced. The second characteristic of the VTCR is the introduction of two-scale approximations with a strong mechanical content: the solution is described as the superposition of an infinite number of plane waves which satisfy the governing equation exactly. All the wave directions are taken into account. The unknowns of the problem are the amplitudes of the waves.

In [Ladevèze et al., 2001] and [Rouch and Ladevèze, 2003], the VTCR was used to predict the vibrational response of a 3D plate assembly. In [Ladevèze et al., 2003a], plates with heterogeneities were taken into account. In [Riou et al., 2004], the theory was extended to shell structures. The use of the VTCR for transient dynamic problems was covered in [Chevreuil et al., 2007]. The extension to linear acoustic problems was presented in [Riou et al., 2008] for 2D acoustics and in [Kovalevsky et al., 2012a] for 3D acoustics. It was shown through many examples that this approach is capable of finding accurate solutions of complex vibration problems while requiring only limited numbers of degrees of freedom (DOFs) and modest computational resources, and is nearly mature enough to become an industrial tool for the resolution of medium-frequency problems.

Although its wide range of applicability and its efficiency on mid-frequency VTRC present two main open issues:

- Its formulation is completely frequency dependent lowering its efficiency on a wide frequency band.
- Being a deterministic method, its extension to consider uncertainty parameters could be computationally inefficient if classical tools (like Monte Carlo simulations) are applied.

The aim of this work is to apply an innovative model reduction technique, called Proper Generalized Decomposition (PGD), in order to solve the two principal weak points of the technique, opening a new era of applications and effectiveness for VTCR.

PGD was proposed many years ago by Ladevèze for the resolution of complex nonlinear thermomechanical problems (see [Ladevèze, 1999]). Under the name "radial approximation", it became one of the main components of the powerful nonincremental and nonlinear LArge Time INcrement (LATIN) solver. More recently, a general separated representation was used in [Ammar et al., 2006] to find approximate solutions of multidimensional partial differential equations. The separated representation was also used in [Nouy, 2007] for the resolution of stochastic equations in which the deterministic variables and the stochastic variables were separated, very much like in [Ladevèze et al., 2010] for the radial space-time approximation of complex multiscale problems and in [Ladevèze and Chamoin, 2011] for finding guaranteed error bounds.

Today, the common name used for techniques involving a separated representation of the variables is Proper Generalized Decomposition (PGD). PGD belongs to the family of Reduced-Order Modeling (ROM) techniques, along with the ROM-POD method [Lieu et al., 2006] and the reduced-basis element method [Maday and Rønquist, 2002], but in the case of PGD the construction of the representation takes into account the nature of the problem directly. The general form of a PGD separated representation of a function u of N variables is $u(x_1,...,x_N) \simeq u^M(x_1,...,x_N) = \sum_{m=1}^{M} u_m^1(x_1) \times ... \times u_m^N(x_N)$, M being the order of the approximation. Many applications of PGD, covering several domains, have already been presented: for example advanced nonlinear solvers using separated space-time representations; multidimensional models; the separation of physical spaces; parametric models; real-time simulations; the quantification of uncertainties and stochastic parametric analysis... [Chinesta et al., 2010a] and [Chinesta et al., 2011] give reviews of recent works on PGD.

In this work PGD, in a first time, is applied to found a separate functional representation over frequency and space of the unknown amplitude of VTCR formulation on a reduced frequency space. This allows to calculate an high quality mid-frequency response over a wide band without a fine frequency discretization, saving computational resources. Moreover the PGD representation of the solution allows to save a huge amount of space in term of storage of the solution over the considered band.

PGD application to VTCR was not straightforward. Despite its effectiveness and efficiency, VTCR brings to a numerically very unpleasant formulation. Resolutive VTCR matrices are complex, non-symmetric and possibly ill-conditioned. From those peculiar characteristics, two consideration can be drawn: Classical Galerkin approach fails due to a strong matrix non-symmetry. Moreover an adapted pre-conditioner is needed to reach a fast convergency in the iterative process despite the ill-condition number. To overcome Galerkin limitation to symmetric problems, different approaches are proposed.

The simplest one is to premultiply the formulation by the complex conjugate of the resolutive matrix. In this way the problem is simply overcome but two major issues (which will be detailed in the work) suggest to find more elegant solutions. The first problem is linked to performances, premultiply a matrix for its complex conjugate its numerically inefficient. The second, and probably even more constraining, is due to the

fact that a premultiplication between two very ill-conditioned matrices, with a lot of very close eigenvalue, brings to introduction of a numerical pollution which could bring to convergency towards an incoherent solution. For those reasons this approach is limited to very simple cases and small bands on the low side of mid-frequency range, where above mentioned effects are limited.

A Petrov-Galerkin algorithm is proposed to overcome those problems. It consist in choosing an adjoint space, in this case the complex conjugate space, and solve the problem on the principal space and its adjoint. Such a kind of solution is clearly appropriate for non symmetrical problems. Moreover Petrov-Galerkin algorithm is intrinsically more stable facing ill-conditioned problems. A pre-conditioner could sensibly improve convergency but it's not a stringent need for such a kind of technique. It will be shown that this approach brings to very good results, compared to a chosen reference, on large mid-frequency cases for several degrees of geometrical complexity. Nevertheless its choice as a definitive PGD algorithm is questionable. Petrov-Galerkin algorithm do not guarante a convergency, due to presence of an adjoint problem computational time are doubled respect a standard Galekin and an unpleasant "step convergency" is present.

For this reason an innovative algorithm is devoted to PGD applied to VTCR for broad band. The key point of this algorithm is to minimize a residual formulation searching for every iteration the minimum error direction. This algorithm guarante a fast and smooth convergency (unlike Petrov-Galerkin) with inexpensive computations over huge mid-frequency bands. Its only week point is a strong sensibility to ill-conditioned problems. In order to not lose the advantages of the method the choice of a good pre-conditioner could be capital. Considering the shape and the nature of VTCR matrices an adapted "block SVD" pre-conditioner has been chosen. A "block SVD" pre-conditioner is a classical SVD bases pre-conditioner applied only on diagonal block of the VTCR matrices, representing the contribution of every sub-domains to the problem. VTCR introduces few big sub-domain so a "block SVD" could lead to several degrees of magnitude of reduction in terms of conditioning at a widely acceptable computational cost.

At the state of the art, an alliance between a residual minimum error direction algorithm and a "block SVD" pre-conditioner is to consider as the definitive choice for PDG-VTCR.

In a second time, PGD technique as been applied to extend its peculiarity to mid-frequency wide band with uncertainty. The technique is still the same, but a third function depending from the uncertainty is added to the previous one in frequency and space. This techniques allows to extend a deterministic method like VTCR to uncertainty over a mid-frequency band without performing any Monte Carlo simulation. Is so possible to exploit calculation otherwise impossible for nowadays computation resources.

The oeuvre is developed in the following way:

- In the first chapter will make a point on the vast state of art on mid-frequency problems and methods.

- The second chapter will introduce and deeply analyze VTCR for linear 2D and 3D acoustic.
- In the third chapter an overview of modal reduction techniques and existing methods will be provided.
- The fourth chapter will analyze deeply generic aspect and state of art of Proper Generalized Decomposition, the innovative modal reduction technique on which the novelties of this work are based.
- Chapter five will constitute the key point of the oeuvre. PGD will be coupled with VTRC in order to achieve for the first time a reduced model over frequency with such a technique. Several algorithms will be introduced. 2D academic case to show the effectiveness of the technique.
- In the last chapter the extension to uncertainty will be proposed. Some example will show the unique performances of the technique.
- In the end a short conclusion will summarize the theoretical and numerical results of the work.

Chapter 1

The Mid-Frequency problem in acoustic

Mid-Frequency problem is an open question and a vast number of methods and relative bibliography are available. Four different strategies have been developed over the years:

- *Low-Frequency methods modified in order to improve numerical performances and reach Mid-Frequency*
- *High-Frequency methods improved to keep into account local Mid-Frequency information*
- *Dedicated Mid-Frequency methods*
- *Hybrid methods combining advantages of Low and High-frequency methods to achieve Mid-Frequency results*

In this chapter a brief synthesis of those methods will be provided. The last part will focus on some bibliographic references about broad band calculation. Due to a vast activity of the scientific community in this field, the literature survey is huge. In this chapter a literature overview will be given at the best of the author's knowledge. In synthesis the aim of this chapter is to introduce the different strategies and provide some significant references.

Contents

1 Reference problem and notation 9

2 Low-Frequency approaches extended to Mid-Frequency 10

2.1 The finite element method and its improvements to tackle mid-frequency 10

2.2 The Boundary Element Method 15

2.3 The enrichment methods 16

2.4 The meshless methods 17

3 High-Frequency approaches extended to Mid-Frequency 18

3.1 The Statistical Energy Analysis 18

3.2 Energy Flow Analysis 19

3.3 Wave Intensity Analysis 20

3.4 Statistical modal Energy distribution Analysis 20

3.5 Ray Tracing Method 20

3.6 Quasi-SEA method 21

3.7 Asymptotical Scaled Modal Analysis 21

4 A Trefftz methods category in order to solve Mid-Frequency problems . 21

4.1 Ultra Weak Variational Formulation 22

4.2 T-elements 22

4.3 The Discontinuous Enrichment Method 23

4.4 Wave Boundary Element Method 23

4.5 Wave Based Method 24

5 Hybrid methods for Mid-Frequency 25

5.1 The Hybrid Finite Element/Statistical Energy Analysis method . . . 26

6 Conclusion 26

1 Reference problem and notation

Let us consider the general 2D interior dynamics problem of a bounded acoustic domain Ω in Figure 1.1, filled with a fluid characterized by sound velocity c_0 and density ρ_0, to be studied in the frequency interval $I =]\omega_0 - \frac{\Delta\omega}{2}; \omega_0 + \frac{\Delta\omega}{2}[$, where ω_0 denotes the central frequency and $\Delta\omega$ the bandwidth of the frequency band being considered. The problem is to find $p(\mathbf{x}, \omega)$, $(\mathbf{x}, \omega) \in \Omega \times I$ such that:

$$\left| \begin{array}{l} \Delta p + k^2 p = 0 \quad \text{over } \Omega \times I \\ p = p_d \quad \text{over } \partial_p \Omega \times I \\ L_v(p) = v_d \quad \text{over } \partial_v \Omega \times I \\ p - Z L_v(p) = h_d \quad \text{over } \partial_Z \Omega \times I \end{array} \right. \tag{1.1}$$

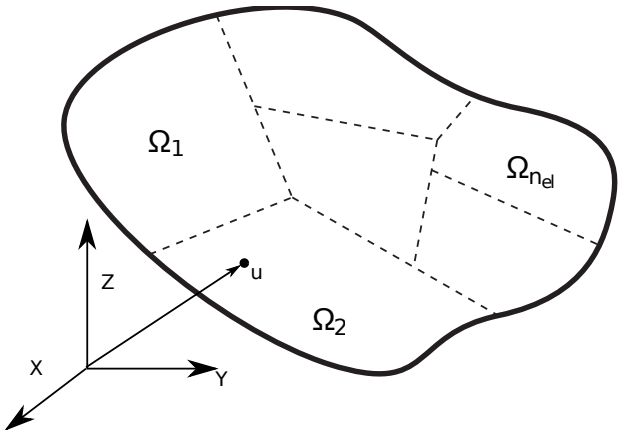

Figure 1.1: Reference problem

where $k = (1 - i\eta)\frac{\omega}{c_0}$ is the wave number (η being the absorption coefficient), p_d a prescribed pressure, v_d a prescribed velocity, Z a given impedance and h_d a given function. Operator $L_v(\square)$ is defined by: $L_v(\square) = \frac{i}{\rho_0 \omega}\frac{\partial \square}{\partial \mathbf{n}} = \frac{i}{\rho_0 \omega}\mathbf{n}^T \nabla(\square)$, $\mathbf{n}$ being the outward normal. The uniqueness of the solution of this reference problem is ensured by η.

If we introduce a partition of Ω into n_{el} non-overlapping elements Ω_e, the following additional equations must be verified in order to ensure the continuity of the solution along $\Gamma_{e,e'} = \Omega_e \cap \Omega_{e'}$:

$$\left| \begin{array}{l} p_e - p_{e'} = 0 \quad \text{along } \Gamma_{e,e'} \times I \\ L_v(p_e) + L_v(p_{e'}) = 0 \quad \text{along } \Gamma_{e,e'} \times I \end{array} \right. \tag{1.2}$$

2 Low-Frequency approaches extended to Mid-Frequency

Low-Frequency methods are well established and very effective when the low frequency are concerned. Unluckily, when a Mid-frequency is to tackle, its cost became prohibitive increasing the considered frequency. Moreover, even if an unlimited computational power is available, dispersion and pollution error still limit this approaches to low-frequencies [Deraemaeker et al., 1999]. For this reason several methods were proposed to raise its limitations.

2.1 The finite element method and its improvements to tackle mid-frequency

In this section a short review of finite element method is presented. Its simple formulation, joint with the inborn characteristic of the method to adapt easily to any possible geometry, made the FEM the principal tool to analyze low frequency problem. Due to these reasons FEM base been developed in many commercial codes, this contributed to definitive success of the technique. Being FEM such an important methods, a natural way to face mid-frequency is to improve FEM limitations. In this section a review of improved FEM is provided.

2.1.1 The Finite Element Method

The Finite Element Method [Zienkiewicz, 1977] is based on a weak approximation of equation (1.1) and an approximation of admissible fields. Let's take into account the reference problem in Section 1. Once discretized the domain, field's approximation is composed by subdomain approximated field. Given the weak formulation, the unknown pressure field $p \in \mathcal{P}_a = \{p \in H_1(\Omega)$ which verify B.C.$\}$ has to satisfy:

$$a(p,p^*) = l(p^*) \quad \forall p^* \in \mathcal{P}_a = \{p \in H^1(\Omega)/p = 0 \text{ on } \partial_p\Omega\} \tag{1.3}$$

with:

$$a(p,p^*) = \int_\Omega \left(\text{grad}(p)\cdot\text{grad}(p^*) + k^2 p p^*\right) \mathrm{d}\Omega + i\int_{\partial\Omega_z} \frac{\rho_0\omega}{Z} p p^* \mathrm{d}S$$

and

$$l(p^*) = i\int_{\partial\Omega_Z} \frac{\rho_0\omega}{Z} h_{ed} p^* \mathrm{d}S - i\int_{\partial\Omega_v} \rho_0\omega v_{ed} p^* \mathrm{d}S + \int_\Omega f p^* \mathrm{d}\Omega$$

The domain Ω is divided in simpler sub-domains Ω_E. The pressure field (solution of Helmotz equation) for every sub-domain is defined by a linear combination of polynomial shape functions:

$$p(\underline{x}) \simeq p^h(\underline{x}) = \sum_{e=1}^{n_{el}} p_e^E \phi_e^E(\underline{x}), \quad \underline{x} \in \Omega_E \tag{1.4}$$

Once the discretization and the shape functions are introduced a matrix notation is introduced:

$$(\mathbb{K} - \omega^2\mathbb{M} + i\omega\mathbb{C})\mathbf{p}^h = \mathbf{F} \tag{1.5}$$

with:

- $\mathbf{p}^h$ discretized unknown vector,
- $\mathbb{K}$ stiffness matrix,
- $\mathbb{M}$ mass matrix,
- $\mathbb{C}$ damping matrix,
- $\mathbf{F}$ loading vector.

One of the advantage of the technique ([Deraemaeker et al., 1999]) is that the error can be majored by:

$$\varepsilon_{\text{EF}} \leq \alpha \left(\frac{kh}{q}\right)^q + \beta kL \left(\frac{kh}{q}\right)^{2q} \tag{1.6}$$

where:

- k is the problem wave number,
- h is the element size,
- q is the polynomial interpolation degree,
- α et β are some problem dependent constants,
- L is a characteristic length of the problem.

The first terms of the equation is linked to the polynomial approximation of the problem. The second concern the pollution error. Pollution error depends from the solution wave number. For Low-Frequency problems the first term is decisive. As a consequence a finer discretization could easily decrease this kind of error and it does not vary if a fixed kh is taken in account. Is to remark that even for a fixed kh, the second term of the error continuously increases with the frequency. For this reason when a mid-frequency is taken in account, the second term of the error increase at fixed kh. This means that mid-frequencies are an inborn limit for FEMs. The pollution's error independence from the discretization makes any refinement of the mesh ineffective, putting an insurmountable limit to classical FEM at higher frequencies. For that reason many improvements for FEM were proposed over the years. Main major finite elements improved versions are described in the following sections.

2.1.2 adaptive Finite Element Methods

Pollution error rises due to the high number of degrees of freedom needed to capture the small wave length at increasing frequency. An possible solution to this problem is to limit the number of degrees of freedom by a non uniform mesh over the domain. In standard FEM the size of discretization is chosen referred to the global frequency of the system. Nevertheless it's non uncommon that "local frequency" varies consistently in different component of the domain. adaptive FEMs is based on this consideration. These methods build a non-uniform mesh with fine discretization where local frequencies are higher and a much coarser mesh elsewhere. An interesting way to find such an optimized mesh is proposed in [Stewart and Hughes, 1996] for acoustical problems. It's based on an *a priori* uniform repartition of the error over the domain in order to chose a so adapted mesh. Different strategy to refine meshes are proposed:

- a *h* strategy like in [Stewart and Hughes, 1997]. In this strategy a finer discretization in terms of element size is proposed,
- *p* strategy like in [Zienkiewicz et al., 2005]. In this strategy higher order polynomials are chosen.
- *ph* strategy which is a combination if previous strategies.

adaptive FEMs allow to push higher in frequency the limits of classical FEM. Of course, the high computational costs are still present and the pollution error lies in the back increasing the frequency. For this reasons these methods can be considered as an excellent choice if the low part of mid-frequency is considered but are not an answer for the complete mid-frequency band.

2.1.3 The stabilized Finite Element

One of the reason why FEM lose its efficacy in approaching higher frequency, derives from the used bilinear form [Deraemaeker et al., 1999]. The quadratic form associated to the bilinear form loses stability at high frequency. For this reason some modification have been proposed to make bilinear form unconditionally stable. Here the most known techniques are summarized:

Galerkin Least-Squares FEM (GLS-FEM)

This technique stabilize classical FEM by adding a term linked to the minimization of the equilibrium residue [Harari and Hughes, 1992]. This work show the evidence of a complete disappearance of the pollution error in 1D cases. Unlikely other works [Thompson and Pinsky, 1995] show that for increasing dimension the

pollution error in suppressed only in some preferential direction.

Galerkin Gradient Least-Squares FEM (G∇LS-FEM)

First time introduced in [Franca and Carmo, 1989] it is similar to the (GLS-FEM) but it aims to improve its performances. This time the stabilizing term minimizes the gradient of the equilibrium residue. This approach showed a high efficiency for structural dynamic problems (where several wave types are present) but a deterioration of the solution in acoustic [Harari and Haham, 1998] do not suggest its application for the problem treated in this manuscript.

Quasi Stabilized FEM

This technique [Babuška et al., 1995] offers a solution to stabilize FEM without and preferential direction. The technique is based on some modification to the finite element matrices in order to perform the desired stabilization. 1D error is suppressed and in 2D, if the mesh is regular enough, is minimized. The price to pay for its effectiveness is a quite complicate implementation.

2.1.4 Domain Decomposition Methods

Pollution error is of course one of the biggest problem in FEM but is not the only limiting factor. Stabilized FEM can suppress or drastically reduce pollution error. Nevertheless the principle that at higher frequency a finer discretization is required, is still inalienable. This could lead to huge computational time and computational resources request. In recent years and in many branches of computational sciences, domain decomposition methods seem to be the most effective tool for huge computational problems. The basic concept is to divide a big domain, which is impossible to tackle due to computational cost, in smaller sub-domain. Once the problem is divided in more affordable problems, each problem could be solved in parallel by several computers and then reconstructed. This operation is quite delicate and the sub-division process have to be kept under control. The communication between sub-domains should be optimal and a too high number of sub-domains could lead to huge computational cost in order to transmit the informations between the domains. Between the others some methods are quoted for their use in vibration problems:

Component Mode Synthesis (CMS)

In this technique [MacNeal, 1971] a preliminary calculation of eigenmodes in every

sub-domain is performed. In a second phase these modes are taken as a basis for the global domain modes. Every sub-domain is treated independently by different calculators in parallel.

Guyan's decomposition

Introduced in [Sandberg et al., 2001], it's based on hierarchic classification of degrees of freedom. Some DoF are classified as slave, and contribute to the calculation of local sub-domain modes. The information is then transmitted to the global system by some and limited in numbers nodes, called masters. Those particular DoFs condense the information of all the slave DoFs. Once again every sub-domain is treated independently by different calculators in parallel.

Finite Element Tearing and Interconnecting (FETI)

Is one of the most popular domain decomposition technique. FETI (Finite Element Tearing and Interconnecting) was first introduced in [Farhat and Roux, 1991]. This is a domain decomposition method based on the FE. The displacement formulation of the discretized problem (decomposed into sub-structures) can be put in the form of a functional minimization under constraints. Constraints correspond to the continuity of the displacement along the interfaces between each substructure. These constraints are taken into account by Lagrange multipliers. After having satisfied the stationarity of the functional, we obtain a matrix problem linking the nodal unknowns and the multipliers. In the FETI method, the primary unknown is composed of inter-efforts between sub-structures, in this case the multipliers. Condensation (substructure by substructure) of nodal unknowns over the multipliers leads to a matrix system that allows to find statically admissible international efforts. An iterative algorithm is used to solve the matrix system. Application of the method in acoustic in present in [Magoules et al., 2000,Farhat et al., 2000,Tezaur et al., 2001]. Coupled vibro-acoustic problem is tackled in [Mandel, 2002]

Domain decomposition methods are very useful to mid-frequency problems. Nevertheless in this work a different philosophical approach is preferred. Domain decomposition is a science on is own and a detailed analysis is out of the aims of this literature review. Further details about this techniques cold be find in the excellent review paper, [Gosselet and Rey, 2006].

2.1.5 Multiscale FE methods

Multiscale FE methods improve performances of standard FE by adding an enrichment where needed with a non-FE refinement. Hence one or several "scale" are added to the

original FE problem. Here two of these methods are described:

Variational Multiscale

Introduced in [Hughes, 1995], it lies on the hypothesis that a solution field u could be constituted as $u = u^P + u^E$. u^p is an approximation of the field at a coarse scale made by FE in any desired form. On the other hand u^E (where E stands for *enrichment*) is an approximation of the field on a very small scale. Being the scale too small for FE other ways have to be followed. In variational multiscale u^E is searched by the introduction of enrichment functions. This functions are boundary zero-trace polynomial.

Residual Free Bubbles (RFB)

The basic principle is the same of Variational Multiscale. This time u^E is searched on a different approximation space. The approximation space on fine scale for RFB is given by bubble function defined on every element [Franca et al., 1997].

2.2 The Boundary Element Method

The Boundary Element Method or BEM is a very common alternative to FEM in acoustic, electromagnetic and unbounded domains [Banerjee, 1993,Bonnet, 1999a]. The technique consists to solve the problem on a boundary $\partial\Omega$ in the place of domain Ω. In a first time the problem is solved only on the boundary. Than, taking in account the solution over the boundary, the solution in the whole domain is extrapolated. Considering $p(x)$ the unknown pressure field, solution of Helmotz equation:

$$c(x)p(x) + \int_{\partial\Omega} \left(\frac{\partial G(x,y)}{\partial n} p(y) - G(x,y) \frac{\partial p(y)}{\partial n} \right) \mathrm{d}\Gamma_y = 0 \quad \forall x \in \Omega \tag{1.7}$$

where:

- $c(x)$is a known function taking into account singularities. It also allows to make a generalization of the expression to consider both the boundary and the domain.
- $G(x,y)$ is the Green function verifing $\mathcal{L}(G(x,y)) = \delta(x-y)\ \forall (x,y) \in \Omega^2$.

The key aspect of the method is the boundary discretization. In this way the domain discretization, typical of FEM, is replaced by the discretization over the boundary. This

allows to drastically reducer the needed DoF needed. On the other hand resulting matrices, even if consequently smaller, are dense and of difficult construction. This is particularly true if x and y coordinate are close each other. This characteristics limit the method to low-frequency problems. To overcome this limitations some improved versions have been proposed during the years:

- The Fast Multipole BEM impose a decoupling hypothesis on y and x. This allows to decouple the integral in (2.2) [Bonnet, 1999b, Bonnet et al., 2008].
- Some so called "clustering methods" allows to treat easier the full BEM matrixes [Hackbusch and Nowak, 1989],
- Partial approximation of martixes [Kurz et al., 2002]

2.3 The enrichment methods

In vibrational analysis the classical definition space of FE is not adapted to the problem. The enrichment methods family try to exploit this gap by improving the definition space of FM taking into account the nature of the problem. In particular shape function are chosen in order to improve the space properties. The infection of new and adapted shape function is problem dependent and needs an *a priori* knowledge of the solution. This enrichment can be performed locally where in needed. The effect of enrichment methods is to reduce DoF but on the others side introduce ill-conditioning on the problem at increasing frequency. Partition Unit Method (PUM) [Melenk and Babuška, 1996, Strouboulis and Hidajat, 2006] and the generalized finite element method [Strouboulis et al., 2000] belong to this family of methods

2.3.1 Partition Unit Method

Partition Unit Method is based on a the following assumption [Melenk and Babuška, 1996]: Let $\phi_j(\underline{x})$ be a a bases function of the compact Ω_j which covers Ω such as:

$$\sum_j \phi_j(\underline{x}) = 1 \quad \forall \underline{x} \in \Omega \tag{1.8}$$

More over a base v_j, approximation of u field is introduced such as:

$$\begin{aligned} ||u - v_j||_{L^2(\Omega_j)} &< \varepsilon_{1,j} \\ ||\underline{\nabla}(u - v_j)||_{L^2(\Omega_j)} &< \varepsilon_{1,j} \end{aligned} \tag{1.9}$$

This means that $\sum_j \phi_j(\underline{x}) v_i$ have to satisfy:

$$
\begin{aligned}
&||u - \textstyle\sum_j \phi_j(\underline{x}) v_j||_{L^2(\Omega_j)} \leq C_1 \sqrt{\textstyle\sum_j \varepsilon_{1,j}^2} \\
&||\underline{\nabla}(u - \textstyle\sum_j \phi_j(\underline{x}) v_j)||_{L^2(\Omega_j)} \leq C_1 \sqrt{\textstyle\sum_j \varepsilon_{1,j} + \varepsilon_{2,j}^2}
\end{aligned}
\tag{1.10}
$$

Such property means that if we construct a partition of unity, it is possible to enrich the local approximation of u by functions v_j having mechanical or topological content. This enrichment is made in a multiplicative way, unlike the FE-multiscale which use an additive strategy.

2.4 The meshless methods

In this methods the domain is discretized by several points and for each point an influence domaine Ω_E is assigned. The overlap between the influence domains is allowed. This is a fundamental difference from FEM where mesh elements are not allowed to overlap. This influence domains provide the support for the p field approximation shape function. It's interesting to denote that the value at point E is an average of the field included in the influence domain. This characteristic makes this method a non-interpolation based method. Several methods exploit this principle but a special attention is given at the Element-Free Galerkin Method for its application in acoustic.

2.4.1 The Element-Free Galerkin Method

The Element-Free Galerkin Method was introduced in [Belytschko et al., 1994] as an improvement of the Diffuse Element Method [Nayroles et al., 1992]. The unknown field u is searched as a linear combination of $\phi_E(\underline{x})$ shape function. The associated coefficients are the u_E values in a surrounding of E point:

$$
u(\underline{x}) \simeq u^h(\underline{x}) = \sum_{E=1}^{n_E} u_E \phi_E(\underline{x}) = u^T(\underline{x}) \underline{\phi}(\underline{x}), \quad \forall \underline{x} \in \Omega \tag{1.11}
$$

$\phi_E(\underline{x})$ shape function are built with a Moving Least Squares as in [Lancaster and Salkauskas, 1981]. Dirichlet boundary condition are taken into account by the use of Lagrange multiplier. This method has been successfully applied in linear acoustic in [Bouillard and Suleaub, 1998, Suleau et al., 2000]. This works shows that the Element-Free Galerkin Method suffer less from pollution error, this is particularly true when using plane wave enrichment. The method could be improved if a multi-level solution is used as in [Lacroix et al., 2003]. In this case a linear base is chosen in order to approximate the wave propagation direction. This directions are then used in a second plane wave based analysis.

3 High-Frequency approaches extended to Mid-Frequency

High frequency analysis are strongly dominated by a tool called Statistical Energy Analysis (SEA) [Lyon and Maidanik, 1962]. Its simple theoretical frame, its inexpensive computational cost and its efficacy (when basic hypothesis are respected) make this tool a obliged choice when high-frequency is to tackle. SEA brings, due to its statistical nature, global previsions in term of energy over a frequency band. No spacial informations are provided. This is not a a problem when, as in high frequency, the diffuse field hypothesis is respected. Unlikely, in mid-frequency this hypothesis is not fully respected. SEA prevision in terms of average energy are still valid but less useful due to a still strong localization of the response. In this section SEA principles will be introduced. As a second step some SEA-based techniques modified to keep into account mid-frequency are presented.

3.1 The Statistical Energy Analysis

Since its introduction in [Lyon and Maidanik, 1962] SEA becomes the preferential tool for high-frequency analysis. Nowadays it's commonly used both as a research tool and as an industrial tool [Troclet, 1995]. The SEA basic idea is to divide the structure in subsystem and then study the energy transmission between the structure to find the vibrational response. This response has to be thought as an average in terms of energy on a wave band. To calculate the energy a power balance on substructures i is to consider:

$$P_{\text{in}}^{i} = P_{\text{diss}}^{i} + \sum_{j} P_{\text{coup}}^{ij} \tag{1.12}$$

where:

- P_{in}^{i} is the input power in the main subsystem,
- P_{diss}^{i} is the dissipated power by i subsystem,
- P_{coup}^{ij} is the coupling power between i and j subsystem.

Coupling between subdomains is supposed proportional to their modal energy difference:

$$P_{\text{coup}}^{ij} = \omega \eta_{ij} n_i \left(\frac{E_i}{n_i} - \frac{E_j}{n_j} \right) \tag{1.13}$$

where:

- n_i is the modal density,

- η_{ij} is the coupling loss factor,
- E_i is the energy of i subdomain,
- E_j is the energy of j subdomain,

The average over frequency is taken into account by ω term. it's to remark that in equation (1.13) the energy is transmitted only to adjacent subsystem. This strong hypothesis is generally true for very high frequency. An other key point to SEA success is the possibility to calculate directly the energy variance in the subsystems [Langley and Brown, 2004, Cotoni et al., 2005]. Basic hypothesis to this extension is the structure ergodicity hypothesis. SEA in an excellent tool but relies on a quite vast set of very strong hypothesis. The field should be diffused in every subsystem and the number of mode should be high enough. An high mold density permit to validate the hypothesis of same probability of natural frequency in a band. As anticipated earlier an other hypothesis is the weak coupling. If the weak coupling is not respected the interaction of two non-adjacent system is to take in account. An excellent review of SEA and its hypothesis can be found in [Mace, 2003].

3.2 Energy Flow Analysis

One inborn limitation of SEA is considering local quantities. One way to improve its capacity in this sense is given by the Energy Flow Analysis where energy flow is denoted by $\mathbf{I}$. The unknown of the problem is the energy density e. Energy flow $\mathbf{I}$ and energy density are connected by this relation:

$$\mathbf{I} = -\left(\frac{c_g^2}{\eta\omega}\right)\nabla e \tag{1.14}$$

with c_g the group velocity. If a power balance is applied to a subsystem the following diffusive relation is obtained:

$$\frac{c_g^2}{\eta\omega}\Delta e - \omega\eta e = -P_{\text{inj}} \tag{1.15}$$

This method has shown its efficacy for simple 1D problems [Lase et al., 1996, Ichchou et al., 1997] but its application to realistic problems is hard due to continuity condition [Langley, 1995]. More over the description of energy with a formulation like (1.15) could be problematic. For such a formulation radiated field by a source in a 2D structure shows a $1/\sqrt{r}$ decay proportion while theory demonstrate a $1/r$ factor [Carcaterra and Adamo, 1999].

3.3 Wave Intensity Analysis

The basic philosophy is the same of SEA but the diffuse field hypothesis is removed. In its place wave field is considered directional [Langley, 1992]. In Wave Intensity Analysis propagative waves are associated with an amplitude. Supposing wave non-correlation, system energy could be expressed as Fourier series:

$$E = \int_0^{2\pi} \sum_p e_p N_p(\theta)\, \mathrm{d}\theta \tag{1.16}$$

A power balance between subsystem provides e_p amplitudes. This method showed considerably better result than SEA on plate assembly [Langley et al., 1997], nevertheless it share with SEA the impossibility of finding local information and the coupling coefficient could be hard to find.

3.4 Statistical modal Energy distribution Analysis

A very interesting extension of SEA to mid-frequency is the Statistical modal Energy distribution Analysis also known as SmEdA [Guyader et al., 1988]. SmEdA relies on the SEA energetic approach but adds a kinetic energy calculation in every subsystem in order improve the information quality and so approach the mid-frequency range. For a vibro-acoustic problem a decouping between the acoustic nature problem and the structural dynamic problem. Evaluation of the energy transfer is based on an *a priori* calculation of all coupled system eigenmodes. A FEM based snapshot technique allows then to find SEA needed coefficient. Successful applications of this method can be found in [Maxit and Guyader, 2001b, Maxit and Guyader, 2001a, Totaro et al., 2009]. This approach provides satisfactory results for plate assemblies. Moreover it allows to understand the influence of geometry and damping on the energy exchanges between each component of the system. The principal weak point of the method is the necessity of a FEM calculation. This is in contrast with SEA simplicity and efficacy, in some case can result very expensive.

3.5 Ray Tracing Method

Derived from linear optic the Ray Tracing Method was first introduced in [Krokstad et al., 1968] to predict acoustic performances in rooms. It proposes to calculate the vibrational field by a set of rays (which are plane waves propagating) whose path is followed until fully dumped. Transmissions and reflections of these rays are computed by classical Snell law. If frequency and damping are high enough, RTM is a inexpensive and accurate method. If not calculation time increases making this technique a non optimal choice. An other difficulty concerns the choice of imposed initial direction for the wave propagation. If the geometry is complex making the optimal choice is an hard task. Exemples of application of this method could be found in [Allen and Berkley, 1979] for acoustic and in [Chae and Ih, 2001] for thin plate.

3.6 Quasi-SEA method

As stated in sub-section 3.1, SEA is limited in high frequency by its strong hypothesis. The basic idea of Quasi-SEA is to introduce a modal energy approach. In [Mace, 2003] SEA hypothesis are analyzed in details and a technique to relax these hypothesis in order to extend the lower limit of validity is proposed. Expressions for the energy influence coefficients of a built-up structure are found in terms of the modes of the whole structure. These coefficients relate frequency average energies of the subsystems to the subsystem input powers. Rain-on-the-roof excitation over a frequency band Ω is assumed. It is then seen that the system can be described by an SEA model only if a particular condition involving the mode shapes of the system is satisfied. Broadly, the condition holds if the mode shapes of the modes in the frequency band of excitation are, on average, typical enough of all the modes of the system in terms of the distribution of energy throughout the system. If this condition is satisfied then the system can be modeled using an quasi-SEA approach, irrespective of the level of damping or of the strength of coupling. However, the resulting model need not be of a proper SEA form, and in particular the indirect coupling loss factors may not be negligible.

3.7 Asymptotical Scaled Modal Analysis

The Asymptotical Scaled Modal Analysis (ASMA) was first introduced for plates in [De Rosa and Franco, 2008, De Rosa and Franco, 2010]. The main hypothesis of ASMA is that the modal frequency response of a system can be approximated by the modal frequency response of a scaled system, when approaching mid-frequency. The main system and the scaled system are linked by an equivalence in terms of quadratic velocity. Quadratic velocity is a global characteristic of the system that can be driven from an inexpensive SEA analysis. If the original system is properly scaled in terms of side lengths and damping, the square velocity is the same. This means that the scaled system keeps energetic properties of the original unscaled system. The new scaled properties makes the system easily solvable by a standard FEM with few modes. The techniques leads to an important reduction of computational costs and can be directly applied to any finite element solver. ASMA has been applied to metallic and composite plates.

4 A Trefftz methods category in order to solve Mid-Frequency problems

Trefftz methods born from the idea to impose an *a priori* solution of the approximation space. These function verifies the equilibrium equation but not the boundary condition. The desired solution in this space converge towards the exact solution under the hypothesis of complete metric space [Herrera, 1984]. This property is called T-completion. [Zienkiewicz, 1997] and [Kita and Kamiya, 1995] provides a review of Trefftz methods applied in different context. Common characteristics of Trefftz methods

are a fast convergency in terms of DOF and a ill-conditioning derived from the chosen approximation space.

4.1 Ultra Weak Variational Formulation

Ultra Weak Variational Formulation is based on a domain discretization in elements. Every element is connected to others by an interface and on this interface a variable is added. This variable must satisfy a weak formulation over the boundary. Pressure is the associated primal variable and it must satisfy Helmotz equation. The vibrational field is approximated by a set of plane waves and a Galerkin routine leads to resolution of a system matrix whose solution is the interface variables' vector. Continuity between the elements is taken into account in the formulation by the intermediary of a dual variable (normal speed) way similar to the method FETI (see subsection 2.1.4). Once the interface variables are computed, the field inside each element can be reconstructed by solving a problem locally. When large problems are solved, the method typically uses a pre-conditioner. Although UWVF allows to make little effort computations, it can present numerical instabilities and remains, in principle, an h-method. It also suffers from poor condition number (as the totality of Trefftz methods). In [Cessenat and Despres, 1998], it is demonstrated that a uniform distributed propagation directions maximizes the determinant of the UWVF matrix, and therefore the distribution is leading to the best possible condition number. A comparison of the method with PUFEM (see section 2.3.1) is presented in [Huttunen et al., 2006] on the problem solving Helmholtz 2D irregular meshes. The authors conclude that both methods provide accurate results with coarse meshes. A general trend is that UWVF seems more efficient than the PUFEM in the high frequencies, while PUFEM is better in low frequencies (which is not surprising being PUFEM a low-frequency derived method). On the other hand, the PUFEM condition number is much better than UWVF (even preconditioned) at higher frequencies. Note also that the work presented in [Gittelson et al., 2009] show that UWVF is a special case of Discontinuous Galerkin approaches (see [Farhat et al., 2003]) using plane waves.

4.2 T-elements

Some indirect approaches use a sub-domain discretization of the studied domain, and seek the solution elements by elements by Trefftz approach. Thus constructed subdomains are called T-elements. Continuity at the interfaces is ensured either by Lagrange multipliers [Freitas, 1999], and in this case sometimes called hybrid Trefftz methods because they can be reconnected to well established finite element (see section 2.1.1). An other method to ensure continuity is by the least square functional. These methods are called Least-Squares T-elements (LST) [Jirousek and Wroblewski, 1996,Monk and Wang, 1999b,Stojek, 1998]. The use of these techniques have a number of advantages compared to the FEM:

- since the only equations that are not verified are the boundary conditions, the size of the numerical model is small.

- complex geometries can be taken into account by using sufficiently small subdomains.
- solution's singularities (acoustic point sources, punctual mechanical efforts) may be taken into account by injecting in the approximation space an adapted function.

Some recent studies have also raised the problems related to the definition of Trefftz's origin (origin of the shape functions) for both direct and indirect approaches. These studies explains why the origin in T-elements is usually placed in the center of the elements or area studied [Chang and Liu, 2004, Yeih et al., 2006].

4.3 The Discontinuous Enrichment Method

The Discontinuous Enrichment Method (DEM) was introduced in [Farhat et al., 2001]. It is very close to multi-scale FE method. However, unlike FE multi-scale which assumes a zero trace u^E fields on the boundaries of the elements, the DEM uses u^E functions defined on a fine scale. They are exact solutions of the equilibrium equation in the interior of each element. These functions do not meet the imposed boundary conditions, neither continuity between field elements. In other to verify these condition Lagrange multipliers are introduced. Enrichment proposed in this method consists of a finite number of plane waves $e^{ik(x\cos\theta+y\sin\theta)}$ propagating in equidistributed directions (θ_1, ..., θ_n). Nevertheless, the definition of the fine scale's space requires particular attention. Indeed, for stability reasons, the number of Lagrange multipliers used on each elements' edge must be directly related to the number of plane waves in each element defined by the *inf-sup* condition [Brezzi and Fortin, 1991]. Therefore, the method should be based on the construction of special elements. Dedicated 2D elements have been proposed in [Farhat et al., 2003, Farhat et al., 2004b, Farhat et al., 2004a]. 3D elements are introduced in [Tezaur and Farhat, 2006]. In [Farhat et al., 2004a] It's shown that the FE approximation, (ex. polynomial functions on the coarse scale) do not improve the quality of the solution when many Helmholtz's problems are considered. This method provides accurate results with coarser meshes than conventional FEM, and the matrices are better conditioned than the PUM [Grosu and Harari, 2008]. Recently, problems of acoustic mobile media were treated in [Gabard, 2007], and problems interacting fluid / fluid and fluid / solid have been treated using evanescent waves in [Massimi et al., 2008]. In conclusion, this method is robust and provides accurate results with a reasonable number of degrees of freedom compared to the FEM, the use of plane waves drastically reduce the effect of pollution. The DEM also allows to take into account complex geometries thanks to the use of a FE mesh. However, this method is constrained by the use of Lagrange multipliers, which hinders flexibility.

4.4 Wave Boundary Element Method

The Wave Boundary Element Method (WBEM) is a direct extension of the BEM. It has been proposed in [Perrey-Debain et al., 2003, Perrey-Debain et al., 2004]. The WBEM in-

troduces a enrichment by propagating plane waves. By this approach boundary elements can be much larger than the conventional BEM approach. The basic idea is that the polynomial functions defined on the boundary are multiplied by plane waves. The number of functions and their propagation direction can be chosen as desired. in [Perrey-Debain et al., 2004] equidistributed distribution is used, but if an *a priori* idea of preferred propagation's directions is known a quite irregular distribution of directions can be introduced. Is to remark that the use of plane waves strongly degrades operators' condition number. The method achieves considerably reduced models compared to a standard approach, particularly if the p approach is chosen.

4.5 Wave Based Method

The Wave Based Method (WBM) is introduced in [Desmet et al., 2002b]. The WBM is based on an approximation of the solution through plane waves. The continuity between interfaces is guaranteed by a weighted residuals' variational technique. Let's take the reference problem defined in Section 1. Acoustical cavity Ω is divided in two sub-cavity Ω_1 and Ω_2. On the two cavities ($E \in \{1,2\}$) the solution is expressed as:

$$p_E = \sum_{m=0}^{\infty} a_m^E \cos\left(\frac{m\pi x}{L_x^E}\right) e^{\pm i\sqrt{\left(k^2-\frac{m\pi x}{L_x^E}\right)^2}y} + \sum_{n=0}^{\infty} a_n^E \cos\left(\frac{m\pi y}{L_y^E}\right) e^{\pm i\sqrt{\left(k^2-\frac{n\pi y}{L_y^E}\right)^2}x} \tag{1.17}$$

where L_x^E and L_y^E are the dimensions of the smallest rectangle which can encompass the Ω_E sub-cavity. These approximations are obviously truncated to perform numerically implementation. In order to chose an appropriate number (n_x^E and n_y^E) of shape functions the following criteria is proposed:

$$\frac{n_x^E}{L_x^E} \simeq \frac{n_y^E}{L_y^E} \simeq T^{\frac{k}{\pi}} \tag{1.18}$$

where T is a truncation parameter chosen by the user. In [Desmet, 1998] this parameter is suggested to impose at least $T = 2$. This ensures that the wavelength $\lambda_m in$ of the shape function is not oscillating larger than the half of the characteristic problem wavelength. The chosen approximation does not verify the boundary conditions and transmission conditions at the interface. In order to verify these conditions further residue equations have to be added:

$$\begin{aligned} R_p^E(\underline{x}) &= p_E^h - p_{de} \quad \underline{x} \in \partial_p\Omega_E \\ R_v^E(\underline{x}) &= \mathcal{L}_v[p_E^h] - v_{de} \quad \underline{x} \in \partial_v\Omega_E \\ R_Z^E(\underline{x}) &= \mathcal{L}_v[p_E^h] - Z_E^{-1} p_E^h \quad \underline{x} \in \partial_v\Omega_E \end{aligned} \tag{1.19}$$

Multiplying each of these residues by a primal test function (δp_E) or by a dual associated test function ($\mathcal{L}_v[\delta p]$) and by integrating on all concerned boundary, the following variational form is obtained:

$$\begin{aligned}&\textstyle\sum_{E=1,2}(\int_{\partial_p\Omega_E}\mathcal{L}_v[\delta p]R_p^E ds+\int_{\partial_v\Omega_E}\delta p_E R_v^E ds+\int_{\partial_Z\Omega_E}\delta p_E R_Z^E ds)\\&\textstyle+\sum_{E=1,E\neq E'}(\int_\Gamma \delta p_E R_{\Gamma v}^{E-E'}-\mathcal{L}_v[\delta p]R_{\Gamma v}^{E-E'}ds)=0\end{aligned}\tag{1.20}$$

This technique leads to the resolution of a matrix sytem $\mathbb{K}\mathbf{X}=\mathbf{F}$ whose solution is the vector of complex wave amplitudes of expression (1.17) Is to remark that in this method, taking into account the transmission conditions at the interface Γ is not very natural. Indeed, in the formulation (1.20) the interface terms are a possible alternative, since *a priori* weighting coefficient associated with the test function is a choice. This choice may make unstable the numerical model, particularly when treated frequency coincides with a natural frequency of substructure. Interface's treatment can be done thanks to a normal impedance condition at the interfaces. It introduces damping in the model, which seems to improve the stability of the method. Numerical tests show that if the chosen impedance factor corresponds to the impedance of the propagation medium ($Z_0=\rho_0 c_0$) formulation is more stable [Pluymers et al., 2007]. The WBM is typically a p-method, and therefore prefer to use elements of large and increasing number of functions used to obtain quality solutions with small models. As all other Trefftz methods WBM suffers of ill-conditioning. This method as been applied in several class of problems. In [Desmet et al., 2002b] application for 3D and 2D acoustic can be found. In [Vanmaele et al., 2007, Vanmaele et al., 2009] it was applied for structural dynamics, and to poroelastic materials in [Deckers et al., 2009, Deckers et al., 2011]. The technique has been as well extended to unbounded domains [Genechten et al., 2010].

5 Hybrid methods for Mid-Frequency

Hybrid methods arise from the consideration that limitation of a single method could be overcome by a simple combination between different methods. In this way is possible to combine advantages of different methods and reduce limitation of both of them. The underling hypothesis to any hybrid methods is that even if a global system's behavior is in mid-frequency it can be decomposed in several subsystem with different local behavior. Let's consider a rod-plate assembly in mid frequency. In this case it's possible to consider rod as low-frequency systems and plate as high-frequency systems. If this hypothesis is confirmed it is possible to use a combined FE-SEA approach [Shorter and Langley, 2005]. On the other hand if a big acoustic cavity with few complex geometrical details is to compute, a hybrid between Trefftz methods and FE can be proposed. The big regular part of the cavity can be modeled with a Treffts methods while the details can be modeled with low-frequency approaches like FE or BEM. This hybrid strategy can be very effective. Trefftz methods are extremely powerful when few big cavities are taken into account. On the other hand low-frequency techniques still inexpensive if low size components are

considered. Some examples of this hybrid technique can be found in [Van Hal et al., 2005, Van Genechten et al., 2011]

5.1 The Hybrid Finite Element/Statistical Energy Analysis method

This methods has been introduced in [Shorter and Langley, 2005, Langley and Cotoni, 2007, Langley and Cordioli, 2009] and an exhaustive literature review can be found in Chapter 6 of [Desmet et al., 2012]. In the hybrid FE/SEA approach the structure is represented as an assembly of (*i*) deterministic FE components, known collectively as the master system, and (*ii*) SEA subsystems with random properties. Without loss of generality it can be assumed that all subsystems are coupled exclusively through the master system, since a set of master system degrees of freedom can always be inserted between two otherwise directly coupled SEA subsystems. The complete set of FE degrees of freedom associated with the master system is denoted by q , while the degrees of freedom associated with the SEA subsystems are the vibrational energies E_j . The physical properties of the master system can be represented by a set of parameters b, the SEA subsystems can be considered to have a set of random physical parameters s (representing density, modulus, geometry etc). The concern is therefore with an ensemble of systems in which the properties s vary across the ensemble. One of the biggest advantage of this technique is to provide directly the ensemble average (μ) and variance (σ^2) of the response of the system in the form:

$$\begin{aligned} \mu_j &= E_s[w_j(s)] \\ \sigma_j^2 &= Var_s[w_j(s)] \end{aligned} \tag{1.21}$$

where w_j represents a general response variable (a subsystem energy, or a cross-spectrum of the master system response), and $E_s[]$ and $Var_s[]$ represent the mean and variance over the ensemble. This ensemble is referred to here as the non-parametric ensemble, due to the fact that the details of the parameters s are never considered in the model is used to describe the statistics of the subsystem natural frequencies and mode shapes. This approach obviates the need for any detailed knowledge of the variability or uncertainty of the parameters s and does not require Monte Carlo simulations to be performed to propagate the uncertainty. The only input needed to describe the SEA subsystems are the geometry and mechanical properties of the nominal system, as in the conventional SEA approach. An extension to uncertainty in order to better keep into account mid-frequency physical behavior is proposed in [Cicirello and Langley, 2012].

6 Conclusion

Despite the immense literature survey, the author has given some fundamental references to better understand the state of the art for mid-frequency problems. This will allow to

the reader to better place the following original work in the right contest. Mid-frequency methods have been classified in four different categories:

- Low-Frequency approaches extended to Mid-Frequency; as shown these approaches try to improve performances of classical low-frequency methods. In this way the left part of mid-frequency range can easily be computed.
- Mid-Frequency approaches extended to Mid-Frequency; these methods allow to extend some of the several advantages of high-frequency approaches ti mid-frequency. Improving this methods allows to compute the upper part of mid-frequency band.
- Trefftz methods category; these methods are dedicated to compute mid-frequency. They are perfectly suited for this kind of problems and the solution's quality generally outperforms other approaches. On the other hand Trefftz approaches bring to numerically very uncommon and unpleasant numerical problems. Moreover their complex formulations do not makes, at the state of art, these methods for wide spread industrial purpose. For these reasons this category of methods is still a open challenge. This manuscripts aims to make a decisive step foward in their efficacy and efficiency.
- Hybrid methods for Mid-Frequency; they propose a combination between well established methods in order to solve mid-frequency problems.

Chapter 2

The Variational Theory of Complex Rays to solve Mid-Frequency acoustical problem

In this third chapter VTCR is presented in details. After a theoretical overview, an exhaustive literature review is provided. After this chapter, the reader will have a clear idea of the state of art VTCR and understand its advantages, its range of applicability and its performances. Moreover the accent will be posed on known issues of the technique that this work proposes to overcome.

Contents

1 An introduction to VTCR 31

2 The basic concepts of the VTCR 31

3 Properties of the VTCR 33

4 Illustration of the performance of the VTCR in acoustical and structural applications 34

4.1 Two-dimensional Helmholtz problems in acoustics 34

4.2 Structural vibration problems 43

4.3 Structures containing holes 49
4.4 Structural vibrations of shells 49
4.5 The Fourier Version of the VTCR 54
4.6 Error estimator 56
4.7 3D acoustics 61
5 VTCR, still an open question? 68

1 An introduction to VTCR

The Variational Theory of Complex Rays (VTCR), which was first introduced in [Ladevèze, 1996], (focus of this chapter and a fundamental starting base of all the work), belong to the Trefftz category presented in chapter 1, section 4.

The first characteristic of the VTCR is the use of a specific weak formulation of the problem which enables the approximations within the substructures to be *a priori* independent of one another. Thus, in each substructure, any type of shape function can be used, provided that it satisfies the governing equation. This gives the approach great flexibility and, consequently, makes it very efficient because any type of approximation function can be easily introduced. The second characteristic of the VTCR is the introduction of two-scale approximations with a strong mechanical content: the solution is described as the superposition of an infinite number of plane waves which satisfy the governing equation exactly. All the wave directions are taken into account. The unknowns of the problem are the amplitudes of the waves.

In [Ladevèze et al., 2001] and [Rouch and Ladevèze, 2003], the VTCR was used to predict the vibrational response of a 3D plate assembly. In [Ladevèze et al., 2003a], plates with heterogeneities were taken into account. In [Riou et al., 2004], the theory was extended to shell structures. The use of the VTCR for transient dynamic problems was covered in [Chevreuil et al., 2007]. The extension to linear acoustic problems was presented in [Riou et al., 2008] for 2D acoustics and in [Kovalevsky et al., 2012a] for 3D acoustics. It was shown through many examples that this approach is capable of finding accurate solutions of complex vibration problems while requiring only limited numbers of degrees of freedom (DOFs) and modest computational resources, and is nearly mature enough to become an industrial tool for the resolution of medium-frequency problems. In this chapter, over fifteen years of development of the VTCR are summarized. First, the general concepts of the method are described. Next, various examples are given in order to illustrate its efficiency for both structural vibration and acoustic problems. In the last paragraph the motivation that brought to life this work, are stressed. This literature review is extensively withdrawn from [Desmet et al., 2012]. The review of VTCR can be found in Chapter 5, one of the coauthors of this VTCR review is also the author of this PhD dissertation.

2 The basic concepts of the VTCR

Let us consider a general steady-state dynamic problem in a d-dimensional region Ω ($d = 2$ or $d = 3$), bounded by $\partial\Omega$ and partitioned into n_{el} non-overlapping subregions Ω_e. The problem to be solved can be stated as follows: find the amplitude u such that, for a given circular frequency,

$$\mathcal{L}(u) = f \qquad \text{within } \Omega \tag{2.1}$$

$$\mathcal{B}(u) = b \qquad \text{over } \partial\Omega \tag{2.2}$$

where f and b are two prescribed functions associated with the prescribed sources located within the regions Ω_e or at their boundaries, $\mathcal{L}$ is a linear differential operator associated with the governing equation and $\mathcal{B}$ is a linear differential operator associated with the boundary conditions and the continuity across the interfaces between the regions Ω_e.

The first characteristic feature of the VTCR is the use of a global formulation of the boundary conditions (2.2), then, problem (2.1)-(2.2) becomes: find $u \in S_{ad}$ such that

$$B(u, \delta u) = r(\delta u) \quad \forall \delta u \in S_{ad,0} \tag{2.3}$$

where $B(\bullet, \bullet)$ and $r(\bullet)$ are a bilinear form and a linear form respectively, which are equivalent to (2.2); S_{ad} is the space of the functions which satisfy (2.1); and $S_{ad,0}$ is the space of the functions which satisfy the homogeneous part of (2.1). Formulation (2.3) is written in such a way that *a priori* independent approximations can be used within the regions Ω_e. Under classical assumptions, one can prove that this formulation is equivalent to the initial reference problem and that its solution is unique.

Then, all that is necessary in order to develop approximations from the VTCR is to define a subspace S^h_{ad} of S_{ad} a subspace $S^h_{ad,0}$ of $S_{ad,0}$, both with finite dimensions. The approximate formulation becomes: find $u^h \in S^h_{ad}$ such that

$$B(u^h, \delta u^h) = r(\delta u^h) \quad \forall \delta u^h \in S^h_{ad,0} \tag{2.4}$$

The second characteristic feature of the VTCR is the use of two-scale approximations with a strong mechanical content to derive space S_{ad}: aside from the particular solution associated with source f in (2.1), which can be easily obtained, the solution of the homogeneous part of (2.1) is described as the superposition of an infinite number of plane waves which satisfy the governing equation exactly. For some classes of steady-state dynamic problems and under some conditions regarding Ω_e, convergence can be proven (see, e.g., [Ochs, 1989] [Colton and Kress, 2001] for 2D and 3D acoustic problems). Then, space $S^h_{ad,0}$ is built using an approximation of the distribution of the wave amplitudes, which can be carried out in different ways in order to benefit from physical and numerical advantages. An important point is that one can prove that for any approximate space $S^h_{ad,0}$ the solution u^h is unique.

Once the discretization in each region Ω_e has been chosen, the VTCR leads to a linear system of equations in the complex domain:

$$\mathbf{K}\,\mathbf{A} = \mathbf{F} \tag{2.5}$$

Matrix $\mathbf{K}$ corresponds to the discretization of the bilinear form of the weak formulation (2.4); $\mathbf{A}$ is the vector of the unknown quantities which approximate the distribution of the wave amplitudes; and $\mathbf{F}$ corresponds to the discretization of the linear form of (2.4). $\mathbf{K}$ itself is not symmetrical, but its symmetric part is related to the dissipation of the problem, which guarantees its invertibility. The VTCR approximate solution of the problem (2.1)-(2.2) is obtained by selecting in S^h_{ad} the functions whose amplitudes are equal to $\mathbf{A}$.

3 Properties of the VTCR

The main properties of the VTCR are:

The weak formulation The VTCR is based on a specific weak formulation of the problem which was developed in order to enable the approximations within the subregions to be *a priori* independent of one another and to take into account both the boundary conditions and the continuity conditions across the interfaces, thus eliminating the need for a specific treatment to guarantee interelement continuity. Any type of shape function can be used within each subregion provided that it verifies the governing equation (2.1), which gives this approach great flexibility and robustness.

Injected waves A two-scale approximation in introduced into the weak formulation (2.3). Only the slowly-varying scale (the scale of the amplitudes of the waves) is discretized. The rapidly-varying scale (the scale of the spatial shape of the waves) is taken into account analytically. These two characteristics give the approximation a strong physical content and several computational advantages.

Properties of Matrix K Matrix $\mathbf{K}$ (see (2.5)) is a block-populated, complex, nonsymmetrical, frequency-dependent matrix. However, since the shape functions are defined over the entire region Ω_e, the matrices of the model are sparse by blocks $\mathbf{K}_{[i,j]}$. Blocks $\mathbf{K}_{[i,i]}$ associated with regions Ω_i are fully populated, but off-diagonal submatrices $\mathbf{K}_{[i,j]}$ are zero if the corresponding regions Ω_i and Ω_j are not connected. These submatrices may be ill-conditioned.

Accuracy of derivatives Due to the fact that in the FEM the primary response variables are usually approximated using simple polynomial shape functions, their higher-order derivatives (e.g. structural stresses and strains, acoustic velocity, ...) are less accurate. In the VTCR, there is no such loss of accuracy because the derivatives of the wave functions are also wave functions.

The problem of complex geometries Complex geometries can be handled by the VTCR because their effects are included in (2.3). However, a proper definition of S_{ad} (and, therefore, of S^h_{ad}) sometimes requires a specific discretization of Ω in Ω_e. One of the main advantage of VTCR is that no hypothesis of convexity of the domains is needed [Weck, 2004].

Computational performance The calculation of the matrix coefficients involves the integration of highly oscillatory functions. Special care must be taken in carrying out these integrations in order to ensure good convergence. Semi-analytical methods can be used in the case of meshes composed of straight lines (2D). Numerical integration can be used for curved boundaries. Graphics Processing Units (GPUs) or parallel computing among multiple servers can also be used to accelerate many of the calculations without

resorting to low-level programming.

4 Illustration of the performance of the VTCR in acoustical and structural applications

Over the last fifteen years, the concepts of the VTCR described previously have been applied to several types of problems. This section gives an general overview of the performance of the method when applied to acoustical and structural vibration problems.

4.1 Two-dimensional Helmholtz problems in acoustics

Let us consider an acoustic cavity Ω divided into two subcavities Ω_1 and Ω_2 connected along a line Γ, and subjected to a prescribed pressure p_{ed} and a prescribed velocity v_{ed} ($e \in \{1,2\}$) as shown in Figure 2.1 [1] The unknowns are the pressures p_1 and p_2. For this problem, (2.1) yields

$$\Delta p_e + k^2 p_e = 0 \quad \text{in } \Omega_e, e \in \{1,2\} \tag{2.6}$$

and (2.2) yields

$$\begin{array}{ll} p_e = p_{ed} & \text{over } \partial_p\Omega_e, e \in \{1,2\} \\ \dfrac{i}{\rho_0 \omega}\dfrac{\partial p_e}{\partial n_e} = v_{ed} & \text{over } \partial_v\Omega_e, e \in \{1,2\} \\ p_1 = p_2 & \text{along } \Gamma \\ \dfrac{i}{\rho_0 \omega}\dfrac{\partial p_1}{\partial n_1} + \dfrac{i}{\rho_0 \omega}\dfrac{\partial p_2}{\partial n_2} = 0 & \text{along } \Gamma \end{array} \tag{2.7}$$

where ω is the frequency, $k = (1 - i\eta)\omega/c_0$ is the wave number (assumed to be constant in $\Omega_e, e \in \{1,2\}$, with c_0 being the velocity of sound and η the damping factor), ρ_0 is the density and n_e is the outward normal to Ω_e. $i = \sqrt{-1}$ is the imaginary unit. This type of problem was studied in [Riou et al., 2008].

Equation (2.6) is the homogeneous Helmholtz equation. Only two types of boundary conditions (prescribed pressure and prescribed velocity) are considered in this sample problem, but other types, such as a normal impedance function or absorbing boundary conditions, could be taken into account (see [Kovalevsky et al., 2012a]).

For that problem, (2.3) becomes: find $(p_1, p_2) \in S_{1,ad,0} \times S_{2,ad,0}$ such that

$$\begin{array}{l} \displaystyle\sum_{e=1,2} \int_{\partial_p\Omega_e} (p_e - p_{ed})\, \delta v_e^* ds + \sum_{e=1,2} \int_{\partial_v\Omega_e} \delta p_e \,(v_e - v_{ed})^*\, ds \\ \displaystyle + \frac{1}{2}\int_\Gamma \left((p_1 - p_2)\,(\delta v_1 - \delta v_2)^* + (\delta p_1 + \delta p_2)\,(v_1 + v_2)^* \right) ds = 0 \\ \forall \delta p_e \in S_{e,ad,0} \end{array} \tag{2.8}$$

[1] This problem can be easily generalized to n_{el}. Here, only two subcavities are considered for the sake of simplicity.

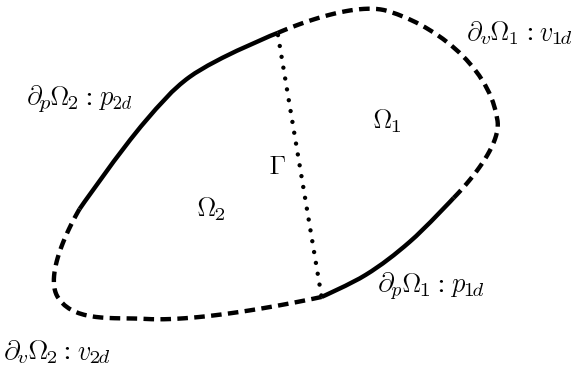

Figure 2.1: Acoustic problem: definition of the geometry

where $v_e = \dfrac{i}{\rho_0\omega}\dfrac{\partial p_e}{\partial n}$, $\delta v_e = \dfrac{i}{\rho_0\omega}\dfrac{\partial \delta p_e}{\partial n}$, and * denotes the conjugate part of a complex quantity.

The plane waves belonging to $S_{e,ad,0}$ are $e^{\mathbf{k_{ea}}\cdot\mathbf{x}}$, with $\mathbf{k}_{ea} = -ik[cos\theta, sin\theta], \theta \in [0, 2\pi[$ (see an example of such a function in Figure 2.2). The superposition of these plane waves leads to $p_e(\mathbf{x}) = \displaystyle\int_{\mathbf{k}_{ea}\in C_{ea}} p_{ea}(\mathbf{k}_{ea}) e^{\mathbf{k_{ea}}\cdot\mathbf{x}} dC_{ea}$, where $\mathbf{x} \in \Omega_e$ and C_{ea} is a circle. As explained in Section 2, the finite-dimension discretized solution is obtained by discretizing the amplitudes p_{ea} of the waves, which can take different forms. Thus, if the discretization is performed point by point, $p_e^h(x) = \displaystyle\sum_{l=1}^{L_e} p_{ea}^l e^{k_{ea}x}$ and $e^{k_{ea}x}$ are plane waves; if the discretization is carried out using piecewise constant functions, $p_e^h(x) = \displaystyle\sum_{l=1}^{L_e}\int_{C_{ea}^l} p_{ea}^l e^{\mathbf{k}_{ea}x} dC_{ea}$ and $\displaystyle\int_{C_{ea}^l} e^{\mathbf{k}_{ea}x} dC_{ea}$ are wave bands.

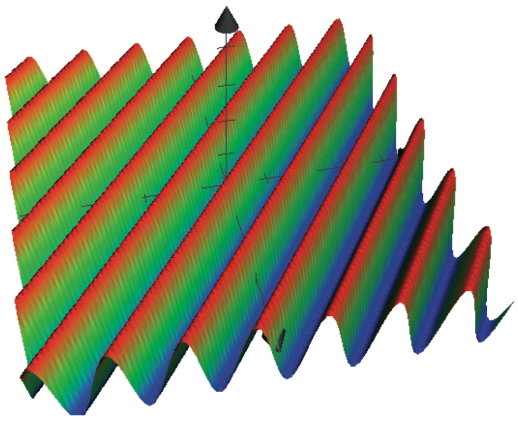

Figure 2.2: An example of a function satisfying (2.6), in this case a propagative wave

Acoustic problem: first numerical example

Let us consider the differential boundary value problem in which $\Omega = [0,a] \times [0,a]$ is a square and p_{1d} is chosen such that the exact solution is $p^{ex} = e^{\mathbf{k}^{ex}x}$, with $\mathbf{k}^{ex} = ik[cos\theta^{ex}, sin\theta^{ex}]$, with $\theta^{ex} = 77.5^o$, $ka = 30$ and $\eta = 10^{-3}$. We compared the VTCR solution given by a single acoustic cavity and complex rays as wave bands to the FEM solution given by a uniform $n \times n$ mesh of $Q1$ and $Q2$ elements. In order to assess the quality of the results from the two strategies, we measured the error according to the following modified H^1-norm:

$$||p - p^{ex}|| = \sqrt{\sum_{e \in E} ||p - p^{ex}||^2_{H^1(\Omega_e)} + \sum_{e' < e, (e,e') \in E^2} ||p - p^{ex}||^2_{L^2(\Gamma_{e,e'})}} \tag{2.9}$$

The results shown in Figure 2.3 correspond to $ka = 30$. They show that the convergence rate was higher in the VTCR than in the FEM. Indeed, for a given level of accuracy, the VTCR required far fewer DOFs.

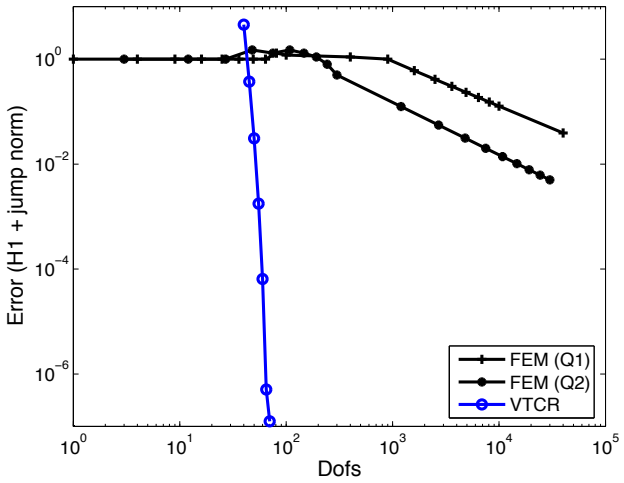

Figure 2.3: Convergence rates for a square acoustic cavity (size $a \times a$, $ka = 30$), using a single acoustic cavity for the VTCR and an $n \times n$ uniform mesh for the FEM

Acoustic problem: second numerical example

In order to study the convergence of the VTCR in the case of acoustic cavities divided into subdomains, let us now consider the two-dimensional acoustic validation example of Figure 2.4. The dynamic solicitation of the air-filled cavity consisted in a unit normal prescribed velocity along the upper part of the boundary, the remaining boundaries being fixed. The density of the air in the cavity was $\rho_0 = 1.225$ kg/m^3, the sound velocity $c_0 = 340$ m/s and the damping $\eta = 10^{-3}$. The L-shaped cavity was divided into two subdomains Ω_1 and Ω_2 as shown in Figure 5. The calculations were performed at two frequencies: $\omega = 2\pi \times 400$ Hz and $\omega = 2\pi \times 650$ Hz. Figure 2.5 shows a comparison of the

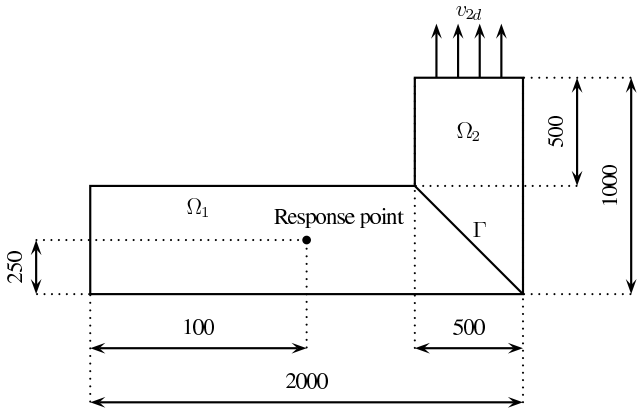

Figure 2.4: An acoustic cavity divided into subdomains

VTCR solution (left) and the FEM solution (right) at $\omega = 2\pi \times 400$ Hz and $\omega = 2\pi \times 650$ Hz. The VTCR solution was obtained using 30 DOFs in each subdomain. The FEM solution was calculated using a relatively large number of DOFs (2,121) to ensure good results. One can see that the VTCR results and the FEM results are similar, even though the former were obtained using far fewer DOFs. This example shows that the VTCR is an efficient means of predicting the response using only a few DOFs, even in the case of an acoustic cavity divided into subdomains. Another indication of the convergence of the VTCR is given by the convergence curves of Figure 2.6, which show the relative error in the predicted pressure at the response point (see Figure 2.4) as a function of the number of DOFs. This error is defined as the difference between the exact and calculated solutions divided by the exact solution. In this case, since the exact solution was unknown, the VTCR solution obtained with a very large number of DOFs was used instead.

The VTCR and FEM convergence curves at $\omega = 2\pi \times 400$ Hz (left) and $\omega = 2\pi \times 650$ Hz (right) confirm that the VTCR leads to better accuracy with a smaller number of DOFs, and also show that its convergence rate (*i.e.* the slope of the convergence curve) is higher.

Acoustic problem: third numerical example

In order to illustrate the efficiency of the VTCR in the case of complex acoustic cavity problems, let us consider the numerical example of Figure 2.7. The dimensions are given in Figure 2.7. The air-filled cavity was solicited by a prescribed normal velocity along the leftmost boundary, all the other boundaries remaining fixed. The density of the air in the cavity was $\rho_0 = 1.225$ kg/m^3, the sound velocity $c_0 = 340$ m/s and the damping $\eta = 10^{-3}$. The calculations were performed at $\omega = 2\pi \times 800$ Hz. Figure 2.8 shows the imaginary part of the pressure in the car cavity given by a VTCR model with 390 DOFs. (For practical implementation reasons, the cavity was divided into 13 subdomains, each with 30 complex rays.) The figure shows that the VTCR solution satisfies the boundary conditions at the rigid boundaries accurately as the pressure lines are perpendicular to the boundaries. Figure 2.9 shows the velocity at the boundary at which the velocity was pre-

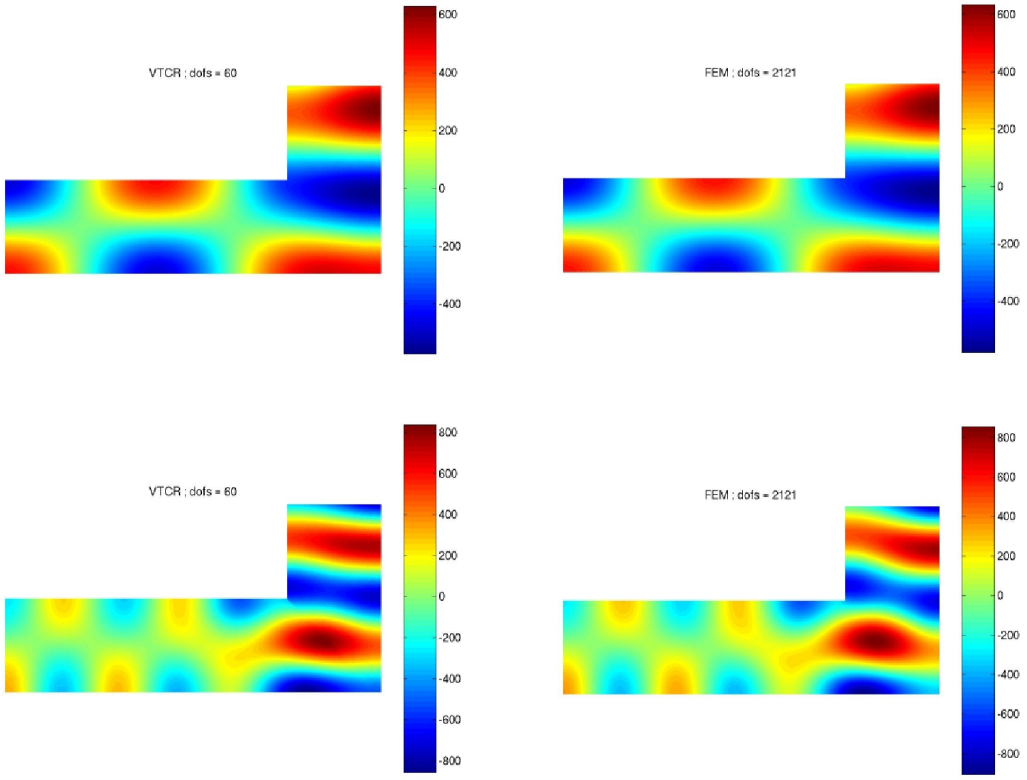

Figure 2.5: The VTCR solution with 60 DOFs (left) and the FEM solution with 2,121 DOFs (right) at $\omega = 2\pi \times 400$ Hz (top) and $\omega = 2\pi \times 650$ Hz (bottom)

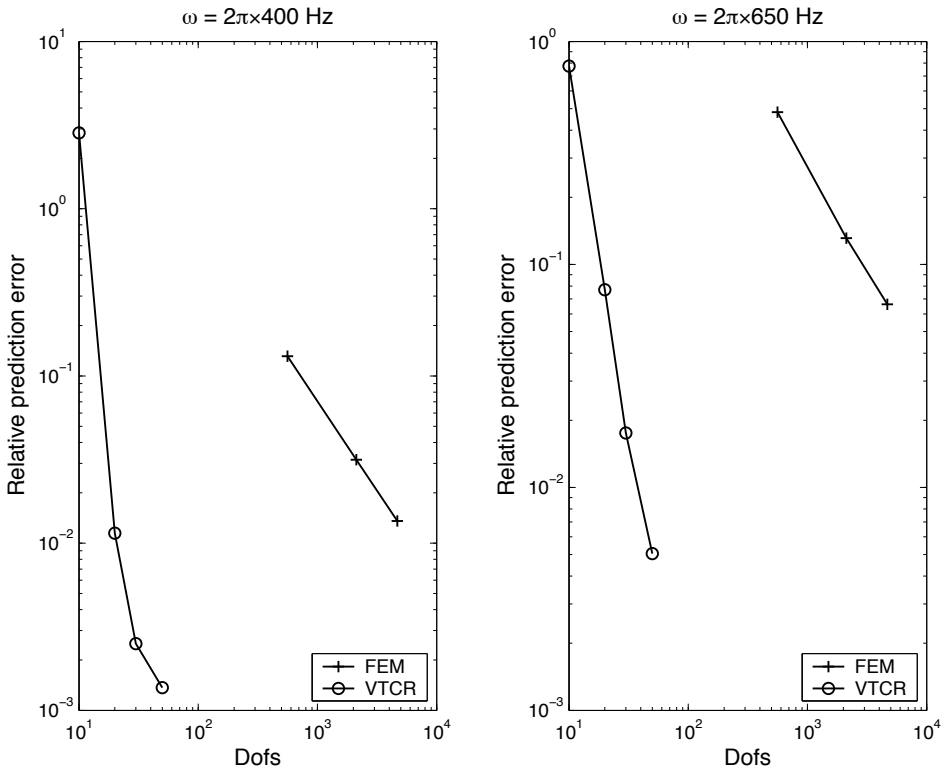

Figure 2.6: The convergence curves at the reference point for the acoustic cavity divided into subdomains (see Figure 2.4)

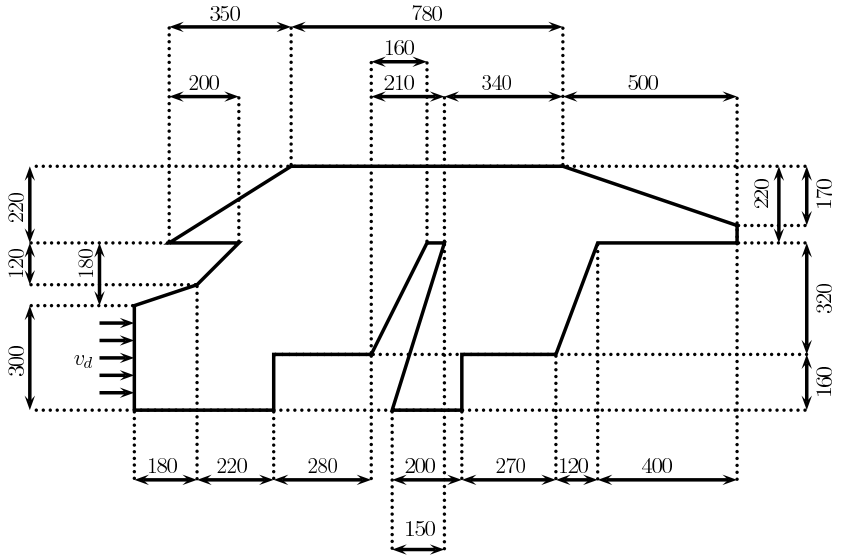

Figure 2.7: Example of the acoustic cavity of a car

scribed (see Figure 2.7), which indicates that the boundary condition along that edge was properly represented. Since the VTCR solution satisfied the governing equation (2.6) exactly and since all the boundary conditions were satisfied accurately, this example shows that the VTCR converged led to an accurate approximation of the acoustic response in the cavity. In order to assess the capabilities of the VTCR compared to the FEM, three FEM models with different numbers of DOFs (750, 1,417 and 3,305) were used. In all three cases, the cavity was discretized into four-node quadrilateral elements. Figure 2.10 shows the imaginary part of the pressure obtained with these three models. Again, the comparison of Figures 2.8 and 2.10 shows that the accuracy of the FEM solution increases when the number of DOFs increases, and this solution converges towards the VTCR solution obtained using only a small number of DOFs.

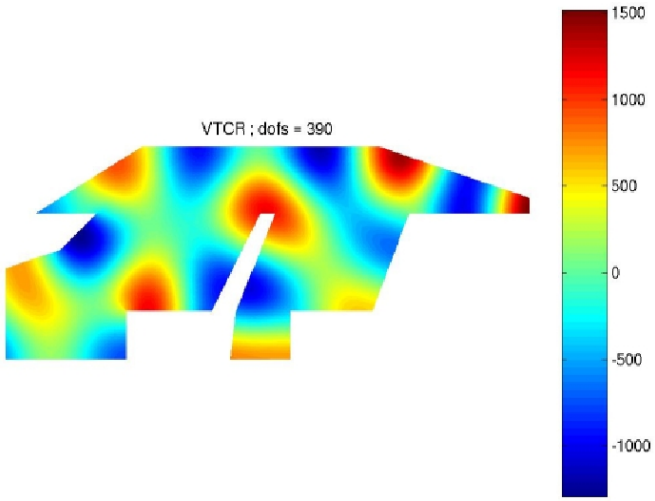

Figure 2.8: The imaginary part of the VTCR pressure in the car cavity (see Figure 2.7)

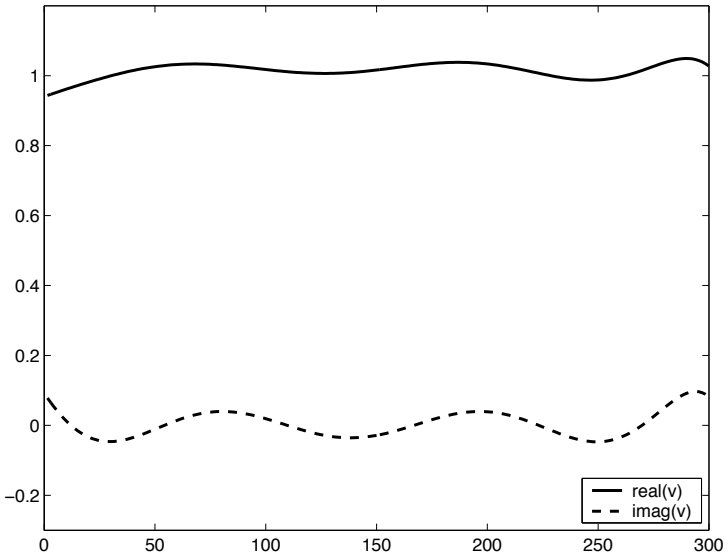

Figure 2.9: The VTCR velocity at the boundary where the velocity was prescribed (see Figure 2.7)

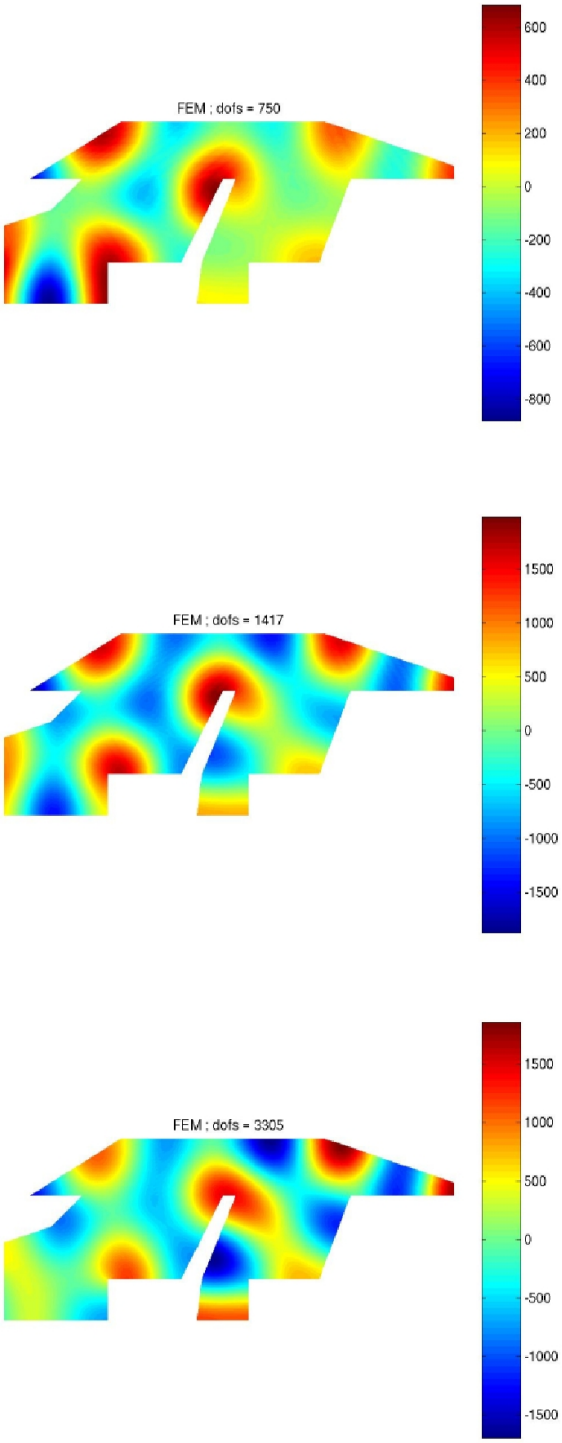

Figure 2.10: The imaginary part of the pressure in the car cavity (see Figure 2.7) using three FEM models: 750 DOFs (top), 1,417 DOFs (middle) and 3,305 DOFs (bottom)

4.2 Structural vibration problems

In order to simplify the presentation of the VTCR for plates, the problem will be formulated for an assembly of two plates, but this can be easily generalized, as was done in [Ladevèze et al., 2003a] and [Rouch and Ladevèze, 2003], to an assembly of n plates. Let us consider two plates S and S' assembled at an angle along boundary Σ. ∂S and $\partial S'$ denote the boundaries of S and S' respectively. We are studying the harmonic vibration of this structure at a fixed circular frequency ω. The action of the environment on S is given

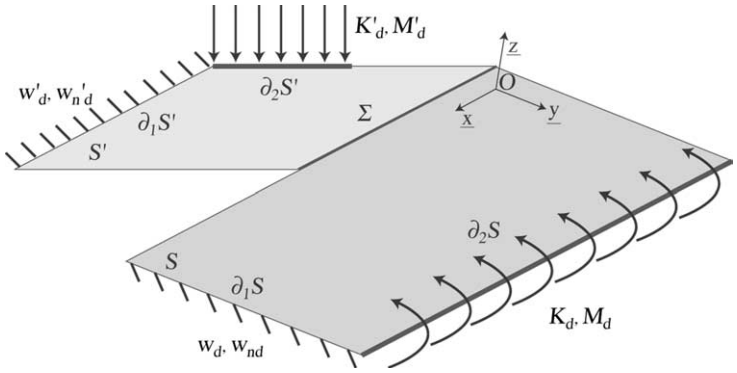

Figure 2.11: The reference problem for plates

by a displacement field w_d, a rotation field w_{nd}, a force density K_d and a moment density M_d (see Figure 2.11). Similar quantities are defined for S'.

The unknowns of the problem are the displacements w over S and w' over S'.

(2.1) leads to:

$$\begin{aligned} &\Delta\Delta w \frac{2(1+i\eta)E_0 h^3}{3(1-\nu^2)} = 2\rho h\omega^2 w \quad \text{over } S \\ &\mathbf{M} = \frac{2h^3}{3}(1+i\eta)\mathbf{K}_{0PS}\mathbf{X}(W) \qquad \text{over } S \end{aligned} \tag{2.10}$$

(2.2) leads to the boundary conditions:

$$\begin{array}{ll} w_{|\partial_1 S} = w_d & w'_{|\partial_1 S'} = w'_d \\ w_{n|\partial_1 S} = w_{nd} & w'_{n'|\partial_1 S'} = w'_{nd} \\ \mathbf{nMn}_{|\partial_2 S} = M_d & \mathbf{n'M'n'}_{|\partial_2 S'} = M'_d \\ (\mathbf{n}\cdot\mathbf{div}[\mathbf{M}] + (\mathbf{tMn})_t)_{|\partial_2 S} = \mathbf{K}_d & (\mathbf{n'}\cdot\mathbf{div}[\mathbf{M'}] + (\mathbf{t'M'n'})_t,)_{|\partial_2 S'} = \mathbf{K}'_d \\ [[\mathbf{tMn}]] = 0 & [[\mathbf{t'M'n'}]] = 0 \end{array} \tag{2.11}$$

and the interface conditions:

$$\begin{array}{ll} w = 0 & \text{along } \Sigma \\ w' = 0 & \text{along } \Sigma \\ w_n + w'_{n'} = 0 & \text{along } \Sigma \\ \mathbf{tMn} - \mathbf{t'M'n'} & \text{along } \Sigma \end{array} \tag{2.12}$$

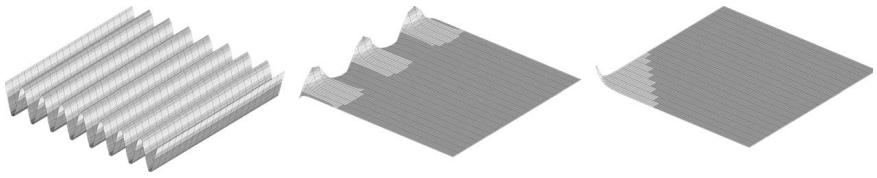

Figure 2.12: Interior, edge and corner modes for a homogeneous plate

where E_0, $2h$, $\mathbf{K}_{0PS}$, ρ, η denote respectively Young's modulus, the plate's thickness, Hooke's plane stress tensor, the density and the damping coefficient (which may depend on the frequency).

Let $S_{ad,0}$ be the space of pairs $(w,\mathbf{M})$ which satisfy (2.10).

(2.3) becomes: find $(w,\mathbf{M}) \in S_{ad,0}$ and $(w',\mathbf{M}') \in S'_{ad,0}$ such that:

$$
\begin{aligned}
&\mathrm{Re}\left\{ -i\omega \left(\int_{\partial_{w_{nd}}\Omega} \mathbf{n}\delta\mathbf{M}\mathbf{n}\,(w_{,n}-w_{nd})^* \,\mathrm{d}\partial\Omega - \int_{\partial_{w_d}\Omega} \delta K_n (w-w_d)^* \,\mathrm{d}\partial\Omega \right.\right. \\
&+ \int_{\partial_{M_d}\Omega} (\mathbf{n}\mathbf{M}\mathbf{n} - M_d)\,\delta w^*_{,n} \mathrm{d}\partial\Omega - \int_{\partial_{K_d}\Omega} (K_n - K_d)\delta w^* \mathrm{d}\partial\Omega \\
&+ \int_{\partial_{w_{nd}}\Omega'} \mathbf{n}'\delta\mathbf{M}'\mathbf{n}' \left(w'_{,n'} - w'_{nd} \right)^* \mathrm{d}\partial\Omega' - \int_{\partial_{w_d}\Omega'} \delta K'_n (w'-w'_d)^* \mathrm{d}\partial\Omega' \\
&+ \int_{\partial_{M_d}\Omega'} \left(\mathbf{n}'\mathbf{M}'\mathbf{n}' - M'_d \right) \delta w'^*_{,n'} \mathrm{d}\partial\Omega' - \int_{\partial_{K_d}\Omega'} (K'_n - K'_d)\delta w'^* \mathrm{d}\partial\Omega' \\
&- \sum_{\partial\Omega \text{ corners}} [[\mathbf{t}\mathbf{M}\mathbf{n}]]\delta w^* - \sum_{\partial\Omega' \text{ corners}} [[\mathbf{t}'\mathbf{M}'\mathbf{n}']]\delta w'^* \\
&+ \int_{\partial\Omega\cap\partial\Omega'} \frac{1}{2} \left[\delta \left(\mathbf{n}\mathbf{M}\mathbf{n} - \mathbf{n}'\mathbf{M}'\mathbf{n}' \right) (w_{,n} - w'_{,n})^* - \delta(K_n - K'_{n'})(w-w')^* \right] \mathrm{d}\partial\Omega \\
&\left.\left. + \int_{\partial\Omega\cap\partial\Omega'} \frac{1}{2} \left[\left(\mathbf{n}\mathbf{M}\mathbf{n} + \mathbf{n}'\mathbf{M}'\mathbf{n}' \right) \delta (w_{,n} + w'_{,n'})^* - (K_n + K'_{n'})\delta(w+w')^* \right] \mathrm{d}\partial\Omega \right) \right\} \\
&= 0 \\
&\forall (\delta w, \delta\mathbf{M}) \in S_{ad,0}, \forall (\delta w', \delta\mathbf{M}') \in S'_{ad,0}
\end{aligned}
\tag{2.13}
$$

where $[[\bullet]]$ and $\bullet^*$ denote respectively the jump and the conjugate of the complex quantity $\bullet$. As usual, an *ad hoc* wave function is injected into the variational formulation (2.13). In such a plate bending problem, different wave functions, such as those which are shown in Figure 6.9, are required to represent interior, edge and corner waves. All the details concerning the proof for plates can be found in [Ladevèze et al., 2003a].

Plates: first numerical example

In order to study the convergence of the VTCR for plate problems, let us consider the example of Figure 2.13. A clamped steel plate is subjected to shear loading on one of its free edges. A reference solution using the NASTRAN code was obtained with ten linear elements per wavelength for good accuracy.

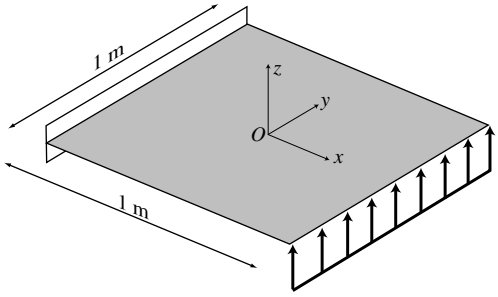

Mechanical properties
E = 2.1 GPa
ν = 0.3
η = 1/100
ρ = 7800 kg/m^3
h = 0.0007 m

Figure 2.13: The reference problem and the action of the environment

Figure 2.14 shows the solutions obtained with NASTRAN and with the VTCR. Further details concerning this example can be found in [Ladevèze et al., 2003a]. One can see that the two solutions are very similar, even though the VTCR was obtained with only 88 DOFs. One can easily note the computational efficiency of the VTCR in such a structural vibration problem.

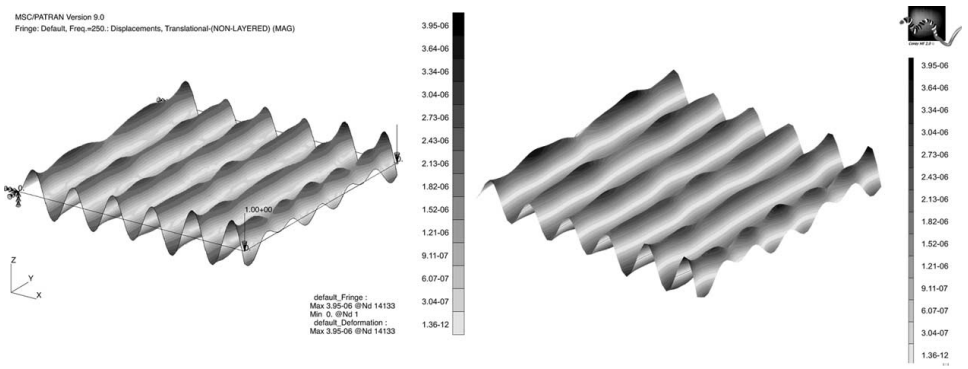

Figure 2.14: The NASTRAN solution with 24,000 DOFs (left) and the VTCR solution with 88 DOFs (right)

Plates: second numerical example

The second problem concerns the structure defined in Figure 2.15, which is a typical stringer from a car chassis. Figure 2.16 shows the solutions in terms of displacements obtained with the VTCR (left) and with NASTRAN (right), along with the total number of DOFs used for each of the three frequencies considered (400 Hz, 800 Hz and 1,500 Hz). The displacement patterns obtained with the two programs are very similar.

One can easily see that the number of DOFs required by the classical FEM increases very quickly with the frequency, whereas with the VTCR the number of DOFs for the same accuracy remains the same. At 1,500 Hz, the number of DOFs required to achieve

very good accuracy using the VTCR is about two orders of magnitude less than for the FEM, which again illustrates the computational efficiency of the VTCR.

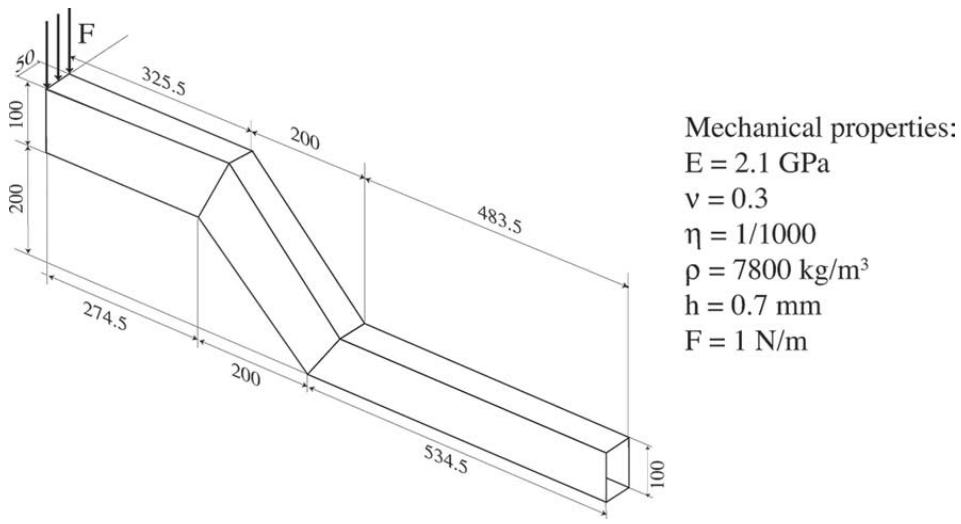

Figure 2.15: The reference problem and the action of the environment (free structure)

Plates: third numerical example

Finally, let us consider the problem of a simplified automotive chassis divided into 43 substructures (see Figure 2.17). The results obtained with the VTCR at 600 Hz and 630 Hz are shown in Figure 2.18.

A comparison of these results with a FEM calculation would be meaningless because the vibrational regime is too oscillatory. In order to assess the accuracy of the VTCR for this problem, the energy density map for all the substructures was compared to that obtained by Statistical Energy Analysis (SEA) using the AutoSEA code (Figure 2.19). One can observe that the two energy density maps are very similar. However, the advantage of the VTCR is that it gives access to the local vibrational states (see Figure 2.18). Thus, one can clearly see that solicitations at two relatively close frequencies can lead to completely different vibration solutions (see Figure 2.18). The solutions at 600 Hz and 630 Hz are very different, so the use of too smooth an approach could have caused some harmful behavior to be overlooked. At 630 Hz, most of the energy is located in the front of the car, as predicted by AutoSEA. Conversely, at 600 Hz, most of the energy is located in the entire front stringer and in the zone under the windshield.

This is a characteristic aspect of medium-frequency behavior.

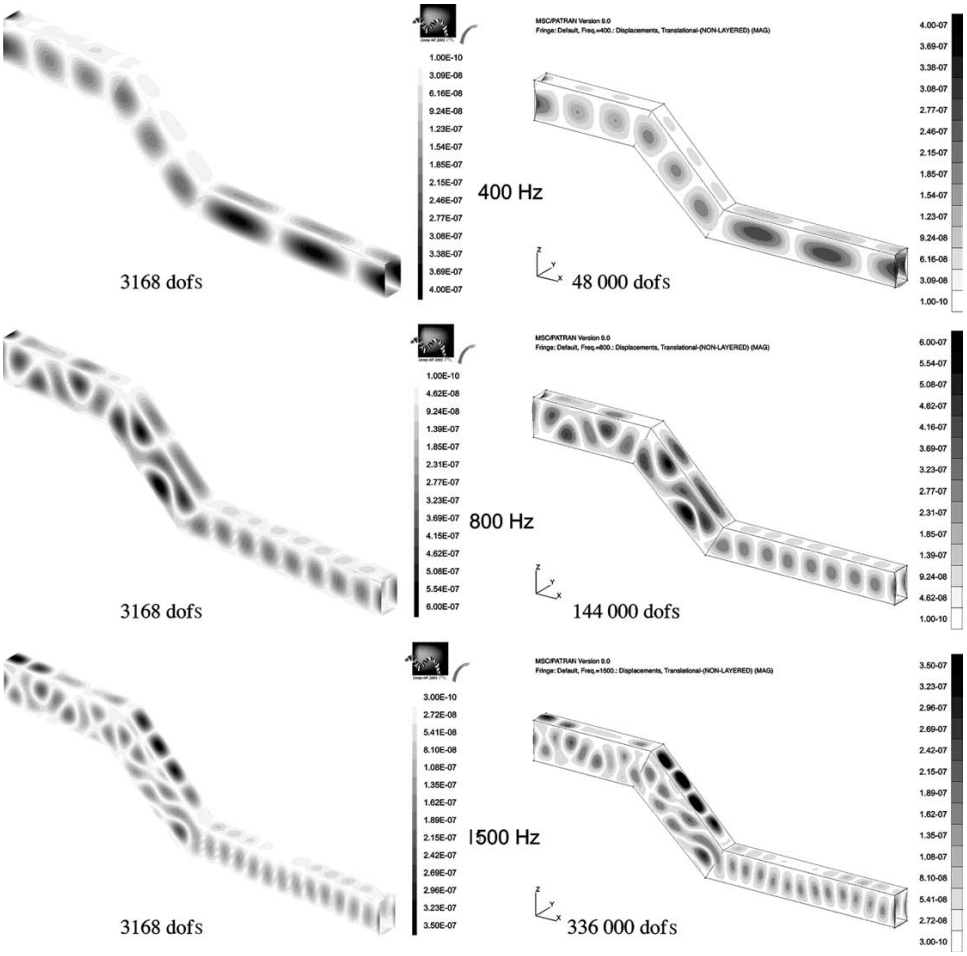

Figure 2.16: Evolution of the number of DOFs *vs.* the frequency for the problem of Figure 2.15

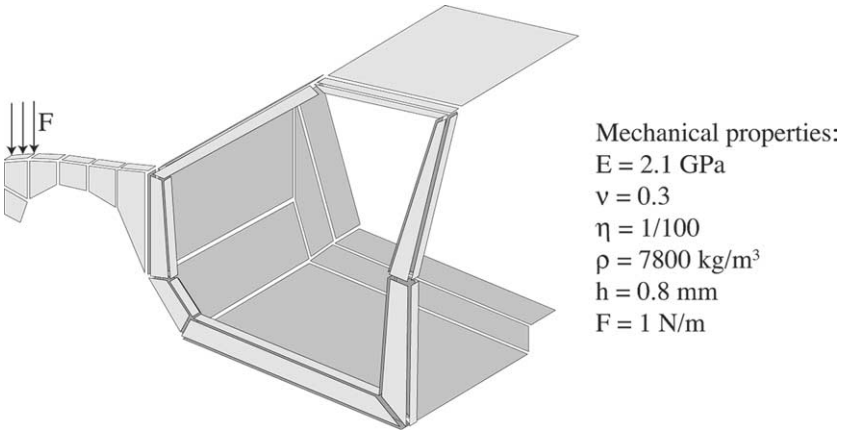

Figure 2.17: The reference problem and the action of the environment

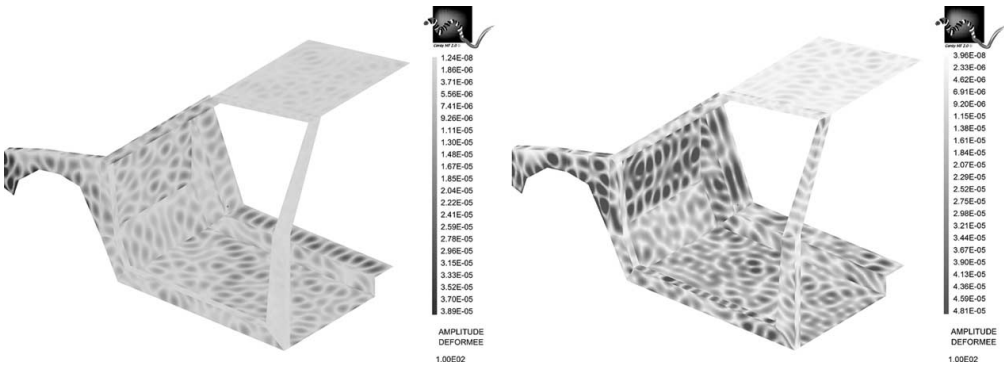

Figure 2.18: The deformed shape for the problem of Figure 2.17 obtained with the VTCR at 630 Hz (left) and 600 Hz (right)

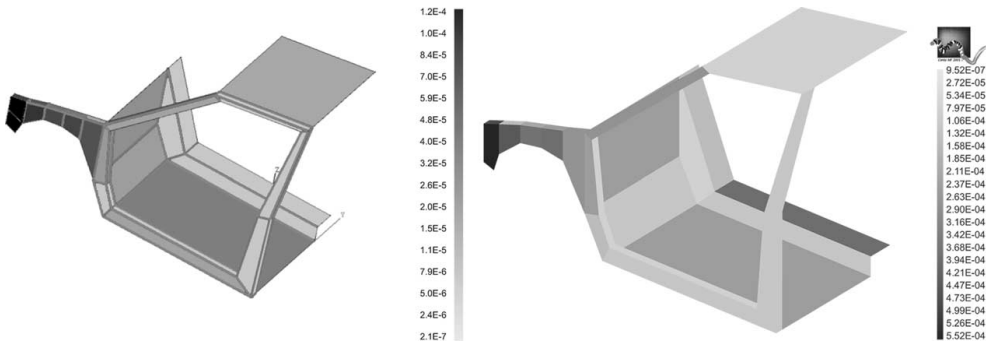

Figure 2.19: Comparison of the energy densities at 630 Hz given by AutoSEA (left) and by the VTCR (right)

4.3 Structures containing holes

One can extend plate results to the case of holed plates by taking into account the perturbation due to local heterogeneity by means of dedicated admissible spaces. The theoretical aspects are explained in details in [Ladevèze et al., 2003a].

Numerical example

Let us consider the problem of a rectangular steel plate of length $L = 1$ m, width $l = 0.8$ m and thickness $h = 0.8$ mm, with a circular hole of diameter 0.11 m at its center. The material properties are $E = 210$ GPa, $\eta = 0.001$, $\nu = 0.3$ and $\rho = 7800$ kg/m^3. The harmonic solicitation is a distributed force $F_d = 1$ N/m of frequency 330 Hz along one of the sides of length l. The plate is fixed along the opposite side. The VTCR solution (Figure 2.20) was calculated using 84 interior waves, 48 edge waves and 8 harmonics of the dedicated hole functions (see [Ladevèze et al., 2003a] for further details). A FEM reference solution is shown in Figure 2.21. The two solutions are very similar, which shows the capability of the VTCR in handling such problems.

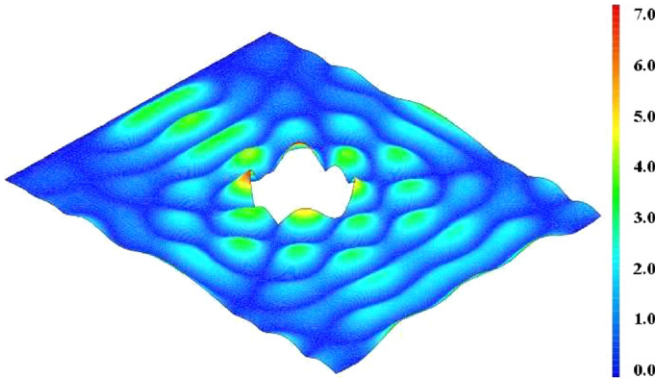

Figure 2.20: The VTCR solution for a holed plate

4.4 Structural vibrations of shells

Thanks to the flexibility of the VTCR formulation, an immediate extension to shell structures is possible. Starting from the VTCR for plates described in the previous section, one simply has to introduce the curvature of the shell. This is explained in details in [Riou et al., 2004]. It is possible to define waves which satisfy the governing equation. As in the case of plates, they can be categorized as interior waves, edge waves and corner waves depending on their shape (see Figures 2.22, 2.23 and 2.24).

Shells: first numerical example

Let us consider the shell structure of Figure 2.25. The mechanical properties are: $E = 75$

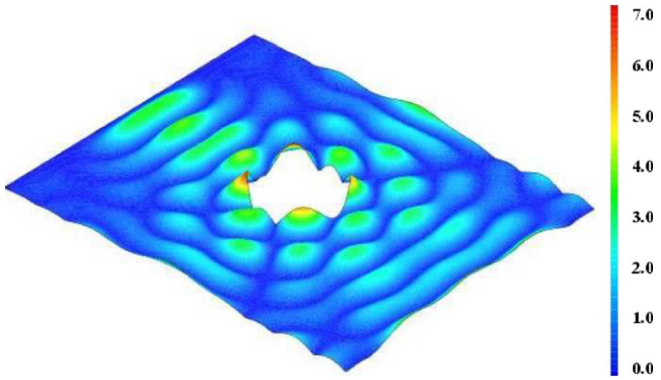

Figure 2.21: The FEM solution for a holed plate

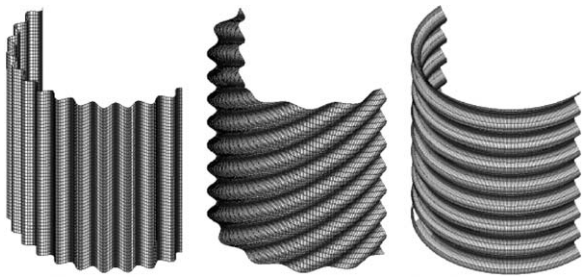

Figure 2.22: Sample waves for the interior zone of a cylinder

GPa, $\eta = 0,0001$, $\mu = 0.3$, $\rho = 2750$ kg/m^3, $\omega = 2\pi.1800$ Hz and $F_d = 1$ N/m. The solution obtained by NASTRAN was used as the reference solution. The mesh seed used in NASTRAN was set to create 10 elements per wavelength. The solution was obtained with $225,000$ DOFs. The VTCR solution used 40 DOFs (20 interior waves, 5 edge waves per edge and 0 corner wave). Figure 2.26 shows that the results given by the VTCR are satisfactory: the two solutions in terms of displacements (distributions of the peaks as well as amplitudes) are similar.

Shells: second numerical example

Let us now consider the 3D assembly of Figure 2.27. The solution obtained with NASTRAN was used as the reference solution. The mesh seed used in NASTRAN was set to create 10 elements per wavelength. The solution was obtained with $1,200,000$ DOFs. For the VTCR solution, the structure was divided into three parts denoted Shell 1, Shell 3 and Plate 2 (see Figure 2.27). The solution was obtained using 132 DOFs (24 interior waves, 5 edge waves per edge and 0 corner wave for each substructure). Figure 2.28 shows that the results given by the VTCR are good: the two solutions in terms of displacements (distributions and amplitudes) are similar.

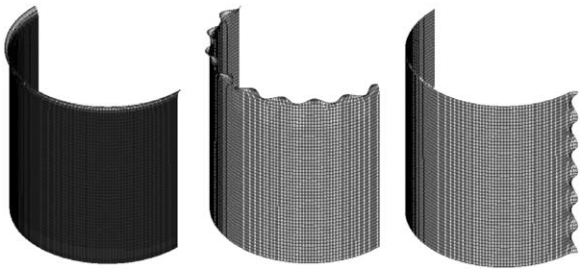

Figure 2.23: Sample waves for the edge zones of a cylinder

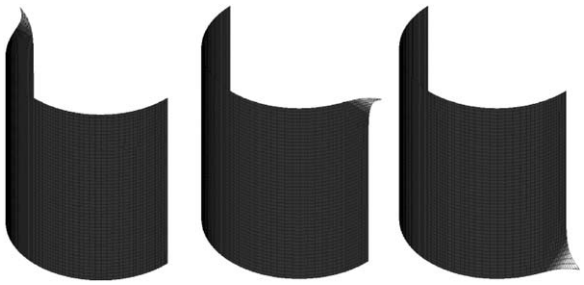

Figure 2.24: Sample waves for the corner zones of a cylinder

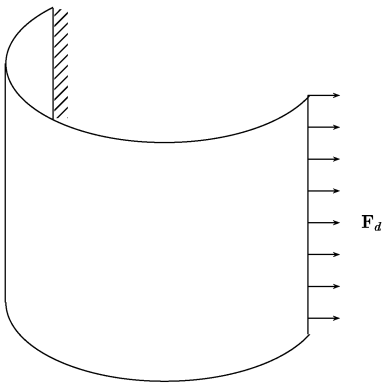

Figure 2.25: The geometric model of a half-cylinder; the cylinder is fixed along one end and a force density F_d is applied along the other

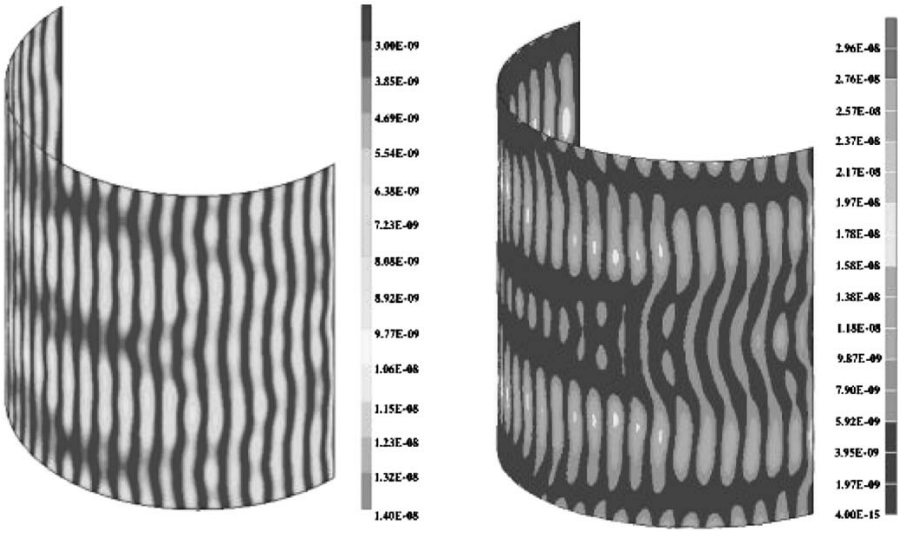

Figure 2.26: The solutions of the half-cylinder problem of Figure 2.25 obtained with the VTCR (left) and with NASTRAN (right)

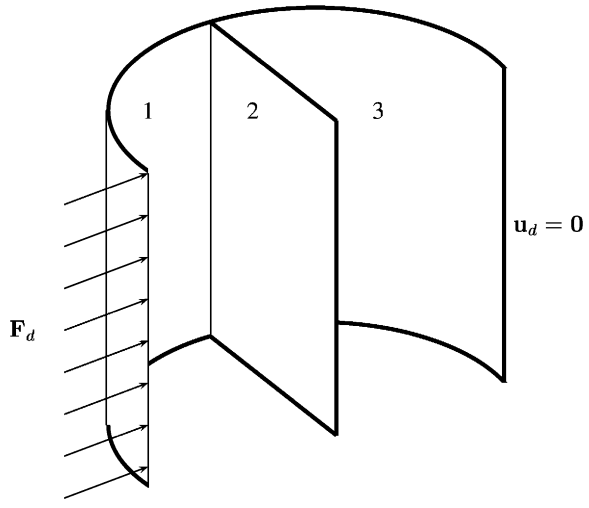

Figure 2.27: The geometry of the 3D assembly. A force density Fd is applied along one side of Shell 1, all the other boundaries being fixed.

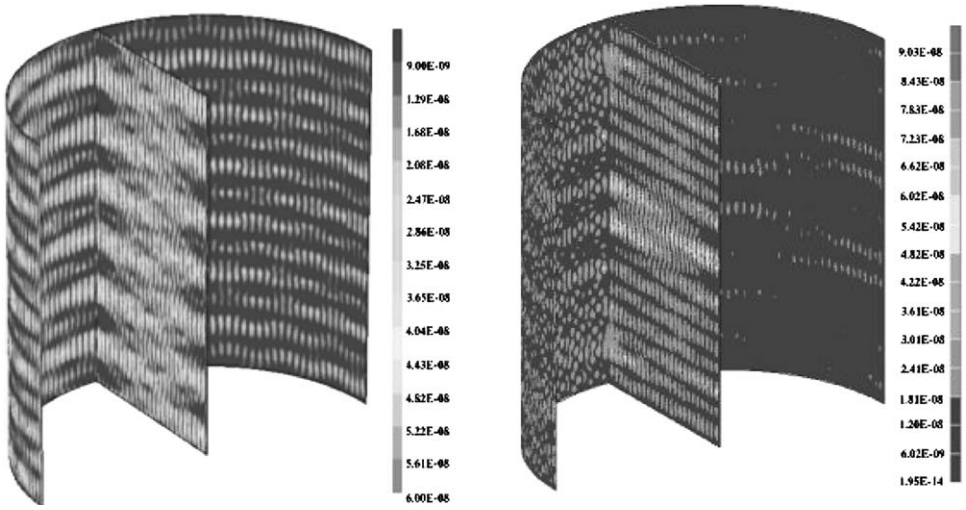

Figure 2.28: The results for the 3D assembly of Figure 2.27 obtained with the VTCR (left) and with NASTRAN (right)

4.5 The Fourier Version of the VTCR

In Section 4.1, we showed that the VTCR is an efficient tool for modeling 2D acoustic problems. However, the representation of the amplitudes of the waves as piecewise constant functions affects the approximation of the wave band which becomes discontinuous with respect to the angular variable θ. To remedy this problem, an alternative representation was recently developed ([Kovalevsky et al., 2012a]) using a new type of shape function based on a Fourier series expansion of the amplitudes of the plane waves which propagate within an acoustic cavity. A, the unknown of the problem (defined by $p_e(\mathbf{x}) = \int_{C_{ea}} A(\mathbf{k}_{ea}) e^{\mathbf{k}_{ea}.\mathbf{x}} dC_{ea}$), is sought, in the approximation space of the functions based on Fourier series, as:

$$\mathcal{S}_{ad}^h = span\left\{ \int_{-\pi}^{\pi} e^{in\theta} e^{ik(x.\cos\theta + y.\sin\theta)} d\theta, n = -N_E, ..., N_E \right\} \tag{2.14}$$

Examples of the real parts of such Fourier-based shape functions are shown in Figure 2.29. This representation makes the angular representation of the wave amplitudes continuous, which may result in a smoother numerical solution.

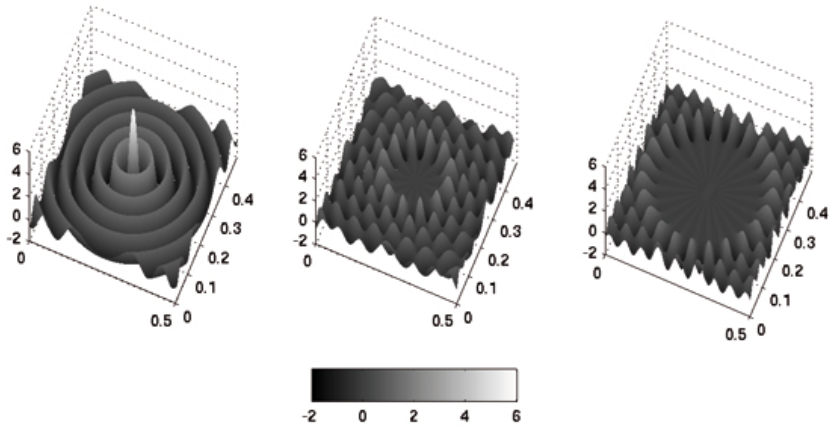

Figure 2.29: Examples of real parts of complex pressure fields associated with Fourier-based functions from (2.14). $\Omega_E = 0.5$ m $\times$ 0.5 m; $k = 120$ m^{-1}; $N_E = 30$; $n = 0$ (left), $n = 12$ (center) and $n = 23$ (right)

Fourier version: first numerical example

In order to assess the performance of the VTCR, let us consider a square domain $\Omega = [0,L] \times [0,L]$ with homogeneous Dirichlet boundary conditions. The loading force is a Dirac function applied at $(x_0; y_0) = (0.1875; 0.1875)$ and the nondimensional wave numbers are $kL = 8, 24, 40, 56, 72$ and 88. An absorption coefficient $\eta = 10^{-5}$ was used. Figure 2.30 shows the VTCR solution along line $y = 0.190625$ obtained with $kL = 8$ and 23 shape functions. Figure 2.31 shows the convergence curves for all the nondimensional

wave numbers considered. One should note that the VTCR gave a very good description of the solution both near the spike caused by the force load and away from that region. The convergence curves of Figure 2.31 also show that for this non-homogenous Helmholtz problem the VTCR behaved quite well in various frequency ranges. Indeed, in all the cases considered, the convergence curves decreased sharply to zero.

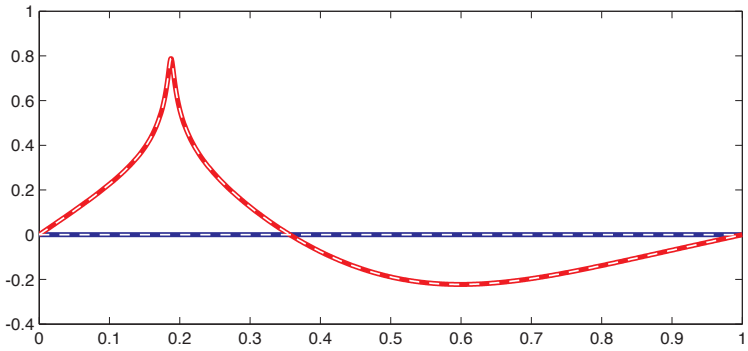

Figure 2.30: Validation using the example of a square domain with homogeneous boundary conditions and a Dirac loading force: comparison of the VTCR solution (continuous line) and the reference solution (dotted line) along the line $y = 0.190625$ with $kL = 8$

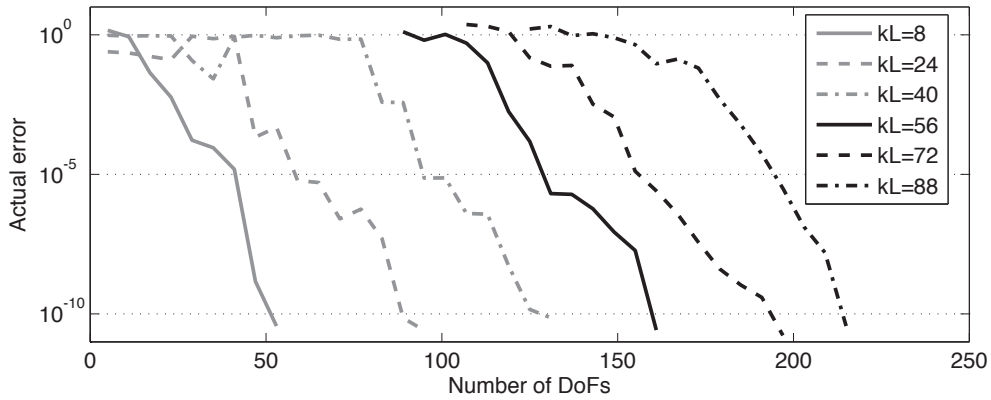

Figure 2.31: Validation using the example of a square domain with homogeneous boundary conditions and a Dirac loading force: convergence curves for nondimensional wave numbers $kL = 8, 24, 40, 56, 72$ and 88

Fourier version: second numerical example

Now, let us consider an L-shaped domain with homogeneous Dirichlet boundary conditions, except for a load applied along half of the lowest horizontal side, as shown in Figure 2.32 (left). The nondimensional wave number is $kL = 8$, L being the width of

the L-shaped domain. For the VTCR, the domain was divided into two symmetrical parallelepipeds and an absorption coefficient $\eta = 10^{-5}$ was used. The VTCR solution is shown in Figure 2.32 (right). Compared to the solution given by [Farhat et al., 2001], this result shows that even though it used very few DOFs (54 DOFs for the calculation if Figure 2.32) the VTCR reproduced the characteristic aspects of the converged solution quite well.

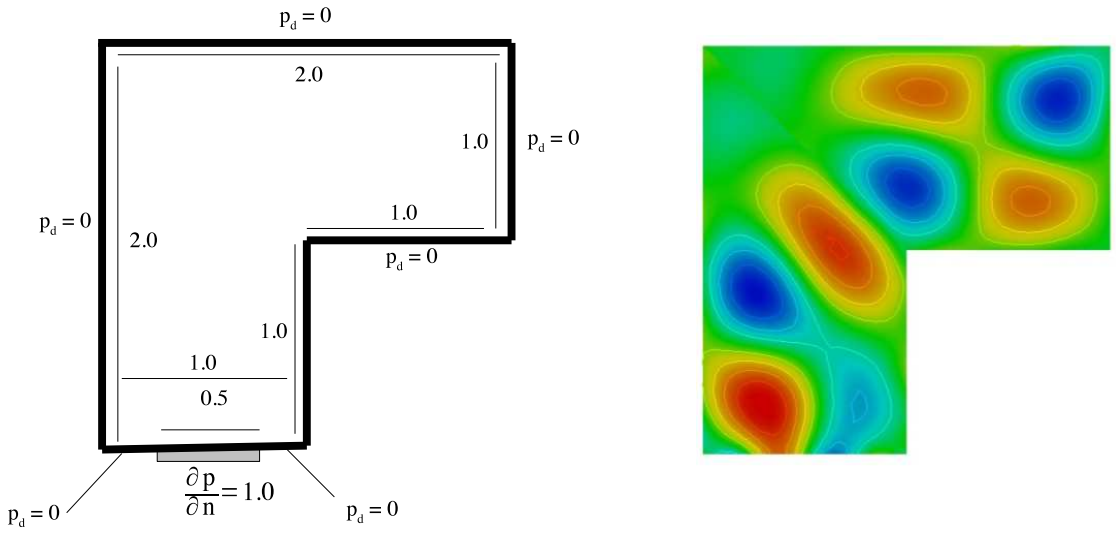

Figure 2.32: Validation using an L-shaped domain with mixed boundary conditions: problem definition (left) and the real part of the VTCR solution for $kL = 8$ with 54 DOFs (right)

Fourier version: third numerical example

The third example concerns the application of the Fourier VTCR to an acoustic cavity of a car filled with air ($\rho_0 = 1.25$ kg.m^{-3}, $c_0 = 340$ m.s^{-1}, $\eta = 10^{-5}$) and subjected to Robin boundary conditions as shown in Figure 2.33. Three circular frequencies were considered: $\omega = 2\pi \times 2,500$ rad.s^{-1}, $\omega = 2\pi \times 4,000$ rad.s^{-1} and $\omega = 2\pi \times 8,000$ rad.s^{-1}. The loading was applied along the leftmost edge. The Fourier VTCR was applied inside each cavity using all the shape functions with an energy greater than 10^{-3}. Figure 2.34 shows the calculated solutions. The quality of these results was good. Even though the solution at $\omega = 2\pi \times 8,000$ rad.s^{-1} (the high-frequency case) involved several dozen wavelengths within the entire acoustic cavity, its calculation using the VTCR presented no difficulty.

4.6 Error estimator

With the Fourier version of the VTCR presented in Section 4.5, it is possible to introduce an *a priori* error estimator. The estimator proposed in [Kovalevsky et al., 2012a] for

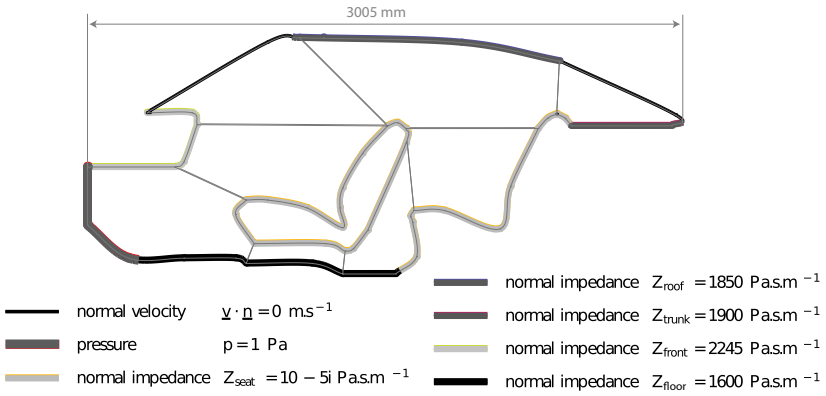

Figure 2.33: Definition of the car acoustic cavity (boundary conditions and internal mesh)

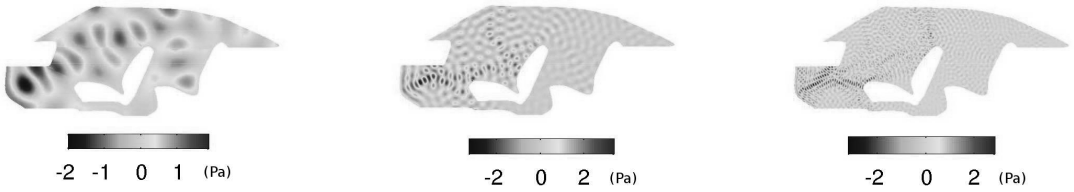

Figure 2.34: Contour plots of the real part of the pressure field in the car acoustic cavity of Figure 2.33 at $\omega = 2\pi \times 2,500$ rad.s^{-1} (left) , $\omega = 2\pi \times 4,000$ rad.s^{-1} (center) and $\omega = 2\pi \times 8,000$ rad.s^{-1} (right)

acoustic problems measures the quality of the pressure p_E^h over Ω_E approximated by the VTCR, and is defined as:

$$\varepsilon_E = \frac{E_{d,\Omega_E}(p_E^h - p_E^{ex})/mes(\Omega_E)}{\sum_E E_{d,\Omega_E}(p_E^{ex})/mes(\Omega)} \tag{2.15}$$

where $E_{d,\Omega_E}(p) = \frac{1}{\omega} Re \int_{\partial\Omega_E} p.\overline{L_v(p)} d\partial\Omega$ is the dissipated energy, $mes(\Omega)$ and $mes(\Omega_E)$ denote respectively the measures of Ω and Ω_E, and p_E^{ex} corresponds to the exact solution of the problem in Ω_E. One can see that this error measures the relative difference between the approximate solution and the exact solution in terms of dissipated energy. The dissipated energy is interesting in the medium-frequency range because at these frequencies it is a relevant quantity; a more local quantity, such as the pressure at a specific point, would be too sensitive to small variations in the problem data. Similarly, a global error indicator can be defined as:

$$\varepsilon = \max_E \varepsilon_E \tag{2.16}$$

The problem with the definition of error (2.15) is that, in general, the exact solution is unknown. Therefore, one needs to define an error estimator. This is not an easy task because there may be some subcavities Ω_E which not touch the boundary $\partial\Omega$. For these subcavities, it is impossible to verify the accuracy of the boundary conditions, which are the only equations of the problem which are not satisfied automatically. (Remember that the shape functions satisfy the Helmholtz equation.) The only way to evaluate the accuracy of the approximate solution in such a subcavity is to verify the continuity in terms of pressure and velocity with all the other subcavities in the vicinity of Ω_E. But this verification is difficult because the solutions in the surrounding subcavities are only approximate solutions.

Based on the previous remarks, we propose the following local error estimator for (2.15):

$$\varepsilon_E^h = \frac{E_{d,\Omega_E}(p_E^h - p_E^{pv})/mes(\Omega_E)}{\sum_E E_{d,\Omega_E}(p_E^{pv})/mes(\Omega)} \tag{2.17}$$

where p_E^{pv} corresponds to the solution of the problem in Ω_E when the pressure and velocity are prescribed at the boundaries of Ω_E in such a way that they correspond to the pressure and velocity in all the $\Omega_{E'}$ adjacent to Ω_E.

In order to verify the effectiveness of error estimator (2.17), let us consider the following example of Figure 2.35: Ω is a 2.3 m $\times$ 1 m rectangular cavity with a curved upper right corner (diameter 1.6 m). This cavity is filled with air (ρ_0 = 1,25 kg.m^{-3}, c_0 = 340 m.s^{-1}, $\eta = 10^{-5}$) and the boundary conditions are such that the exact solution is $p_{ex}(\mathbf{x}) = \int_{\theta=-\pi}^{\pi} A^{ex}(\theta).e^{i\mathbf{k}(\theta).(\mathbf{x}-\mathbf{x}_C)} d\theta$, with $A^{ex}(\theta) = (3+i)\cdot(\theta-2\pi)\cdot(\theta-\pi)\cdot\theta+2\cos\theta\cdot\sin\theta\cdot\cos 4\theta$, $\mathbf{x}_C = [0.62; 0.42]$, $\mathbf{k}$ being the wave vector . This is an interesting case because its solution cannot be easily expanded as a Fourier series. The boundary conditions used combine all the possible types (prescribed pressure, prescribed velocity and Robin condition). The VTCR decomposition of the cavity is shown in Figure 2.35.

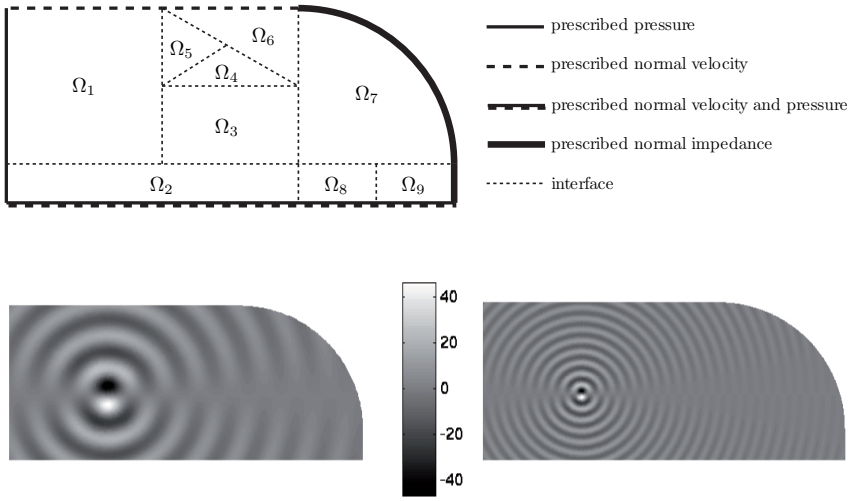

Figure 2.35: Top: description of the example. Bottom: the real part of the exact pressure field for $k = 30$ m^{-1} (left) and for $k = 90$ m^{-1} (right)

With the two circular frequencies chosen ($k = 30$ m^{-1} and $k = 90$ m^{-1}), the characteristic length of Ω was about 10 and 30 wavelengths respectively. The true local error (2.15), the local error estimator (2.17) and the H^1 relative error in each of the subdomains are compared in Figure 2.36. One can see that our proposed error, which is based on a *more physical* interpretation of the solution (the dissipated energy), comes very close to the classical H^1 error and, therefore, is a relevant error measure for assessing the quality of the calculated solution.

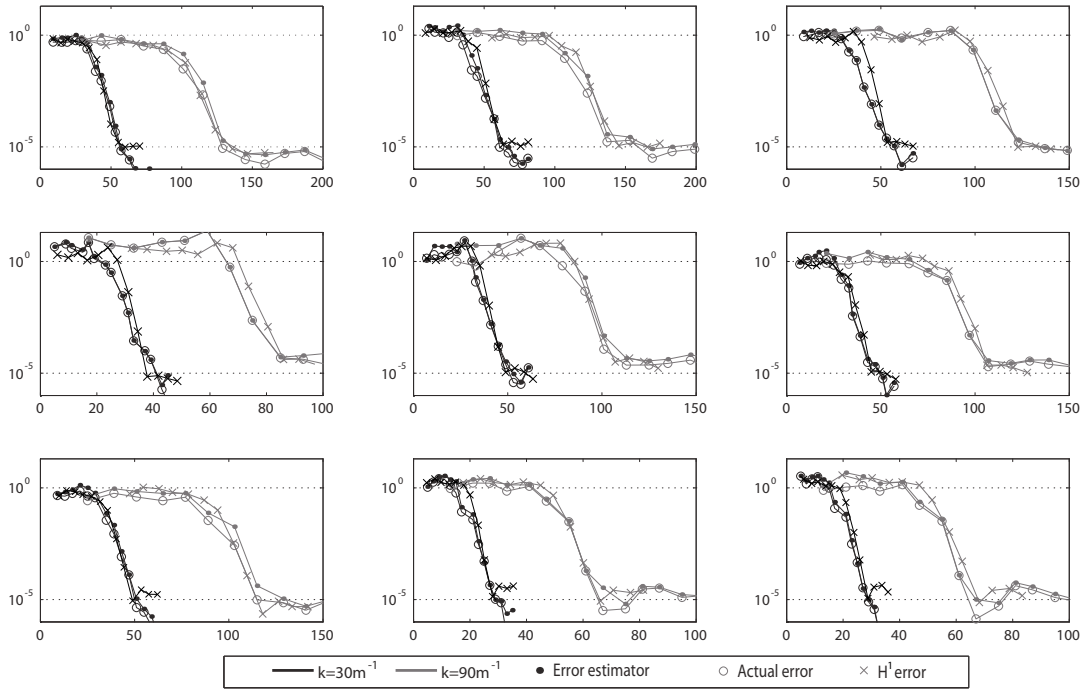

Figure 2.36: Comparison of the true local error (2.15), the local error estimator (2.17) and the H^1 relative error for the example of Figure 2.35 in the case of a Fourier-based approximation (2.14)

4.7 3D acoustics

One the main advantages of the Fourier approximation introduced in Section 4.5 is that it can be extended easily and effectively to 3D problems using spherical harmonics expansion (see [Kovalevsky et al., 2012b]).

In the 3D acoustic case, the distribution of plane waves is defined in the unit sphere:

$$p_E(\mathbf{x}) = \int_{\theta=-\pi}^{\pi}\int_{\varphi=0}^{\pi} A_E(\theta,\varphi).e^{i\mathbf{k}(\theta,\varphi).(\mathbf{x}-\mathbf{x}_E)}d\theta sin\varphi\, d\varphi \tag{2.18}$$

where A_E describes the amplitudes of plane waves propagating in the (θ,φ) spherical direction. In order to avoid the quadrature of the unit sphere which would be necessary to define the ray or wave band shape functions and to take advantage of the Fourier decomposition, a truncated Laplace series is used to describe the amplitude profile $A_E(\theta,\varphi)$. This is a direct extension of Fourier series to three dimensions. Then, the discrete space S^h_{ad} can be expressed as:

$$\begin{aligned} S^h_{ad} &= span\{\int_{\theta=-\pi}^{\pi}\int_{\varphi=0}^{\pi} Y_l^m(\theta,\varphi)e^{i\mathbf{k}(\theta,\varphi).(\mathbf{x}-\mathbf{x}_C)}d\theta sin\varphi\, d\varphi, \\ &\qquad m=-l,...,l, l=0,...,N_E\} \\ &= span\{\Phi_l^m(\mathbf{x}), m=-l,...,l, l=0,...,N_E\} \end{aligned} \tag{2.19}$$

where

- $\mathbf{k}(\theta,\varphi)$ is the wave vector of the plane wave propagating in the direction (θ,φ) in spherical coordinates;

- $Y_l^m(\theta,\varphi) = \sqrt{\frac{2.(l-m)!}{(l+m)!}}.P_l^m(cos\theta).e^{im\varphi}$,
  with $P_l^m(X) = \frac{(-1)^m}{2^l.l!}\left(1-X^2\right)^{m/2}\frac{\partial^{m+l}(X^2-1)^l}{\partial X^{m+l}}$ being the Legendre polynomial, is the spherical harmonics of non-negative index l and momentum m. Parameter m varies from $-l$ to l. The set $\left\{Y_l^m(\theta,\varphi)\right\}_{|m|\leqslant l\leqslant\infty}$ forms a complete orthogonal system on the unit sphere associated with the classical L^2 scalar product. The first spherical harmonics are shown in Figure 2.37. One can observe that these harmonics correspond to a regular decomposition of the possible spherical wave propagation directions.

For a given parameter N_E in (2.19), the number of shape functions to be used is $(N_E+1)^2$.

3D acoustics: first numerical example

The first example concerns a simple wave guide problem. Ω is an $L\times L\times L$ cubic domain subjected to Robin conditions so that the exact solution is a plane wave propagating in spherical direction $(\theta_{ex}=0.8,\varphi_{ex}=2.3)$. One can note that the wave direction does not

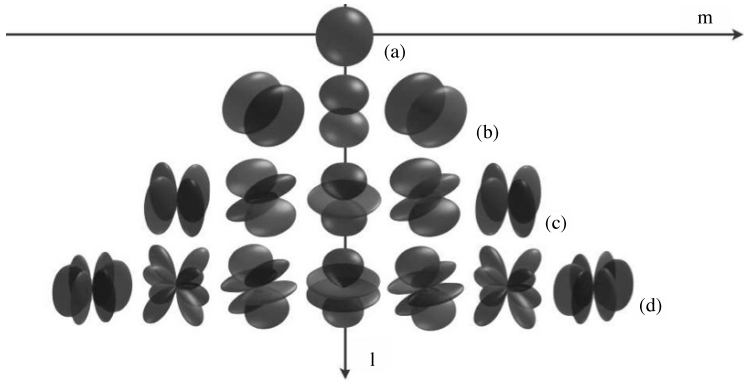

Figure 2.37: Representation of the functions $Y_l^m(\theta,\varphi)$ used in (2.19). Line (a) corresponds to $l=0$ and $m=0$. Line (b) corresponds to $l=1$ and $m=-1,...,1$. Line (c) corresponds to $l=2$ and $m=-2,...,2$. Line (d) corresponds to $l=3$ and $m=-3,...,3$ *(courtesy of Wikipedia)*

characterize a specific set of spherical coordinates. Cavity Ω was not subdivided. The convergence with respect to the number of shape functions used in S_{ad}^h (see (2.19)) was evaluated for wave numbers such that $kL=5$, $kL=10$ and $kL=15$.

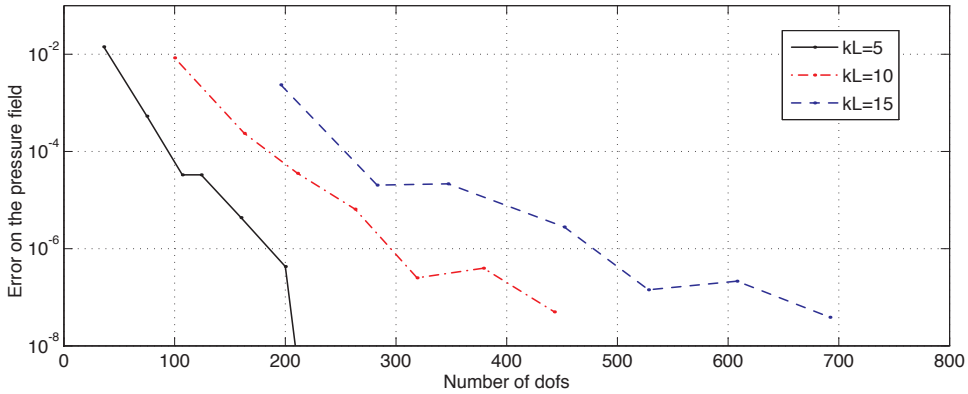

Figure 2.38: The convergence curves of the pressure field given by the 3D VTCR for a cubic wave guide problem with Robin boundary conditions: $kL=5$, $kL=10$ and $kL=15$

The relative error ($\varepsilon(\square)=\dfrac{||\square-\square_{ref}||^2}{||\square_{ref}||^2}$) of the approximate pressure field is shown in Figure 2.38. One can observe that the convergence rate of the VTCR was very good.

3D acoustics: second numerical example

The second example is the sound-hard scattering of a plane wave by a sphere of radius $R_1=0.5$ m. In order to solve this problem, a prescribed velocity defined by $L_v(p)=-\dfrac{i}{\rho_0\omega}\dfrac{\partial p_{scat}}{\partial \mathbf{n}}$, p_{scat} being a plane wave propagating in the spherical direction $(\theta,\varphi)=$

$\left(\frac{\pi}{2},0\right)$, was applied over the boundary of the sphere, and an absorbing boundary condition defined by $Z=-\frac{\rho_0\omega}{k}$ and $h_d=0$ was applied over the exterior boundary, which is a spherical surface of radius $R_2=1.8$ m. The domain was divided into 32 subcavities, as illustrated in Figure 2.39.

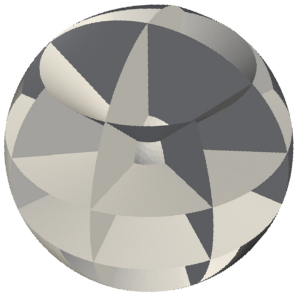

Figure 2.39: Scattering by a sphere: the discretized computational domain

This problem has an exact analytical solution thanks to the following Hankel function expansion in spherical coordinates:

$$p^{ex}(r,\theta,\varphi)=\sum_{n=0}^{\infty}a_n(\theta,\varphi)H_n^{(1)}(kr)+b_n(\theta,\varphi)H_n^{(2)}(kr) \tag{2.20}$$

where $H_n^{(1)}$ and $H_n^{(2)}$ are the spherical Hankel functions of the first and second kind and the coefficients a_n and b_n are obtained by enforcing the boundary conditions.

We studied three circular frequencies defined by $2kR_1=7$, $2kR_1=12$ and $2kR_1=17$. The real parts of the scattering pressure fields are shown in Figure 2.40.

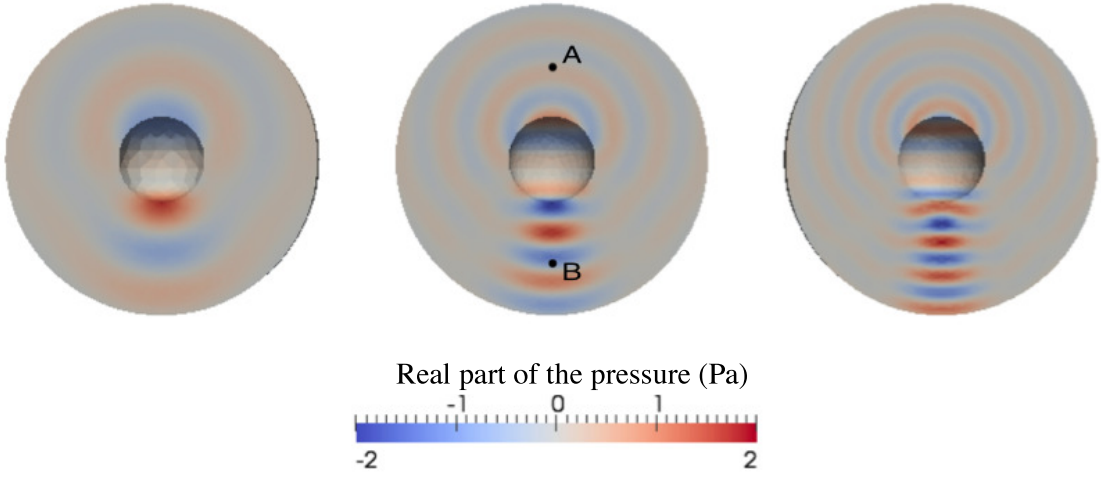

Figure 2.40: The scattering pressure fields for $2kR_1=7$ (left), $2kR_1=12$ (middle) and $2kR_1=17$(right)

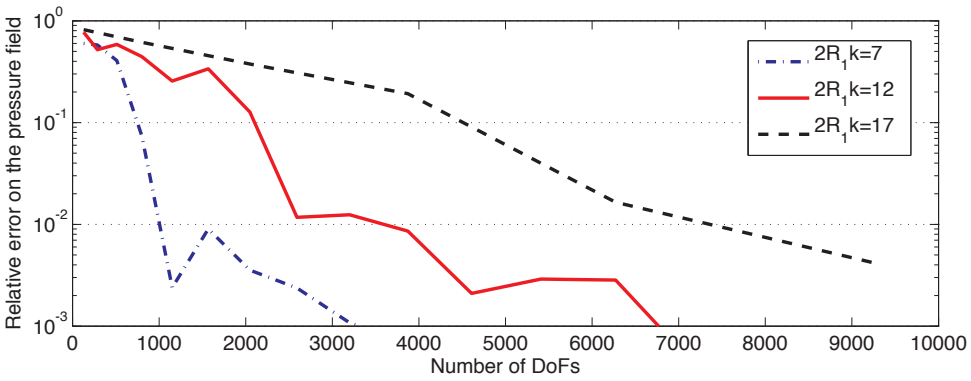

Figure 2.41: Convergence curves of the sound-hard scattering by a sphere, in relative L^2 norm, as a function of the number of DOFs for $2kR_1 = 7$, $2kR_1 = 12$ and $2kR_1 = 17$

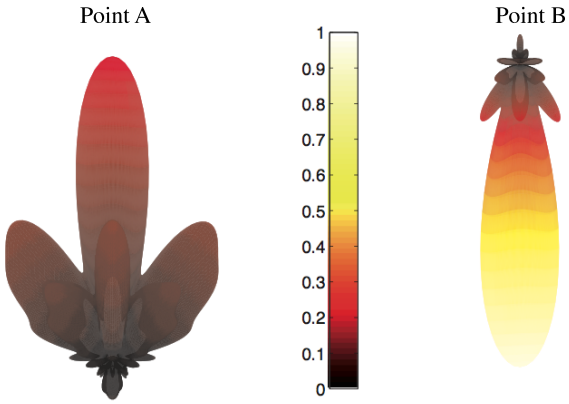

Figure 2.42: The regularized amplitude profiles calculated at points A (left) and B (right) of Figure 2.40 with $2kR_1 = 12$

Figure 2.41 shows the evolution of the results as a function of the total number of DOFs. One can observe that the convergence rate is very good for the three frequencies considered. Indeed, the numbers of DOFs which are necessary in order to achieve a relative accuracy of 10^{-2} are about 1,000, 3,500 and 7,500 for $2kR_1 = 7$, $2kR_1 = 12$ and $2kR_1 = 17$ respectively. In comparison, the corresponding classical FEM meshes with 5 elements per wavelength would represent about 10,000, 40,000 and 80,000 nodes.

The amplitude profiles $A_E(\theta, \varphi)$ of the waves (see (2.18)) calculated at points A and B of Figure 2.40 for $2kR_1 = 12$ are shown in Figure 2.42. One can observe that the main wave propagation direction can be clearly identified, which helps understand the physics of the problem. In order to obtain such a result, it is necessary to use some regularization tools (see [Kovalevsky et al., 2012b]).

3D acoustics: third numerical example

Finally, the 3D Fourier VTCR was used to solve an acoustic problem in a simplified car cavity. This cavity, the boundary conditions and the domain decomposition into 34 subcavities are described in Figure 2.43. The cavity, filled with air (ρ_0 = 1,2 kg.m^{-3}, c_0 = 344 m.s^{-1} and $\eta = 10^{-5}$), was solicited by a point source located on the front right. The boundary conditions were normal impedance conditions with impedance $Z = 845 - 55i$ Pa.s.m^{-1} at the level of the seats and $Z = 615.4 - 1887i$ Pa.s.m^{-1} at the other boundaries, except for the front and rear windows which were modeled as hard walls.

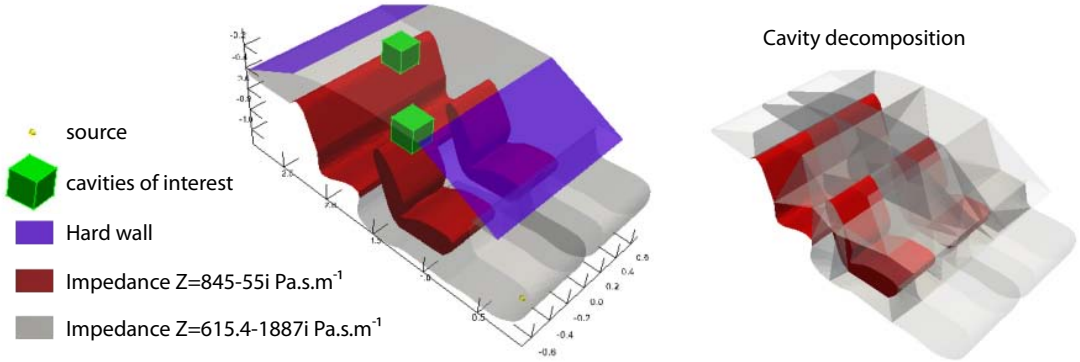

Figure 2.43: Definition of the acoustic car cavity

The results at 700, 1,200 and 1,700 Hz are shown in Figures 2.44, 2.45 and 2.46 respectively. One can observe that the quality of these solutions is good.

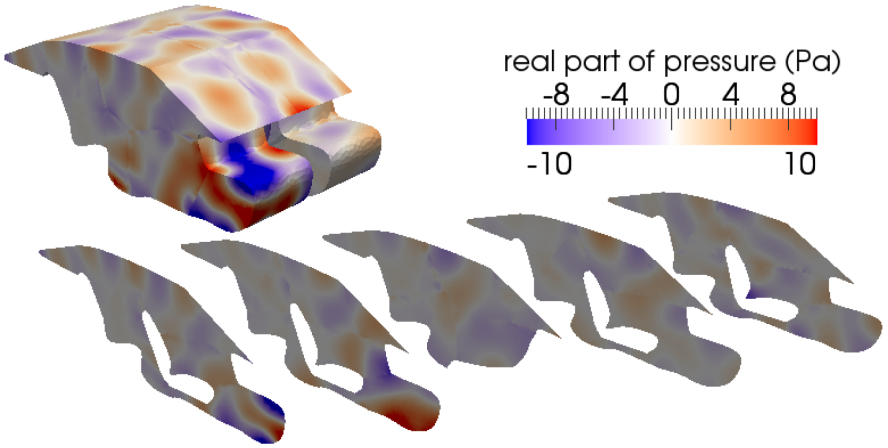

Figure 2.44: The real part of the pressure field obtained with the 3D Fourier VTCR for the problem of Figure 2.43 at 700 Hz

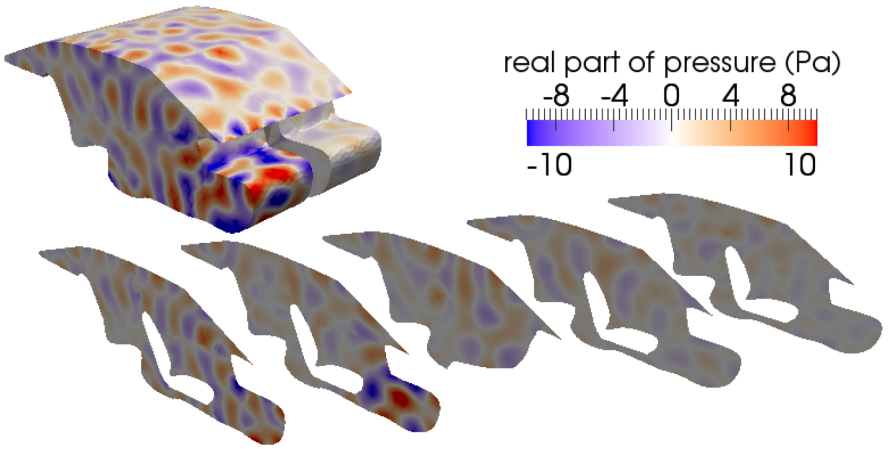

Figure 2.45: The real part of the pressure field obtained with the 3D Fourier VTCR for the problem of Figure 2.43 at 1,200 Hz

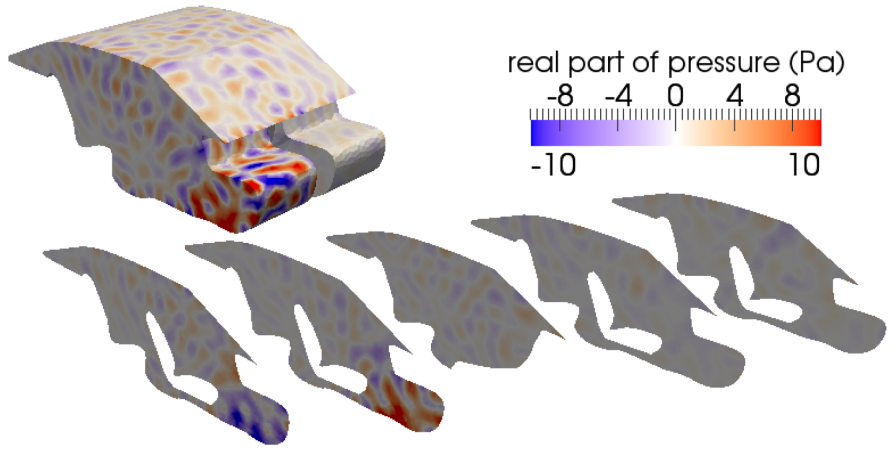

Figure 2.46: The real part of the pressure field obtained with the 3D Fourier VTCR for the problem of Figure 2.43 at 1,700 Hz

5 VTCR, still an open question?

In this chapter potentiality and advantages of VTCR has been extensively discussed. At the state of art the technique could seem quite a mature one. Both 3D and 2D problems in structural dynamics and acoustic are dealt by the technique. Recent enhancements extended the technique to vibro-acoustic coupling and unbounded problems. Moreover Fourier approximation introduced robustness in the approach and the possibility to built a all-user multipurpose code. Nevertheless the technique still needs some decisive improvements. The aim of this work is to act on principal weak points in other to make a decisive step in the maturity of the technique. Being VTCR a Trefftz method (see Chapter 1 Section 4), it shares with those methods some know major issues. In particular we can remark some key points:

- Matrix **K** has very unpleasant characteristics. It's a non-positive full populated by blocks matrix with complex values a bad condition number and strongly non-symmetrical. Even if these characteristics are not decisive in terms of convergency and efficacy of the method, the global robustness is strongly undermined by them. Unluckily these limits are inborn in Trefftz methods nature.

- VTCR formulation is completely frequency dependent. This means that in order to take into account frequency bands, a very fine frequency discretization is needed. This is a very weak point compared to FEM techniques where the solving matrices are frequency independent. Indeed, high performances calculation seen in this chapter, lose effectiveness if a large band is considered. Even though in a single frequency calculation VTCR outperforms classical FEM, on large bands this could not be true due to frequency dependency.

- VTCR is a fully deterministic approach. That means that there is no easy way to propagate uncertainty in the technique. This is against mid-frequency nature. In this range of frequency there is a quite strong sensibility to uncertainty so add a stochastic information can be vital to an industrial user. The most common way to extend deterministic methods to uncertainty is the Montecarlo simulation [Metropolis, 1987]. This is a very well established tool which allows to introduce uncertainty over deterministic methods. Despite its easiness and effectiveness it's a very costly tool. For this reason its application is to avoid. This is particularly true when uncertainty over a frequency band is to take in account. The simple alliance between a fine VTCR frequency mesh calculation and a Montecarlo could lead to unacceptable computational costs.

As remarked there isn't a lot to do to improve in matrix **K** characteristics. Nevertheless in the following of the work a new dedicated pre-conditioner will be introduced

to stabilize the technique. This stabilization in terms of conditioning makes possible to improve VTCR performances and, more important, it makes possible some iterative post-processing which are major points of this work.

The situation is different for the other two points. Recently a new class of numerical tool, called Reduced Order Model (ROM) techniques, is arising. These techniques allows to solve very complex problems choosing a consistent reduced basis (generally through a snap-shooting process) and than project the complex problem on it. This means calculate an approximation of a complex problems with just few information. An overview of these methods will be provided in the following chapter. The main idea of this work is to apply a particularly effective ROM technique, called Proper Generalized Decomposition (PGD), to VTCR. In a first step PGD is proposed to solve wide bands problem. A reduced model over frequency is built and this allows to make accurate and inexpensive predictions over a frequency band. This overcome the second major limitation of VTCR.

Concerning the extension to stochastic, again a combination between PGD and VTCR is proposed. In this way is possible to take in account uncertainty over a frequency band without passing through Montecarlo simulation. Preliminary results, shown in the last chapter, suggest that such a technique is a very valuable research path and could be an answer to the third VTCR major issue.

Chapter 3

The Reduced Order Model techniques

In this chapter Reduced Order Model techniques are introduced. In recent years these techniques raised as an answer to very complex numerical problem. Despite them young history the basis of these techniques were laid in the beginning of 1900. This basic technique is called Proper Orthogonal Decomposition and it is briefly introduced in the chapter. From this technique ROM-POD and Reduced Basis have been recently developed to solve complex problem on reduced base. In the end of the chapter the Proper Generalized Decomposition is finally introduced.

Contents

1 Reduced Order Model techniques 72

2 The Proper Orthogonal Decomposition 72

2.1 Reduced Order Model based on POD 72

3 The Proper Generalized Decomposition 73

1 Reduced Order Model techniques

Before discussing in details the model order reduction techniques of interest a remark about the semantic is necessary. Reduced model is a very generic term used in several domains. Concerning acoustic and structural dynamics works, reduced models are used in [Soize, 1998]. A Padé approximation based reduction for acoustic can be found in [Collins, 1993, Rumpler et al., 2011].

In the context of this manuscript, Reduced Order Model (ROM) is referred to an ensemble of techniques capable to solve complex numerical problems on a reduced spaces. The basic concept of these methods is to substitute a far too complex problem with a surrogate model defined on a simpler reduced space. On this space a reduced base is built. In the end the reduced base is used to solve the initial problem. Most of ROM technique are based on greedy algorithms. The reduced based is enriched in an iterative process until a desired convergency to the right solution.

2 The Proper Orthogonal Decomposition

The intuition of ROM methods rises from an old numerical technique called Proper Orthogonal Decomposition (POD) [Pearson, 1901]. The same technique, depending on the way to construct the POD approximation, is also known as Karhunen-Loeve decomposition [Karhunen, 1946, Loeve, 1955] or Singular Value Decomposition [Eckart and Young, 1936]. If u is a function defined over time t and space x, POD technique search the approximation of the function as:

$$u(x,t) \approx u_m(x,t) = \sum_{i=1}^{m} \Lambda_i(x)\lambda_i(t) \tag{3.1}$$

where $\Lambda_i(x)$ are space dependent functions and $\lambda_i(t)$ are time dependent functions. The POD decomposition is so composed by a sum of time and space dependent functions. The approximation is built in order to minimize the error between the original function and the approximation in respect a chosen norm:

$$||u-u_m|| = \min_{[\lambda_i]_{i=1}^m, [\Lambda_i]_{i=1}^m \in \mathscr{L}_2^m} ||u - \sum_{i=1}^{m} \Lambda_i(x)\lambda_i(t)|| \tag{3.2}$$

2.1 Reduced Order Model based on POD

A POD decomposition as built in 3.3 manage to approximate complex problems with few couples introducing an high data compression ratio. On the other hand the complete knowledge of the initial model is required. The idea, in order to introduce a predictive power to the technique is to reduce a complex problem in a simpler one (from which reduced order model). POD decomposition in so chosen to build a base of the reduced problem which act like a reduced base for the initial problem. If this reduced base is

chosen in a proper way the approximation will be close to the problem solution. To guarantee this property in necessary to establish a reliable error criteria and to put in place some greedy algorithm to enrich the reduced base and reduce the error between the approximated and the actual solution. A way to reduce the model is to search the solution of $u(x,t)$ on a reduced test space of m dimension:

$$u(x,t) \approx u_m(x,t) = \sum_{i=1}^{m} \Lambda_i(x)\lambda_i(t) \tag{3.3}$$

where $\Lambda_i(x)$ are known functions and base on the test space, $\lambda_i(t)$ are unknown of the problem. The approximation error of the solution is much smaller if the reduced test space is relevant. A basic example of relevant base is the modal base for vibration found after a preliminary calculation by considering the structure without solicitation. When no relevant basis can be withdrawn directly from the problem, it is possible to use the POD to extract a minimum size base from a sampling process. The choice of a representative sample is critical. Inaccurately chosen snapshot could lead to enormous mistakes. Let us consider a space-time process. A first strategy can be to solve the complete problem only on initial time steps than the withdrawn POD space base is used as a reduced base on the other time steps. A second strategy can be to solve a coarse time discretization of the problem and then project the full time problem on the reduced POD space base. The techniques applying this kind of process are called ROM-POD techniques. They have been used with success in dynamic problem [Krysl et al., 2001] and in transient thermal analysis in [Białecki et al., 2005]. This method was also used to perform a fluid structure interaction analysis of a complete aircraft [Lieu et al., 2006]. Projection on the base could be very expensive, so an improvement is proposed in [Ryckelynck et al., 2006]. This method called A Priori Hyper Reduction Method (APHR) proposes a strategy to chose only few significant snapshot to improve performances. Adding an error criterion in the resolution allows enrichment of the projection base and thus circumvent the critical points of the choice of an appropriate sample [Kunisch and Volkwein, 2001]. An other important family of method is the Reduced Based method [Fink and Rheinboldt, 1983, Machiels et al., 2000, Maday and Rønquist, 2002, Patera and Rozza, 2007]. The technique defines an error which is used to enrich the base, where the error is the largest. This definition allows a high quality of the reduced model.

3 The Proper Generalized Decomposition

As ROM-POD and Reduced Bases the Proper Generalized Decomposition in based on a sum of function product representation of the solution. The way to get to the solution is slightly different. Such a representation was proposed many years ago by Ladevèze for the resolution of complex nonlinear thermomechanical problems (see [Ladevèze, 1999]). Under the name “radial approximation”, it became one of the main components of the powerful non-incremental and nonlinear LArge Time INcrement (LATIN) solver. More recently, a general separated representation was used in [Ammar et al., 2006] to find

approximate solutions of multidimensional partial differential equations. The separated representation was also used in [Nouy, 2007] for the resolution of stochastic equations in which the deterministic variables and the stochastic variables were separated, very much like in [Ladevèze et al., 2010] for the radial space-time approximation of complex multiscale problems and in [Ladevèze and Chamoin, 2011] for finding guaranteed error bounds.

Today, the common name used for techniques involving a separated representation of the variables is Proper Generalized Decomposition (PGD). PGD belongs to the family of Reduced-Order Modeling techniques but in the case of PGD the construction of the representation takes into account the nature of the problem directly. The general form of a PGD separated representation of a function u of N variables is $u(x_1,...,x_N) \simeq u^M(x_1,...,x_N) = \sum_{m=1}^{M} u_m^1(x_1) \times ... \times u_m^N(x_N)$, M being the order of the approximation. Many applications of PGD, covering several domains, have already been presented: for example advanced nonlinear solvers using separated space-time representations [Boucard and Ladeveze, 1999]; multidimensional models and the separation of physical spaces [Néron and Ladevèze, 2010]; parametric models [Chinesta et al., 2010b]; real-time simulations [Monserrat et al., 2001]; the quantification of uncertainties and stochastic parametric analysis [Nouy, 2007]. A study on error and verification of the technique is found in [Ladevèze and Chamoin, 2011]. [Chinesta et al., 2010a] and [Chinesta et al., 2011] give reviews of recent works on PGD. An exhaustive collection of possible algorithm and an excellent theoretical framework were presented in [Nouy, 2010]. Proper Generalized Decomposition is the main object of this manuscript and details about the technique and its application to mid-frequency problems will be provided in the following chapters.

Chapter 4

PGD-VTCR, an alliance to tackle mid-frequency broad band

In this chapter an overview of the interest of combing PGD with VTCR is provided. A first simple algorithm will be introduced. Numerical result will show the strong limitation of this approach. After a deep numerical analysis, reason for this fail is found. A Petrov-Galerkin approach is consequently introduced to overcome this numerical issue. In the end of the chapter a significant numerical example is provided in order to show potentiality of the Petrov-Galerkin approach. Some significant imperfections of the technique are underlined planting the seeds for more performing algorithms proposed in the next chapter

Contents

1 Proper Generalized Decomposition and VTCR: a ROM technique to perform efficient frequency band calculations 77

1.1 The reference problem and the choice of the approximation 77

2 A simple algorithm to introduce PGD-VTCR 79

2.1 A numerical example 80

2.2 A surprising numerical problem 82

3 A Petrov-Galerkin algorithm 85
3.1 A numerical example 87
3.2 How to proper dimension matrices 93
3.3 Petrov-Galerkin algorithm's limitations 96
4 Conclusion 97

1 Proper Generalized Decomposition and VTCR: a ROM technique to perform efficient frequency band calculations

The basic idea of this thesis work is to combine the Variational Theory of Complex Rays, fully introduced in Chapter 2, with the Proper Generalized Decomposition, discussed in the previous chapter. VTCR is a very effective technique which lacks of an immediate way to keep into account frequency dependence and uncertainty parameters. On the other hand PGD showed excellent performances in reducing complex problem (see Chapter 4) and propagating uncertainty. In this chapter only the frequency reduction is considered. Let us take into account the VTCR solving problem on matrix form:

$$\mathbf{K}(\omega)\mathbf{X}(\omega) = \mathbf{F}(\omega) \tag{4.1}$$

The equation (4.1) is fully drawn in Chapter 2. Here $\mathbf{X}(\omega)$ is the unknown amplitude vector and ω the problem's frequency. It is useful to remind that:

$$p_e(\mathbf{x},\omega) \in S^e_{ad,0} \Leftrightarrow p_e(\mathbf{x},\omega) = \int_{\theta=0}^{2\pi} X_e(\theta,\omega) e^{i\mathbf{k}(\theta,\omega)\cdot\mathbf{x}} d\theta \tag{4.2}$$

with $S^e_{ad,0} = \left\{ p_e ; \Delta p_e + k^2 p_e = 0 \text{ over } \Omega_e \times I \right\}$. So if $\mathbf{X}(\omega)$ is known, the pressure field, solution of reference problem (1.1) is known. In formula (4.1) the complete frequency dependance is underlined. The main idea is to reconstruct amplitude $\mathbf{X}(\omega)$ over a frequency band $I =]\omega_0 - \frac{\Delta\omega}{2}; \omega_0 + \frac{\Delta\omega}{2}[$ in PGD form:

$$\mathbf{X}(\omega) \simeq \mathbf{X}_M(\omega) = \sum_{m=1}^{M} \mathbf{X}_m \lambda_m(\omega) \tag{4.3}$$

where $\mathbf{X}_m$ are constant vectors related to the wave propagation in all possible 2D directions, $\lambda_m(\omega)$ are frequency-dependent functions and M is the order of PGD decomposition. It's to underline that making an approximation on amplitudes means switch the problem from Helmotz equation solution space to another. This is of fundamental importance. Try to solve directly Helmotz equation by PGD brings to find frequency functions on its definition space. In this case frequency dependence, particularly in mid frequency, has a very irregular shape. As we stated in Chapter 4 PGD gives its best when fairly regular solution is to approximate. For this reason is strongly not recommended to do a direct approximation on Helmotz definition space. If so, building a good approximation could be more expensive than solve the direct problem. A switch of the problem to the VTCR amplitude approximation brings the regularity that PGD needs to give its best and allows the powerful reduction that will be explained in the following.

1.1 The reference problem and the choice of the approximation

In the following of the work the reference problem is the one posed in Chapter 1 Section 1. A more accurate analysis has to be done regarding the VTCR approximation choice.

In VTCR history (see Chapter 2) three different approximations of Herglotz wave amplitudes were proposed: rays, wave bands and Fourier. After some trials and errors and a theoretical study, Fourier approximation demonstrated not only to be the most performing one but also the more adapted to work in alliance with PGD. Let us see in details why:

- Fourier's approximation has shown the best performances in terms of convergency (see Chapter 2 Section 4.5).
- It's formulation allowed for the first time an extension to 3D problems (see Chapter 2 Section 4.7).
- Fourier's approximation has shown the best performances in terms of conditioning number (see Chapter 2 Section 4.5). The importance of this point for a non-Petrov-Galekin iterative PGD algorithm will be explained in the next sections.
- PGD algorithms requires a resizing of matrixes to a same size. Fourier expansion is based on nested function. This allows to resize matrices for every frequency without losing numerical stability. Further details on its practical implementation will be given in the following of the chapter (see section 3.2).
- Fourier approximation give a regularization opportunity for VTCR amplitude portrait (see [Kovalevsky, 2011]). In general VTCR solution, as well as other Trefttz methods, tends to explode when increasing the number of DoFs. Fourier approximation allows to control this unpleasant phenomena.

To ease the reading of the chapter, give a coherent notation and introduce frequency dependency, here are recalled the principal equations of Fourier approximation. A Fourier series expansion of the wave amplitudes $X_e(\theta,\omega))$ (see (4.2)) limited to the first $2N_e+1$ terms is taken into account:

$$X_e(\theta,\omega) = \sum_{n=-N_e}^{N_e} X_e^n(\omega)\mathrm{e}^{in\theta} \tag{4.4}$$

where N_e is sufficiently large to lead to a good approximate solution. In other words, the approximate solution consists in an expansion of p_e over a finite-dimension subspace of Ω_e generated by functions $\Phi_e^n(\mathbf{x},\omega)$:

$$p_e(\mathbf{x},\omega) \simeq \sum_{n=-N_e}^{N_e} X_e^n(\omega)\Phi_e^n(\mathbf{x},\omega) \tag{4.5}$$

where $\Phi_e^n(\mathbf{x},\omega) = \displaystyle\int_{\theta=0}^{2\pi} \mathrm{e}^{in\theta}\mathrm{e}^{i\mathbf{k}(\theta,\omega)\cdot\mathbf{x}}\mathrm{d}\theta$. A complete overview of Fourier approximation can be found in Chapter 2 Section 4.5 of this manuscript.

2 A simple algorithm to introduce PGD-VTCR

Coherently with what stated until now, the approximation of the amplitude is searched in PGD form as in (4.3). The simplest way to build this approximation is to minimize residue norm of the scalar product with a simple Galerkin approach. The residue R_M is defined as:

$$\mathbf{R}_M(\omega) = \mathbf{F}(\omega) - \mathbf{K}(\omega)\mathbf{X}_M(\omega) = \mathbf{F}(\omega) - \mathbf{K}(\omega)\left(\sum_{i=m}^{M} \mathbf{X}_m(\theta)\lambda_m(\omega)\right) \tag{4.6}$$

In order to minimize equation (4.6) with a Galerkin approach some characteristic of matrix $\mathbf{K}$ are required. The matrix should be symmetric and defined positive. Unluckily none of these properties are verified in VTCR. The simples way to obviate to this problem is to multiply the formulation by $\mathbf{K}^*$. In this way the resulting right side matrix $\mathbf{K}\mathbf{K}^*$ will respect required property. Is to remark that the product $\mathbf{K}\mathbf{K}^*$ could be very expensive from a numerical point of view. The equation 4.1 is so transformed:

$$\mathbf{K}^*\mathbf{K}(\omega)\mathbf{X}(\omega) = \mathbf{K}^*\mathbf{F}(\omega) \tag{4.7}$$

Consequently equation (4.6) becomes:

$$\int_{\omega_0-\Delta\omega}^{\omega_0+\Delta\omega} \| \mathbf{K}^*\mathbf{R}_M(\omega) - \mathbf{K}^*\mathbf{K}(\mathbf{X}_{M+1}(\theta)\lambda_{M+1}(\omega)) \|^2 \, \mathrm{d}\omega = \left(\| \mathbf{K}^*\mathbf{R}_M(\omega) - \mathbf{K}^*\mathbf{K}(\mathbf{X}_{M+1}(\theta)\lambda_{M+1}(\omega)) \|^2 \right)_\omega \tag{4.8}$$

In order to perform the scalar product a convenient $[\mathbf{K}^*\mathbf{K}]^{-1}$ matrix is chosen. From the minimization problem (4.8) two equations are drawn:

$$\lambda_{M+1}(\omega) = \frac{\Re(\mathbf{R}_M^*\mathbf{K}\mathbf{X}_{M+1})}{\mathbf{X}_{M+1}^*\mathbf{K}^*\mathbf{K}\mathbf{X}_{M+1}} \tag{4.9}$$

$$\mathbf{X}_{M+1} = \left(\int_{\omega_0-\frac{\Delta\omega}{2}}^{\omega_0+\frac{\Delta\omega}{2}} \lambda_{M+1}^*\mathbf{K}^*\mathbf{K}\lambda_{M+1}\mathrm{d}\omega \right)^{-1} \left(\int_{\omega_0-\Delta\omega}^{\omega_0+\Delta\omega} \lambda_{M+1}^*\mathbf{K}^*\mathbf{R}_M\mathrm{d}\omega \right) \tag{4.10}$$

Equations (4.9) and (4.10) are interdependent one to the other. For this reason an iterative process is needed to find every couple.

Algorithm 1: Galerkin approach PGD for brad band problems

Initialization of $\mathbf{R}_0 = \mathbf{F}$;
for $m = 1$ *to* M **do**
  Initialization of λ_m^0;
  for $k = 1$ *to* k_{max} **do**
    Compute:
    $\mathbf{X}_m^{k-1} = \mathcal{F}(\lambda_m^{k-1}) \rightarrow (4.10)$;
    Normalize $\mathbf{X}_m^{k-1}$;
    $\lambda_m^k = \mathcal{F}(\mathbf{X}_m^{k-1}) \rightarrow (4.9)$;
    Stationarity check $(\mathbf{X}_m^k, \lambda_m^k)$;
  Update of $\mathbf{R}_{m+1} = \mathbf{R}_m - \mathbf{K}\mathbf{X}_m\lambda_m^k$;
  Convergency check;

where $\mathcal{F}()$ represent a generic functional operator. It's to remark that any initialization would leads to convergency but, an initialization choice somehow linked to the problem could leads to a sensible faster convergency.

2.1 A numerical example

Let's consider the simple numerical example in Figure 4.1 on a frequency band $\omega \in [\omega_0 - \frac{\Delta\omega}{2}, \omega_0 + \frac{\Delta\omega}{2}]$.

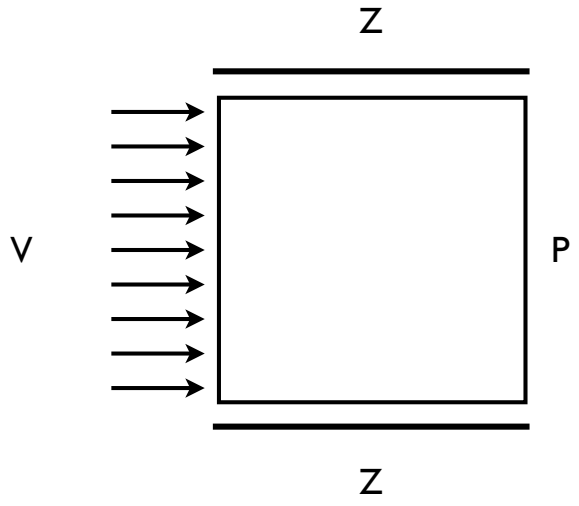

Figure 4.1: Square cavity under different boundary conditions

The domain in a square cavity where $\rho_0 = 1.25\ [kg/m^3]$, $c_0 = 340\ [m/s]$, $V = 1\ [m/s]$, $P = 0\ [Pa]$, $Z = 2000(1+i)\ [Pa \cdot s/m]$, $\omega_0 = 2\pi 1900\ [Hz]$, $\Delta\omega = 2\pi 200\ [Hz]$. The procedure used to built the approximation on this example is described in Algorithm 2:

Algorithm 2: Approximation building algorithm

for $j = 1$ *to "frequency test point number"* **do**
  Find $\mathbf{K}_j = \mathbf{K}(\omega_j)$;
  Find $\mathbf{F}_j = \mathbf{F}(\omega_j)$;
Apply algorithm 1 $\leftarrow (\{\mathbf{K}\}_j, \{\mathbf{F}\}_j)$;
  $\hookrightarrow$ PGD modes $\{(\mathbf{X}(\theta), \lambda(\omega))\}_m$

For this problem a PGD approximation with 40 modes has been constructed. A frequency discretization every 5 Hz has been chosen. In Figure 4.2 an energy comparison between a VTCR reference, calculated with a very fine frequency discretization, and the approximation is made. Good results in term of energy are confirmed by a compared pressure

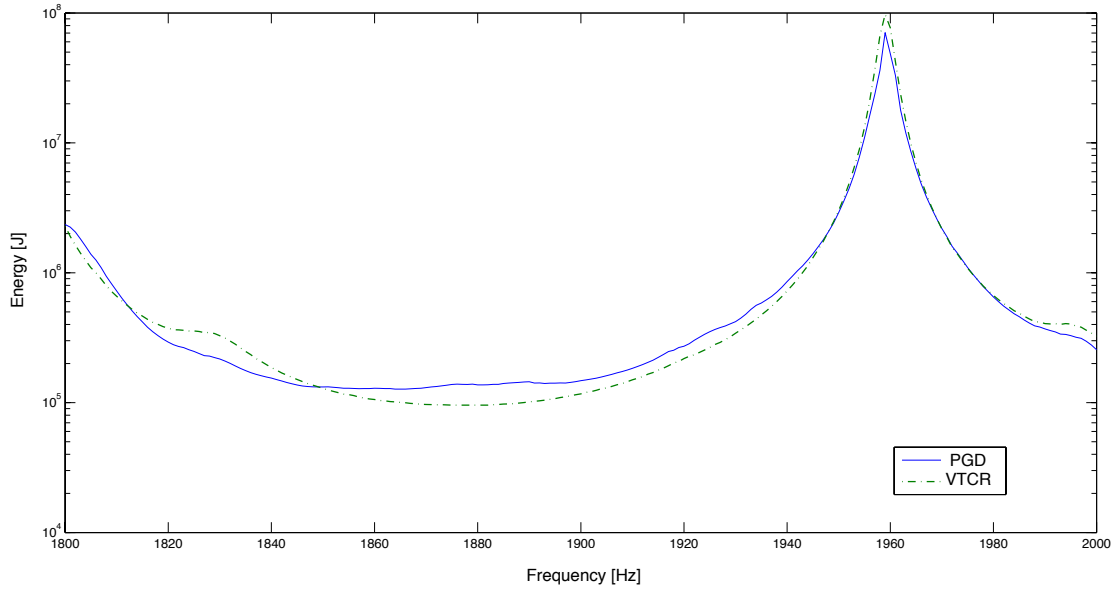

Figure 4.2: PGD with 40 modes vs. Regular VTCR

field plot in Figure 4.3. It is evident the high quality of PGD approximation, only few negligible errors can be identified in respecting pressure and velocity boundary condition. Of course some deeper analysis on this example are possible. Nevertheless, as we can see in Figure 4.2, this example concerns a very narrow frequency band and the frequency behavior is too simple to be considered as mid-frequency. For this reasons further analyses are reserved to a more complex case.

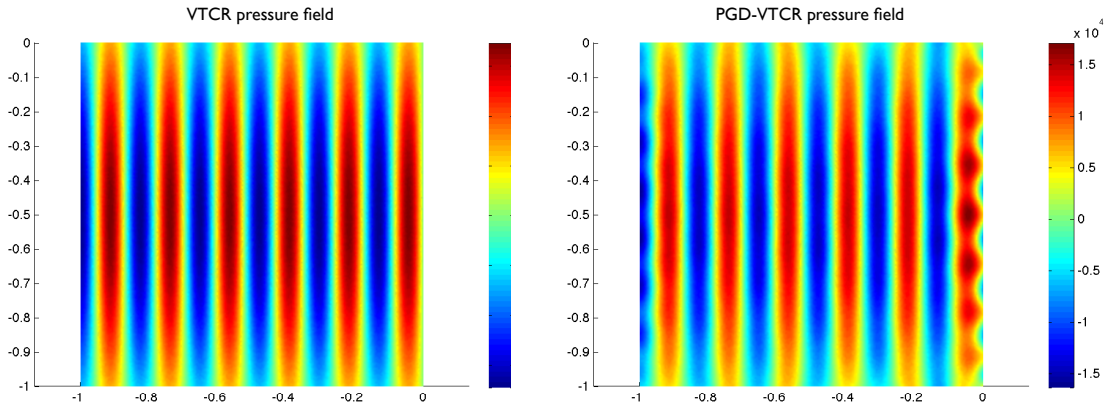

Figure 4.3: VTCR reference real pressure field (left) compared to PGD real pressure field (right) at resonance frequency $\omega = 2\pi 1959[Hz]$

2.2 A surprising numerical problem

To increase the complexity level of the problem a more challenging example is provided in Figure 4.4.

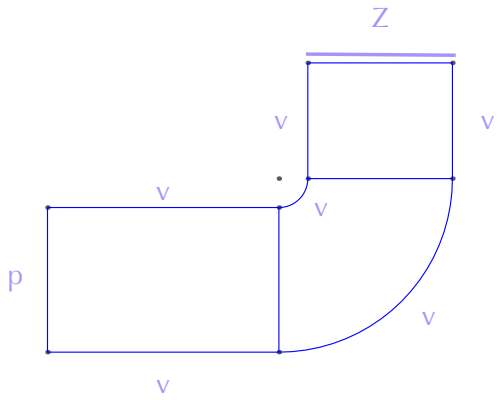

Figure 4.4: L-shaped cavity

The cavity is filled with a fluid with air $\rho_0 = 1.25\ [kg/m^3]$, $c_0 = 340\ [m/s]$ and with $V = 1\ [m/s]$, $P = 0\ [Pa]$, $Z = 850 + 50i\ [Pa \cdot s/m]$, $\omega_0 = 2\pi 1900\ [Hz]$, $\Delta\omega = 2\pi 200\ [Hz]$. This example is more challenging to VTCR. It presents a subdivision in subdomains. On this example the Algorithm 2 is used as on the previous example. Surprisingly, the good results obtained for the geometry in Figure 4.1 were not confirmed. This is evident in Figure 4.5. Pressure field is completely inconsistent with the reference solution which means that the PGD approximation is ineffective on this example. With the aim of better understanding the phenomena, let us come back to the example in Figure 4.1. This time a

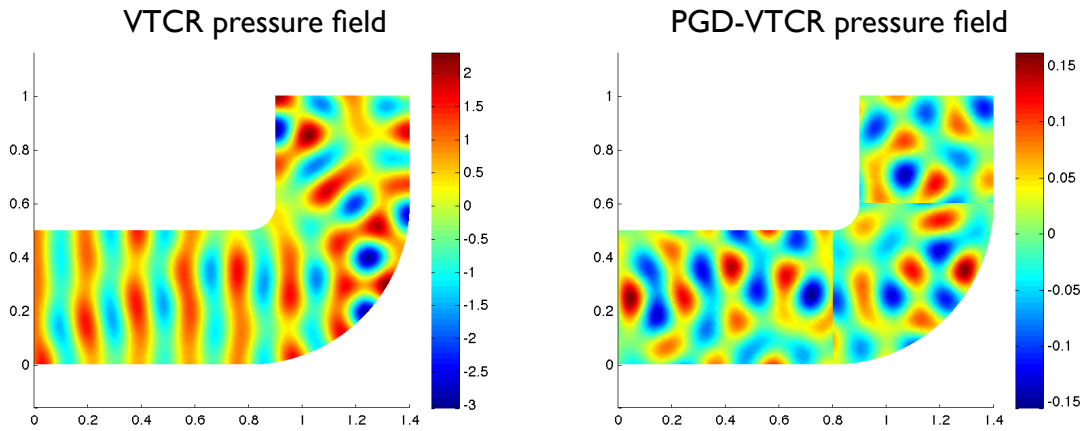

Figure 4.5: VTCR reference real pressure field (left) compared to PGD real pressure field (right) at $\omega = 2\pi 1900[Hz]$

sub-discretization is introduced as in Figure 4.6. Sub-discretization do not bring any loss

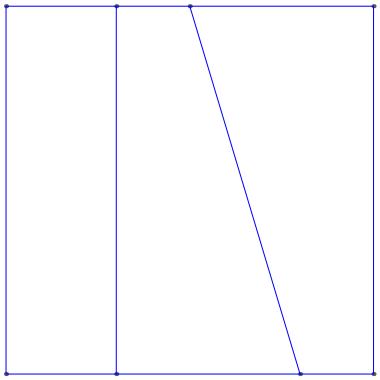

Figure 4.6: Sub-discretized square cavity

of informations so the expected results are of the same kind of Figure 4.3. Nevertheless, when PGD approximation is performed, pressure field appears discontinuous and wrong in terms of pressure level (see Figure 4.7) in complete disagree with the result in Figure 4.3. The only difference between examples in Figures 4.3 and 4.7 lies in the introduction of two interfaces. This do not increases complexity of the problem (which is, from a physical point of view, exactly equivalent) but increases numerical complexity of matrix $\mathbf{K}$. From this consideration arises the intuition of analyze numerical properties of matrix $\mathbf{K}$ in order to find the problem. In Figure 4.8 is shown the comparison between the eigenvalue of $\mathbf{K}^*\mathbf{K}$ for the sub-discretized problem (in blue) and the the non sub-discretized one (in red) This astonishing result brings to one conclusion; the quality of $\mathbf{K}$ tends to drop increasing its complexity and dimension. It is enough to add some interfaces to

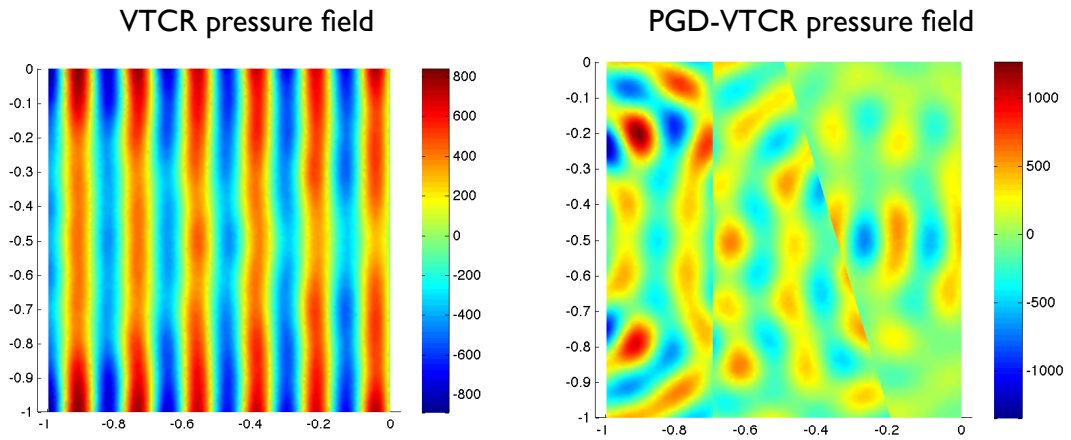

Figure 4.7: VTCR reference real pressure field (left) compared to PGD real pressure field (right) for a sub-discretized square cavity

dramatically bring into the matrix a lot of numerical pollution (of course linked to bad condition number) which explodes when the operation of symmetrization is performed by multiplying for $\mathbf{K}^*$.

This surprising discover obliges to overcome standard Galerkin approach with something different. Two different paths were explored. As a first step a different type of algorithm directly taking into account non-symmetry and robust to ill-conditioning was introduced. This algorithm, based on a Petrov-Galerkin technique, is introduced in the next section. The other way is to work on a dedicated pre-conditioner to improve quality of matrix $\mathbf{K}$ and after put in place some more sophisticated algorithm to avoid performing $\mathbf{K}^*\mathbf{K}$ product. These numerical difficulties makes PGD-VTCR, not only an interesting strategy for mid-frequency, but a hard benchmark for PGD itself. In its young history the technique is for the first time used to solve such a complex numerical problem.

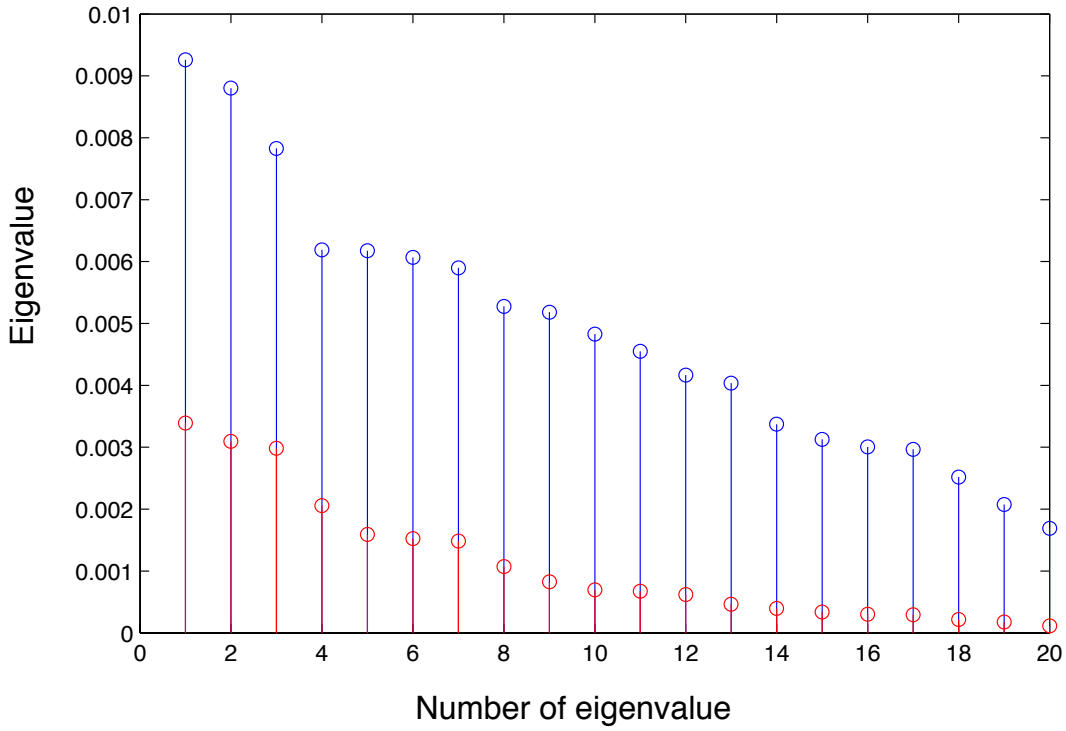

Figure 4.8: Comparison between first eigenvalues of $\mathbf{K}^*\mathbf{K}$ for the sub-discretized problem (in blue) and the the non sub-discretized one (in red), as we can see eigenvalues are completely difference in the two cases.

3 A Petrov-Galerkin algorithm

Due to previous considerations, a natural choice to overcome Galerkin algorithm limitation is a Petrov-Galerkin algorithm. This algorithm was proposed for PGD application in [Nouy, 2010] and its application to linear acoustic in [Barbarulo et al., 2012] (from which this section is mostly withdrawn). Petrov-Galerkin algorithm is capable to deal with non symmetrical problems and, moreover, is constitutionally robust when ill-conditioning is present.

The Petrov-Galerkin-based PGD algorithm requires the definition of the variational formulation of the problem being considered. In our case, (4.1) can be expressed as: find $\mathbf{X}(\omega)$ such that

$$\mathcal{K}(\mathbf{X},\mathbf{Y}) = \mathcal{F}(\mathbf{Y}) \quad \forall \mathbf{Y} \in C^N \tag{4.11}$$

where $\mathcal{K}(\mathbf{X},\mathbf{Y}) = \int_{\omega_0-\frac{\Delta\omega}{2}}^{\omega_0+\frac{\Delta\omega}{2}} \mathbf{Y}^*(\omega)\mathbf{K}(\omega)\mathbf{X}(\omega)\mathrm{d}\omega$ and $\mathcal{F}(\mathbf{Y}) = \int_{\omega_0-\frac{\Delta\omega}{2}}^{\omega_0+\frac{\Delta\omega}{2}} \mathbf{Y}^*(\omega)\mathbf{F}(\omega)\mathrm{d}\omega$. C is the complex conjugate adjoint space and N depends on the approximation space chosen for the functions of the Fourier series. In order to develop the algorithm, let us assume that the pairs $\{(\mathbf{X}_m,\lambda_m)\}_{m=1\ldots M-1}$ are known from the previous iteration and that we are now

seeking the enrichment pair $(\mathbf{X}_M, \lambda_M)$. The method for calculating these terms consists in using the following two orthogonality criteria:

$$\mathcal{K}(\mathbf{X}_{M-1} + \mathbf{X}_M\lambda_M, \mathbf{Y}\gamma) = \mathcal{F}(\mathbf{Y}\gamma) \quad \forall \mathbf{Y} \in C^N \tag{4.12}$$

$$\mathcal{K}(\mathbf{X}_{M-1} + \mathbf{X}_M\lambda_M, \mathbf{Y}\gamma) = \mathcal{F}(\mathbf{Y}\gamma) \quad \forall \gamma \in X \tag{4.13}$$

where $(\mathbf{Y}, \gamma)$ is another pair of a constant vector and a frequency-dependent function. Of course, additional equations must be added to (4.12) and (4.13) in order to define functions $(\mathbf{Y}, \gamma)$. We use the following equations:

$$\mathcal{K}(\mathbf{X}'\lambda_M, \mathbf{Y}\gamma) = << \mathbf{X}'\lambda_M, \mathbf{X}_M\lambda_M >> \quad \forall \mathbf{X}' \in C^N \tag{4.14}$$

$$\mathcal{K}(\mathbf{X}_M\lambda', \mathbf{Y}\gamma) = << \mathbf{X}_M\lambda', \mathbf{X}_M\lambda_M >> \quad \forall \lambda' \in Y \tag{4.15}$$

$<< ., . >>$ denotes the inner product defined by
$<< \mathbf{X}\lambda, \mathbf{Y}\gamma >> = \int_{\omega_0 - \frac{\Delta\omega}{2}a}^{\omega_0 + \frac{\Delta\omega}{2}} \gamma^*(\omega)\mathbf{Y}^*\mathbf{H}(\omega)\mathbf{X}\lambda(\omega)\mathrm{d}\omega$, with $\mathbf{H}(\omega) = \tilde{\mathbf{H}}\tilde{h}(\omega)$, $\tilde{\mathbf{H}}$ being the mean value of matrix $\mathbf{K}(\omega)$ over the frequency band of the diagonal. $\tilde{h}(\omega)$ is the frequency-dependent function which corresponds to the mean value of the coefficients of the diagonal of $\mathbf{K}(\omega)$. With that particular choice, the following separation property holds:

$$<< \mathbf{X}\lambda(\omega), \mathbf{Y}\gamma(\omega) >> = \left(\mathbf{X}^*\tilde{\mathbf{H}}\mathbf{Y}\right) \int_{\omega_0 - \frac{\Delta\omega}{2}}^{\omega_0 + \frac{\Delta\omega}{2}} \lambda(\omega)\tilde{h}(\omega)\gamma(\omega)\mathrm{d}\omega \tag{4.16}$$

This accelerates the calculations because the mathematical algorithm is specific to the initial physical problem. Then, the idea of the algorithm is to derive the pairs $(\mathbf{X}_M, \lambda_M)$ and $(\mathbf{Y}_M, \gamma_M)$ which verify Equations (4.12), (4.13), (4.14) and (4.15) simultaneously. In order to do that, one must solve these equations many times until convergence, *i.e.* until each function has reached a fixed value. If $(\mathbf{X}_M^{(q)}, \lambda_M^{(q)})$ denotes the pair $(\mathbf{X}_M, \lambda_M)$ calculated at the current iteration with the exponent (q-1) from the previous iteration, we use the following stopping criterion:

$$\int_{\omega_0 - \frac{\Delta\omega}{2}}^{\omega_0 + \frac{\Delta\omega}{2}} \overline{\left(\mathbf{X}_M^{(q)}\lambda_M^{(q)}(\omega) - \mathbf{X}_M^{(q-1)}\lambda_M^{(q-1)}(\omega)\right)^*} \left(\mathbf{X}_M^{(q)}\lambda_M^{(q)}(\omega) - \mathbf{X}_M^{(q-1)}\lambda_M^{(q-1)}(\omega)\right) \mathrm{d}\omega < \delta_q \tag{4.17}$$

where δ_q is related to the accuracy of this power-type iteration procedure.

After $(\mathbf{X}_M, \lambda_M(\omega))$ has converged, the procedure must be repeated until the convergence of the global enrichment procedure $\mathbf{X}(\omega) \simeq \mathbf{X}^M(\omega) = \sum_{m=1}^{M} \mathbf{X}_m\lambda_m(\omega)$. In our numerical applications, the stopping criterion was:

$$\varepsilon_M(\mathbf{X}^M) = \frac{\int_{\omega_0 - \frac{\Delta\omega}{2}}^{\omega_0 + \frac{\Delta\omega}{2}} \overline{\left(\mathbf{K}(\omega)\mathbf{X}^M(\omega) - \mathbf{F}(\omega)\right)^*} \left(\mathbf{K}(\omega)\mathbf{X}^M(\omega) - \mathbf{F}(\omega)\right) \mathrm{d}\omega}{\int_{\omega_0 - \frac{\Delta\omega}{2}}^{\omega_0 + \frac{\Delta\omega}{2}} \overline{\mathbf{F}(\omega)^*}\mathbf{F}(\omega)\mathrm{d}\omega} < \delta_M \tag{4.18}$$

where δ_M is related to the accuracy of the PGD separated representation of the solution of Problem (4.1). Therefore, we introduce the iterative algorithm described in Algorithm 3:

Algorithm 3: Petrov-Galerkin approach PGD for brad band problems

Initialization of $\mathbf{R}_0 = \mathbf{F}$;
for $m = 1$ *to* m_{max} **do**
  Initialization of λ and γ;
  for $q = 1$ *to* q_{max} **do**
    Compute:
    $\mathbf{X}_m^{(q)}$ using (4.12) and $\mathbf{Y}_m^{(q)}$ using (4.14);
    Normalize $\mathbf{X}_m^{(q)}$ and $\mathbf{Y}_m^{(q)}$;
    Compute $\lambda_m^{(q)}$ using (4.13) and $\gamma_m^{(q)}$ using (4.15);
    if *convergence (4.17)* **then**
      break
  Set $\mathbf{X}_m(\omega) = \mathbf{X}_{m-1}(\omega) + \mathbf{X}_M^{(q_{\max})}\lambda_M^{(q_{\max})}(\omega)$;
  if *convergence (4.18)* **then**
    break

It is important to note again that several consistent initialization choices can lead to convergence, but a proper choice could make the convergence faster. This is why it is recommended to choose an initialization which is somewhat related to the problem. In the present work, we used:

$$\lambda(\omega) = \gamma(\omega) = \sqrt{\overline{(\mathbf{K}(\omega)\mathbf{X}^{m-1}(\omega) - \mathbf{F}(\omega))}^{*} (\mathbf{K}(\omega)\mathbf{X}^{m-1}(\omega) - \mathbf{F}(\omega))} \tag{4.19}$$

The most time-consuming part of the method is the resolution of (4.12) and (4.14), which are matrix problems. (4.13) and (4.15) are scalar equations and can be solved easily and inexpensively. Thus, the proposed strategy requires the resolution of only $2 \times M \times Q$ matrix problems (M being the number of functional pairs and Q the total number of internal power-type iterations required to obtain an approximate solution to the desired accuracy levels δ_q and δ_M). In comparison, a standard incremental strategy which calculates the solution one frequency at a time requires the resolution of N_I matrix problems (N_I being the number of frequencies considered for I), which, depending on the accuracy, can be extremely costly, especially in the medium-frequency range where the response is very sensitive to the data and requires a very refined frequency discretization.

3.1 A numerical example

In order to test the efficiency of Algorithm (3), we studied an L-shaped acoustic cavity (see Figure 4.9) filled with a fluid ($\rho_0 = 1.25\ [kg/m]^3$, $c_0 = 340\ [m/s]$, $\eta = 0.0005$) and subjected to boundary conditions in the form of a pressure $P = 0\ [Pa]$ and a velocity $V = 1\ [m/s]$. Three bandwidths ($\Delta\omega_1 = 2\pi 100\ [Hz]$, $\Delta\omega_2 = 2\pi 200\ [Hz]$ $\Delta\omega_3 = 2\pi 400\ [Hz]$)

around the same central frequency $\omega_0 = 2\pi 1,200\ [Hz]$ were considered. This example is complex enough in terms of both the shape of the domain and the boundary conditions to be viewed as a benchmark.

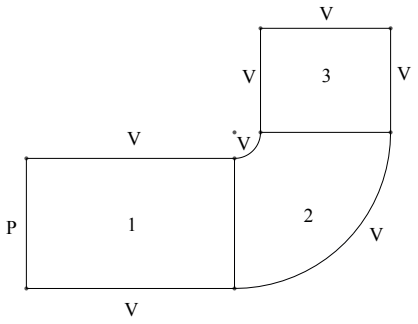

Figure 4.9: L-shaped acoustic cavity (with a prescribed pressure $P = 0\ [Pa]$ and a prescribed velocity $V = 1\ [m/s]$) to test the efficiency of Algorithm (3)

This problem was solved using the VTCR in its Fourier version as presented in Chapter 2. In order to do that, domain Ω was divided into 3 subdomains (see Figure 4.9). Seventy shape functions (4.5) were used in each subdomain. The reference solutions for the three frequency bands considered were obtained with the VTCR using these parameters along with a very refined frequency discretization. These results were chosen as the reference solution because the VTCR is known to be an efficient method for acoustic problems (see [Riou et al., 2008] and [Kovalevsky et al., 2012a]). Besides, since our objective is to test the efficiency of Algorithm (3), which is based on the VTCR formulation (4.1), the introduction of another reference solution would have led to uncontrolled errors related to the comparison with another numerical method, a question whose discussion is outside of the scope of this example.

The iterative search for each pair of functions (X_m, λ_m) in Algorithm (3) is controlled by two parameters: δ_q, the stopping criterion (4.17), and $q_{\max}$, the maximum number of iterations. Figures 4.10, 4.11 and 4.12 show the error $\varepsilon(\mathbf{X}^M)$ (4.18) as a function of the number of pairs of the decomposition for different values of these parameters and for the three frequency bands $\Delta\omega_1 = 2\pi 100\ [Hz]$, $\Delta\omega_2 = 2\pi 200\ [Hz]$ and $\Delta\omega_3 = 2\pi 400\ [Hz]$.

The figures on the left show that a proper criterion ($\delta_q = 0.0001$) suffices to guarantee a satisfactory convergence rate. The figures on the right show that choosing a proper $q_{\max}$ also leads to convergence. This suggests that one should choose a relatively small $q_{\max}$ and stop the iterations even if the convergence criterion (4.17) has not been entirely satisfied. Evidence of the effectiveness of this strategy is shown in Figure 4.13.

Figure 4.13 shows a convergence comparison for the most severe case $\Delta\omega_3 = 2\pi 400$ Hz between an algorithm stopped at a chosen value of the convergence criterion ($\delta_q = 0.0001$ with $q_{\max} = \infty$) and the same algorithm stopped after a small specified number of iterations ($q_{\max} = 8$ with $\delta_q = 0$). The convergence achieved with the two calculations was very similar. It took the algorithm 30 iterations to reach the required convergence criterion ($\delta_q = 0.0001$). This was necessary to guarantee the convergence of the pairs, but

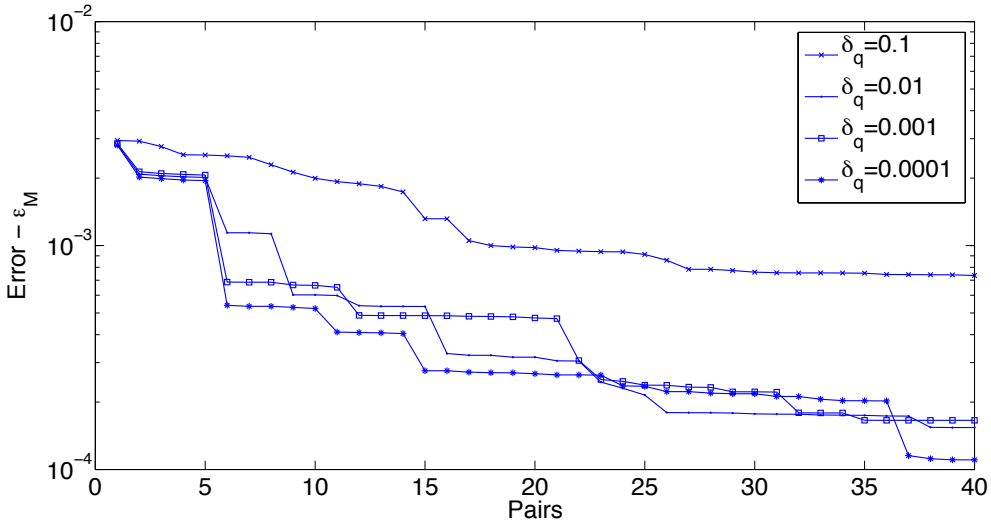

(a)

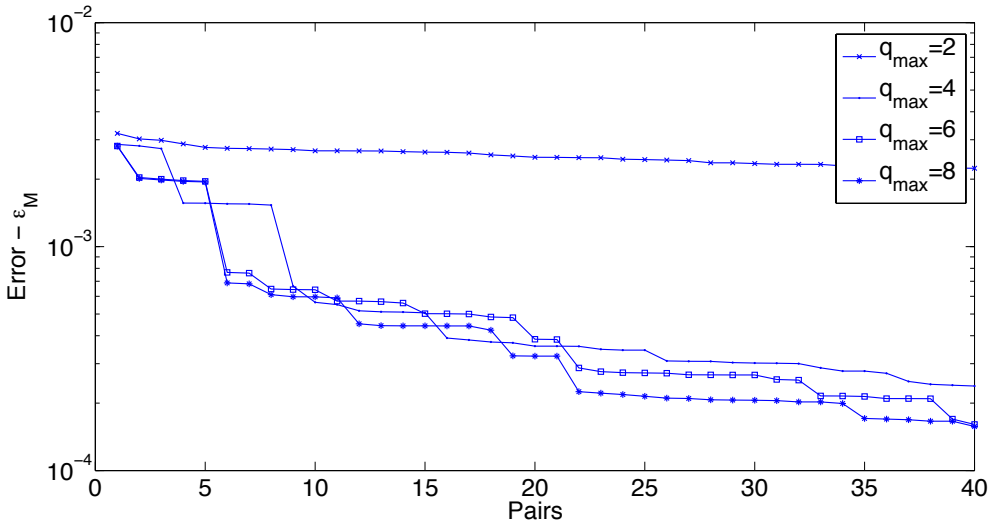

(b)

Figure 4.10: The relative error $\varepsilon(\mathbf{X}^M)$ (4.18) for different δ_q with $q_{\max} = \infty$ (a) and for different $q_{\max}$ with $\delta_q = 0$ (b). $\Delta\omega_1 = 2\pi 100\ [Hz]$.

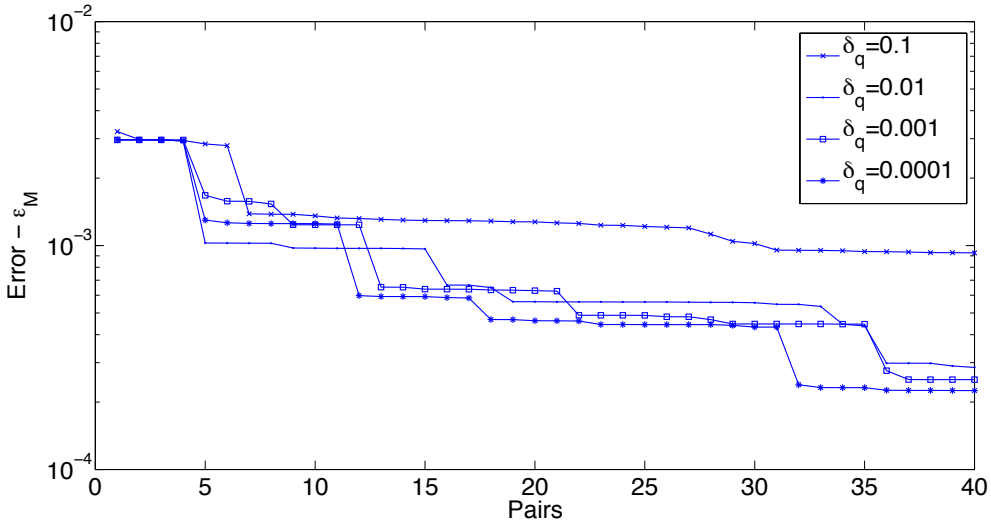

(a)

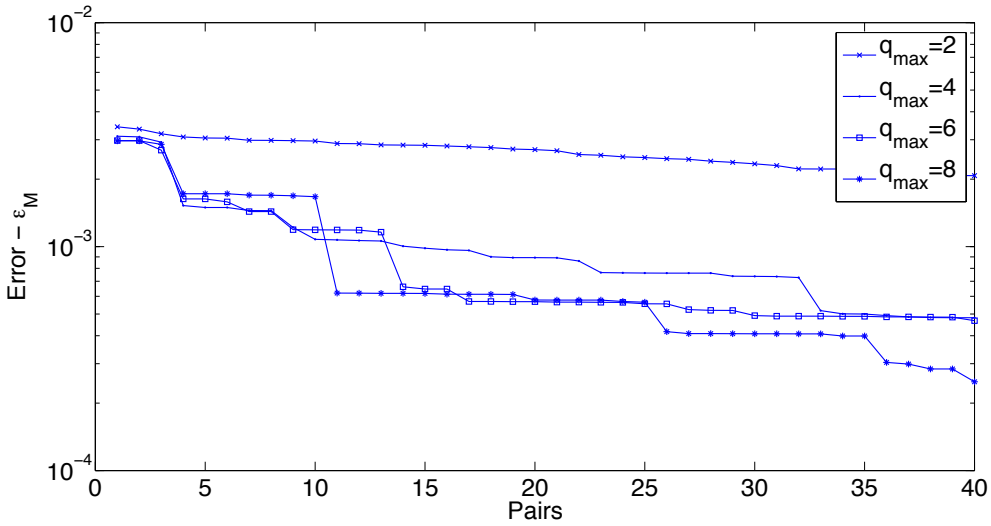

(b)

Figure 4.11: The relative error $\varepsilon(\mathbf{X}^M)$ (4.18) for different δ_q with $q_{\max} = \infty$ (a) and for different $q_{\max}$ with $\delta_q = 0$ (b). $\Delta\omega_2 = 2\pi 200\ [Hz]$.

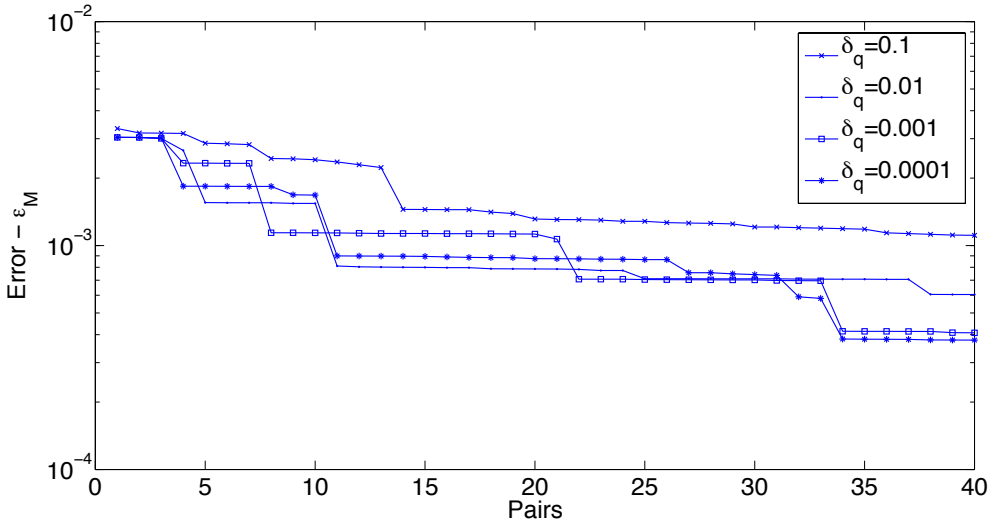

(a)

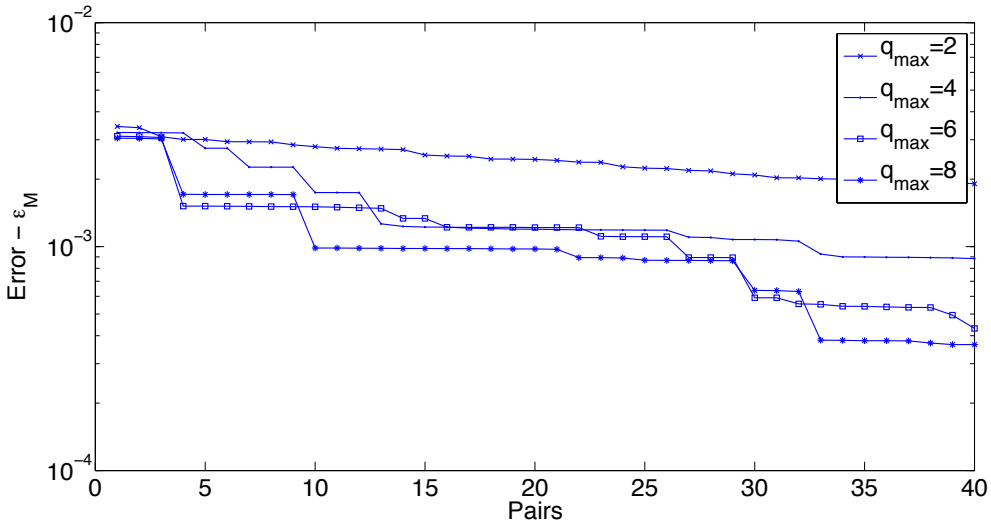

(b)

Figure 4.12: The relative error $\varepsilon(\mathbf{X}^M)$ (4.18) for different δ_q with $q_{\max} = \infty$ (a) and for different $q_{\max}$ with $\delta_q = 0$ (b). $\Delta\omega_3 = 2\pi 400\ [Hz]$.

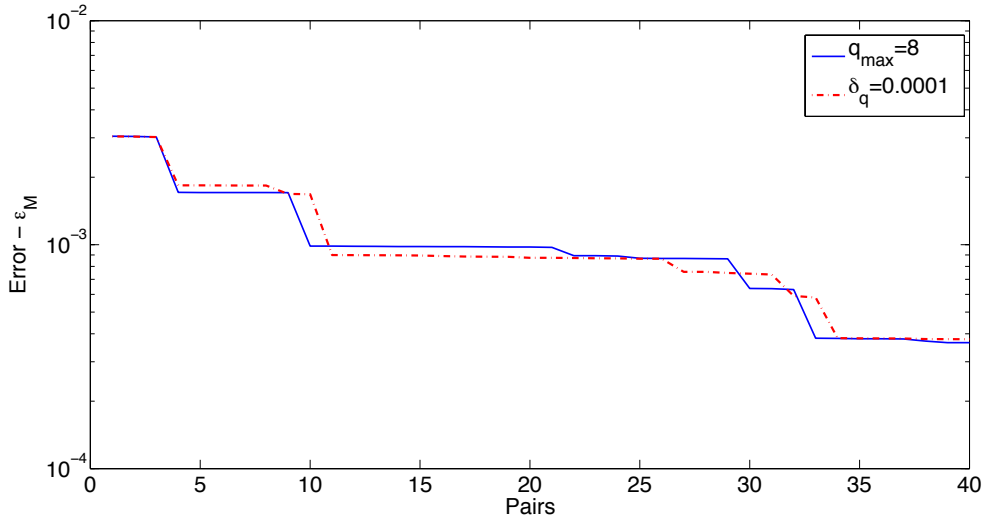

Figure 4.13: The relative error $\varepsilon(\mathbf{X}^M)$ (4.18) for $\delta_q = 0.0001$ and $q_{\max} = 8$. $\Delta\omega_1 = 2\pi 400$ $[Hz]$.

had no decisive influence on the relative error $\varepsilon(\mathbf{X}^M)$ (4.18). Conversely, setting a small number of iterations ($q_{\max} = 8$) precluded full convergence of the pairs, but still gave a satisfactory relative error $\varepsilon(\mathbf{X}^M)$ (4.18). Therefore, it is computationally more efficient not to seek full convergence, but to stop the iterations after a smaller number of iterations $q_{\max}$, thus saving on the number of iterations for each pair and, consequently, on the overall computation time.

Figure 4.14 shows, for the most computationally intensive frequency band ($\Delta\omega_3 = 2\pi 400$ Hz), a comparison of the frequency response functions obtained with our different approximations of the reference problem for various expansion orders M. The PGD solution was calculated with a coarse frequency discretization (one test point every 3 Hz). These frequency response functions represent the global energy of the structure. As one can see, for the frequency band considered, Approximation (4.3) reproduces the reference solution very well. Of course, the quality of the approximation is less good for M small (although the general trend of the reference FRF is respected), but becomes better when M increases. This confirms what could be anticipated from Figure 4.13. Only 15 PGD pairs are needed to represent the global energy completely throughout the band.

Figure 4.15 shows the approximate solution of the problem for $\omega = \omega_0 - \dfrac{\Delta\omega_3}{2}$, $\omega = \omega_0$ and $\omega = \omega_0 + \dfrac{\Delta\omega_3}{2}$ in the case of frequency band $\Delta\omega_3 = 2\pi 400$. The reference solution is also shown on the figure. All the solutions are very similar, which proves the effectiveness of the proposed algorithm.

Figures 4.13, 4.14 and 4.15 clearly illustrate the effectiveness of Algorithm (3), which manages to recover the reference solution over a very large frequency band with only a few terms in Representation (4.3). These figures show that, overall, the proposed method

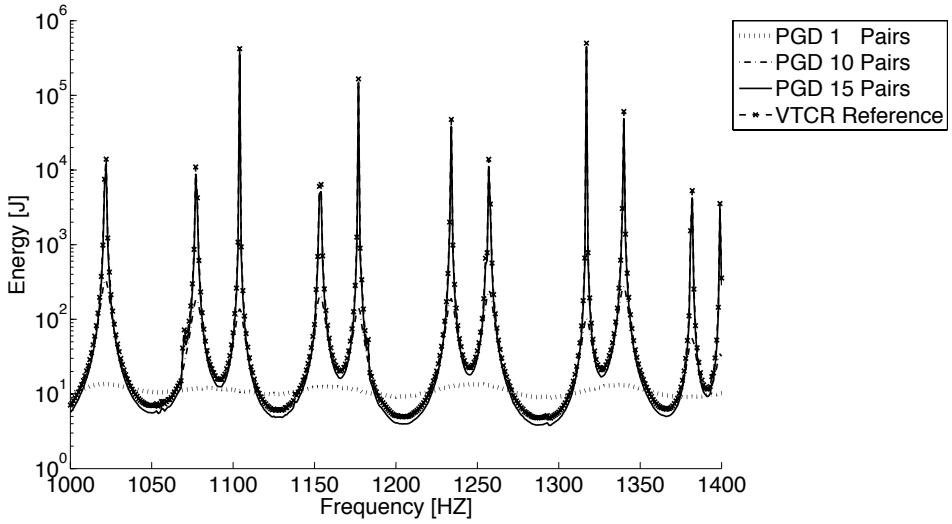

Figure 4.14: The frequency response functions of the various approximations of the reference problem for different expansion orders M

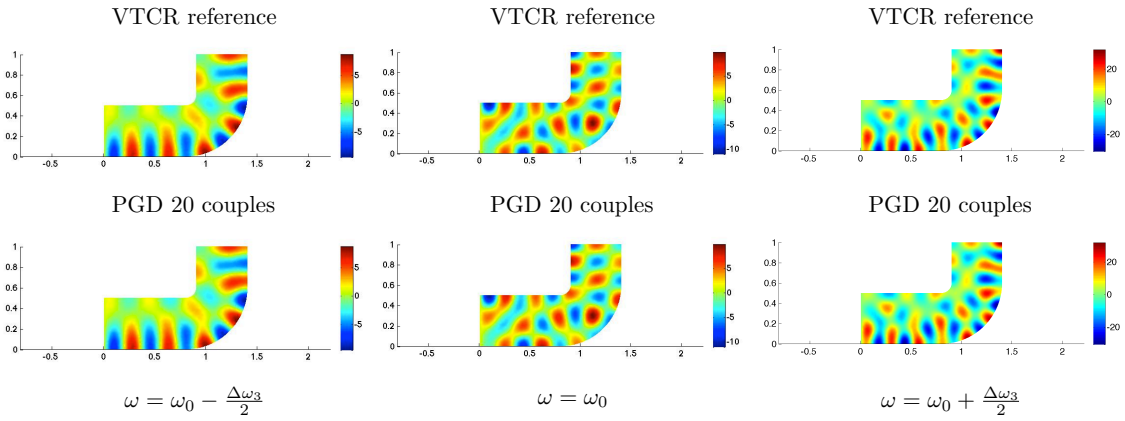

Figure 4.15: Comparison of the approximate and reference real pressure fields for $\omega = \omega_0 - \dfrac{\Delta\omega_3}{2}$, $\omega = \omega_0$ and $\omega = \omega_0 + \dfrac{\Delta\omega_3}{2}$

outperforms the previous strategies developed for broadband calculation [Ladevèze et al., 2003b], [Ladevèze and Riou, 2005].

3.2 How to proper dimension matrices

A non trivial point has been unsaid until now. As stated before **K** is frequency dependent. What is to remark is that not only its coefficients varies with the frequency but in order to respect criteria in Chapter 2 Section 4.6 its size also increases as in Figure 4.16.

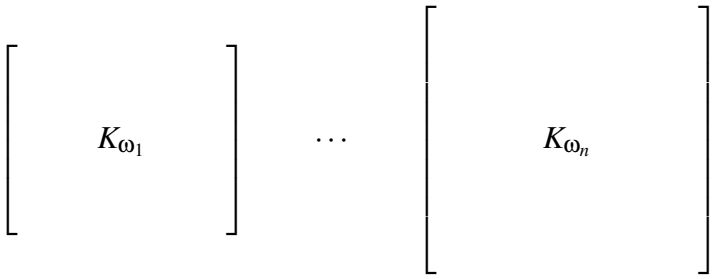

Figure 4.16: K size increasing with frequency

This is not compatible with PGD. Indeed the algorithm needs to process all matrices of the same size. The idea is to size every matrix on the maximum number of DoFs. If a Fourier approximation is considered, it is extremely easy to resize smaller matrices to the maximal size one. Due to the nested function property is enough to add some *virtual DoFs* by adding some zero energy contribution functions to the approximation. The resizing is explained in Figure 4.17. Here is shown how to resize the first subdomain for a three subcavity domain (as in Figure 4.9). Of course for other subdomains the process is identical. This expansion is very simple if Fourier series are taken into account. This property gives

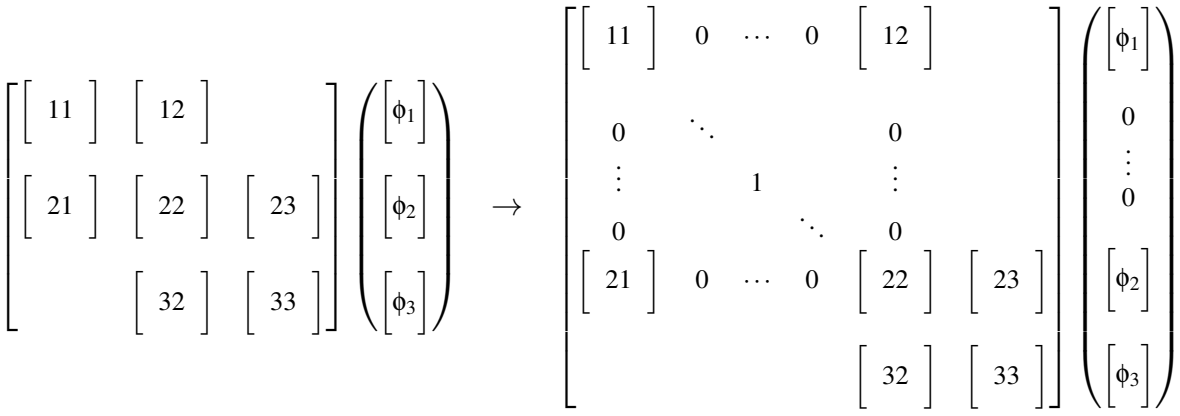

Figure 4.17: K resizing according to ϕ bases

a decide advantages to Fourier approach over other approaches. As stated before this expansion do not change matrix properties. If this expansion is not performed we can choose between two other strategies. The first possibility is to fix the maximal **K** size for higher frequency and compute VTCR solutions at lower frequency with the maximal number of DoFs. This approach will guarantee convergency on the upper side of the band. On the other side matrix condition number and matrix properties will be very bad at lower frequency. This effect could be seen for the geometry in Figure 4.18 where $\rho_0 = 1.25$ $[kg/m^3]$, $c_0 = 340$ $[m/s]$, $V = 1$ $[m/s]$, $P = 0$ $[Pa]$, $Z = 850 + 50i$ $[Pa \cdot s/m]$, $\omega_0 = 2\pi 1200$

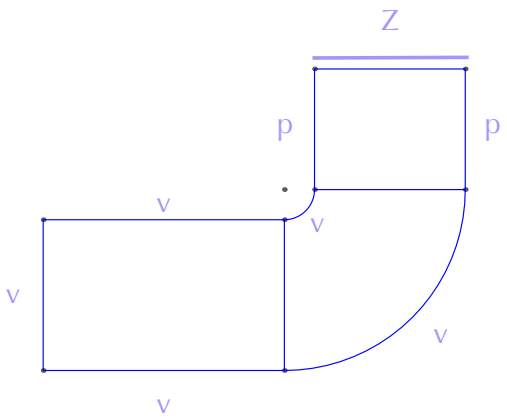

Figure 4.18: L-shaped acoustic cavity to test sizing effect

$[Hz]$, $\Delta\omega = 2\pi 200\ [Hz]$. The effect of this strategy is shown in Figure 4.19. As foreseen

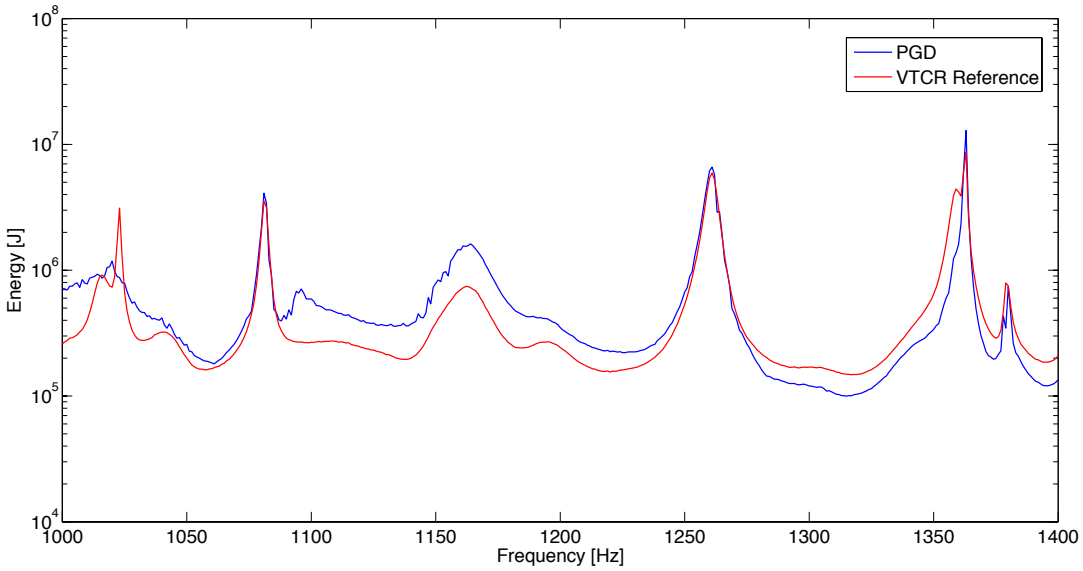

Figure 4.19: Energy response for non-expanded matrices

the quality of the prediction is very high for higher frequency, while bad numeric ruins the lower frequency response prediction. Of course it is possible to choose the opposite strategy and size everything to the lower frequency and than compute VTCR solution with this number of DoFs. In this case bad numerical properties are not a problem but VTCR solution will not reach convergency. An explanation to this phenomena is given in Chapter 2 and an example of not converged solution can be found in Figure 4.20. For these reasons a Fourier approximation is to prescribe to avoid numerical problem related

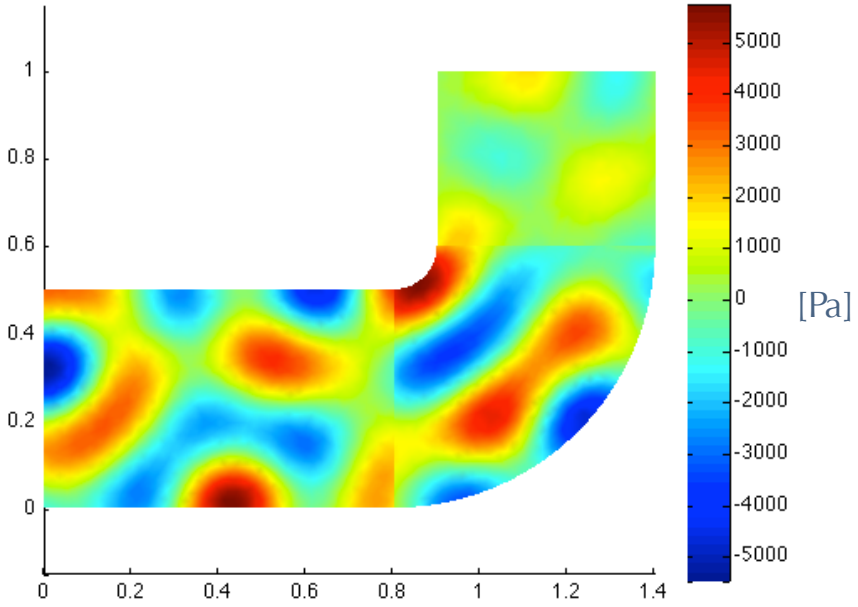

Figure 4.20: Not converged real pressure field for $\omega = 2\pi 1200\ [Hz]$

to a brute force sizing criteria.

3.3 Petrov-Galerkin algorithm's limitations

As shown in Section 3.1 Petrov-Galerkin approach is effective and reliable. Its robustness and its way to deal with non-symmetrical problems make this algorithm, as a first glance, the perfect choice to combine PGD and VTCR. Nevertheless some consideration on Petrov-Galerkin approach's inborn characteristics can suggest some improvement in algorithm's choice. The first limitation of Petrov-Garelkin concerns the necessity of research an adjoint solution on an adjoint space (see Algorithm 3). For this reason in every PGD sub-iteration we are forced to compute an adjoint solution only to overcome the non-symmetry problem. This means that this algorithm costs, in term of sub-iterations, the double respect to a classic Galerkin. An other problem of the technique is evident from Figure 4.13. An unpleasant step convergent is present. The consequence of this convergency shape is that we are not able to catch immediately the optimal PGD modes, this effect has also been found in [Nouy, 2010]. Once again the formulation asks us to pay a computational cost for information of no direct utility. A last issue is about convergency properties. Petrov-Galerkin algorithm, in opposite to Galerkin one, do not guarantee any convergency. Of course the PGD algorithm inherits properties of the chosen approach so we can guarantee no convergence either. For these reasons Petrov-Galerkin based PGD is to consider as very good choice in dealing such kind of problems but the door is open to search for better solution. Next Chapter will be dedicated to research of improved algorithms.

4 Conclusion

In this Chapter the path that brought to a first time excellent performing PGD approximation over a frequency band has been described. In the beginning a very limited Galerkin approach has been proposed. Despite its significant limitations, it has conducted to an intensive study of the problem properties. Once the problem has been identified a Petrov-Galerkin approach has been proposed. Moreover an important numerical subtlety has been remarked to show how make a correct resizing and give an addition proof of Fourier approximation interest. Numerical results has been widely satisfactory but a series of performance considerations pushed the author to continue searching for other possible algorithms.

Chapter 5

A new class of algorithms

In this chapter a new strategy to couple PGD and VTCR will be proposed. In order to improve performances in terms of convergency and computational efficiency, a non Petrov-Galerkin strategy will be introduced. The base of this new class of algorithm is the introduction of a dedicated pre-conditioner. In this way the numerical problems explained previously are mostly solved and the choice of the most performing algorithm is easier. After the introduction of the pre-conditioner two new algorithms are introduced. Performances are studied on an academic test case.

Contents

1 A dedicated pre-conditioner for VTCR 100

2 An improved algorithm for PGD-VTCR 102

3 Minimal residue direction algorithm: the state of the art for PGD-VTCR on frequency bands 104

3.1 A numerical example 106

4 Conclusion 109

1 A dedicated pre-conditioner for VTCR

As discussed in Chapter 1 Section 4 all Trefftz methods suffer from ill-conditioning. VTCR, belonging in this category, is not an exception. An energy based pre-conditioner was introduced in [Kovalevsky, 2011]. This pre-conditioner is of simple implementation, fast to compute and introduces a strong regularization in amplitude portraits. On the other hand its effect on conditioning number is light.

When dealing with iterative solutions of ill-conditioned problems (as PGD does), the condition number plays a fundamental role. Despite the meagre literature on the subject an extensive analysis of the problem can be found in [Bayliss et al., 1983, Erlangga et al., 2004,Erlangga, 2008]. These articles show clearly the importance of conditioning number in iterative solving of Helmotz equations and propose the introduction of pre-conditioners as the only way to get efficient iterative solutions.

Starting from these considerations is here proposed a pre-conditioner particularly effective for VTCR. The aim is to improve enough the conditioning number to allows less robust algorithm (facing ill-conditioning) to properly work. To ease the choice of the right pre-conditioner a preliminary analysis of **K** shape can be useful. As we can remark

$$\begin{bmatrix} \begin{bmatrix} 11 \end{bmatrix} & \begin{bmatrix} 12 \end{bmatrix} & \\ \begin{bmatrix} 21 \end{bmatrix} & \begin{bmatrix} 22 \end{bmatrix} & \begin{bmatrix} 23 \end{bmatrix} \\ & \begin{bmatrix} 32 \end{bmatrix} & \begin{bmatrix} 33 \end{bmatrix} \end{bmatrix} \begin{pmatrix} \begin{bmatrix} \phi_1 \end{bmatrix} \\ \begin{bmatrix} \phi_2 \end{bmatrix} \\ \begin{bmatrix} \phi_3 \end{bmatrix} \end{pmatrix}$$

Figure 5.1: K matrix shape for a generic three subdomain problem

in Figure 5.1 two different kind of blocks are present in the matrix. Diagonal block matrices represent the contribution of a single subdomain. Off diagonal matrices represent subdomains coupling contribution. Is to remark that VTCR tends to privilege few big subdomains. This characteristic, common to most of Trefftz approach, is at the base of its strong performances. From these considerations rise the idea at the basis of a new pre-conditioner. The proposition is to apply a strong SVD pre-conditioner only to diagonal block of the matrix as in Figure 5.2. In this way computational costs will not explode due to the presence of few subdomains. Taking into account the i^{th} diagonal matrix of **K**, we can write:

$$\mathbf{K}_{ii} = \mathbf{U}_i \mathbf{D}_i \mathbf{V}_i \tag{5.1}$$

where :

- **D** is a diagonal matrix of the eigenvalue of matrix $\mathbf{K}_{ii}$,

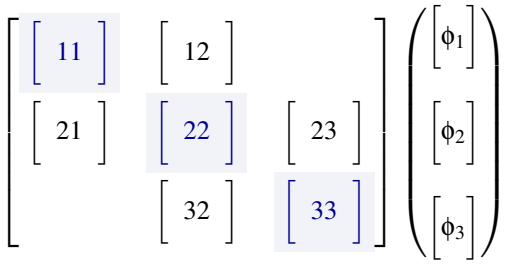

Figure 5.2: SVD application subdomains (in blue)

- **V** (resp. **U**) is composed by an orthonormal base of "enter" vectors (resp. "exit").

Following matrices are so created:

$$\mathbf{U} = \begin{bmatrix} \mathbf{U}_1 & 0 & 0 \\ 0 & \mathbf{U}_2 & 0 \\ 0 & 0 & \mathbf{U}_3 \end{bmatrix} \qquad \mathbf{D} = \begin{bmatrix} \mathbf{D}_1 & 0 & 0 \\ 0 & \mathbf{D}_2 & 0 \\ 0 & 0 & \mathbf{D}_3 \end{bmatrix} \qquad \mathbf{V} = \begin{bmatrix} \mathbf{V}_1 & 0 & 0 \\ 0 & \mathbf{V}_2 & 0 \\ 0 & 0 & \mathbf{V}_3 \end{bmatrix} \tag{5.2}$$

It's so possible to rewrite the matrix system (4.1) as:

$$\begin{aligned} \mathbf{K}\mathbf{X} = \mathbf{F} &\Leftrightarrow \mathbf{U}^* \mathbf{D}^{-1/2} \mathbf{K} \mathbf{D}^{-1/2} \mathbf{V}^* (\mathbf{D}^{-1/2} \mathbf{V}^*)^{-1} \mathbf{X} = \mathbf{U}^* \mathbf{D}^{-1/2} \mathbf{F} \\ &\Leftrightarrow \mathbf{K}^c \mathbf{X}^c = \mathbf{F}^c \end{aligned}$$

where

- $\mathbf{K}^c = \mathbf{U}^* \mathbf{D}^{-1/2} \mathbf{K} \mathbf{D}^{-1/2} \mathbf{V}^*$
- $\mathbf{X}^c = (\mathbf{D}^{-1/2} \mathbf{V}^*)^{-1} \mathbf{X}$
- $\mathbf{F}^c = \mathbf{U}^* \mathbf{D}^{-1/2} \mathbf{F}$

This pre-conditioner is an expensive one but the gain in terms of stability of the method and of PGD applicability justify the choice. In Figure 5.3 superior performance of the new pre-conditioner are shown. Is to remark that in this example a very strict convergency criteria has been chosen to test its performance under the worst condition. A gain of over ten order of magnitude in term of conditioning number is present. Moreover, increasing frequency and DoFs a stabilization phenomena appears.

If a more realistic convergency criteria is chosen, condition number does not get over 10^2. This order of magnitude is completely compatible with most of iterative algorithm of which PGD related ones.

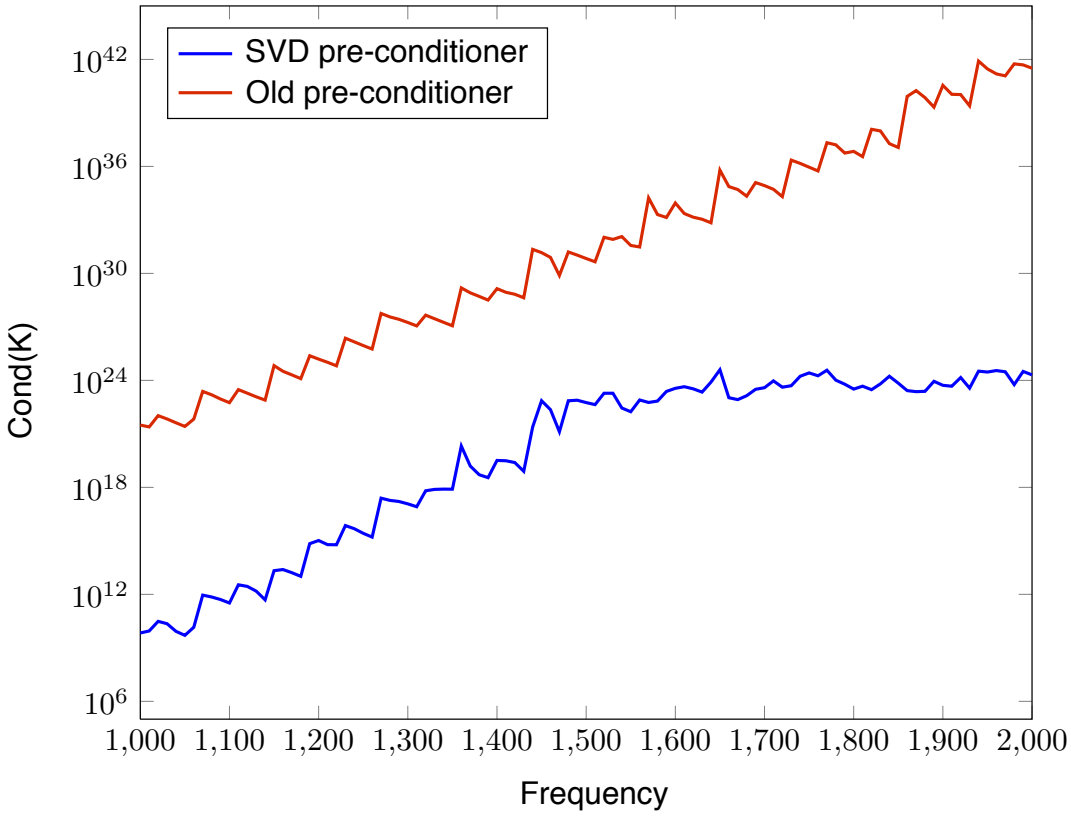

Figure 5.3: Comparison between SVD based pre-conditioner and old energy based pre-conditioner

2 An improved algorithm for PGD-VTCR

With the stability acquired from the pre-conditioner it is possible to reformulate the Algorithm 1 with some improvements. As done in Chapter 4 Section 2 the solution of VTCR problem is searched in PGD form:

$$\mathbf{X}(\omega) \simeq \mathbf{X}_M(\omega) = \sum_{m=1}^{M} \mathbf{X}_m \lambda_m(\omega) \tag{5.3}$$

Again the residue of the problem is written as:

$$\mathbf{R}_M(\omega) = \mathbf{F}(\omega) - \mathbf{K}(\omega)\mathbf{X}(\omega) = \mathbf{F}(\omega) - \mathbf{K}(\omega)\left(\sum_{i=m}^{M} \mathbf{X}_m(\theta)\lambda_m(\omega)\right) \tag{5.4}$$

Supposing M order of approximation known, to find the new PGD mode $(\mathbf{X}_{M+1}(\theta), \lambda_{M+1}(\omega))$ could be found minimizing:

$$\int_{\omega_0-\frac{\Delta\omega}{2}}^{\omega_0+\frac{\Delta\omega}{2}} \| \mathbf{R}_M(\omega) - \mathbf{K}\mathbf{X}_{M+1}(\theta)\lambda_{M+1}(\omega) \|^2 \, \mathrm{d}\omega = \left(\| \mathbf{R}_M(\omega) - \mathbf{K}\mathbf{X}_{M+1}(\theta)\lambda_{M+1}(\omega) \|^2 \right)_\omega \tag{5.5}$$

with $\| \bullet \| = (\bullet, \bullet^*)$ where $\bullet^*$ is the conjugate transpose operator. From the minimization problem (5.5) two equation are drawn:

$$\lambda_{M+1}(\omega) = \frac{\Re(\mathbf{R}_M^* \mathbf{K}\mathbf{X}_{M+1})}{\mathbf{X}_{M+1}^* \mathbf{K}^* \mathbf{K}\hat{\mathbf{X}}_{M+1}} \tag{5.6}$$

$$\mathbf{X}_{M+1} = \left(\int_{\omega_0-\Delta\omega}^{\omega_0+\Delta\omega} \lambda_{M+1}^* \mathbf{K}^* \mathbf{K} \lambda_{M+1} \mathrm{d}\omega \right)^{-1} \left(\int_{\omega_0-\Delta\omega}^{\omega_0+\Delta\omega} \lambda_{M+1}^* \mathbf{K}^* \mathbf{R}_M \mathrm{d}\omega \right) \tag{5.7}$$

This time in order to improve the stability and performances of the method $\lambda(\omega)$ functions are calculated differently. Combining equation (5.6) and (5.7) the associated Rayleigh quotient can be drawn:

$$\mathcal{R}(\lambda) = (\lambda \mathbf{R}_m^* \mathbf{K})(\lambda \mathbf{K}^* \mathbf{K} \lambda)^{-1} (\lambda \mathbf{K}^* \mathbf{R}_m) \tag{5.8}$$

where $\mathcal{R}(\lambda)$ is the Rayleigh quotient associated to λ. Let us recall that for a generic Rayleigh quotient in the form:

$$\mathcal{R}(\mathbf{x}) = \frac{\mathbf{x}^* \mathbf{M} \mathbf{x}}{\mathbf{x}^* \mathbf{N} \mathbf{x}} \tag{5.9}$$

stands the following eigenvalue problem:

$$\mathbf{M}\mathbf{x} = \alpha \mathbf{N}\mathbf{x} \tag{5.10}$$

where $\mathbf{x}$ is a eigenvector, $\mathbf{M}$ and $\mathbf{N}$ are matrices and α is an eigenvalue. For this reason from the lowest eigenvalue of Rayleigh quotient it is possible to find the lowest eigenvector of the associated eigenvalue problem. In the case of a PGD approach the lowest eigenvalue corresponds to the desired λ. This is an important theoretical result which shows how PGD approximation is linked to an eigenvalue problem. Finally is possible to write a PGD algorithm involving the Rayleigh quotient:

Algorithm 4: Rayleigh quotient based PGD algorithm for brad band problems

Initialization of $\mathbf{R}_0 = \mathbf{F}$;
for $m = 1$ *to* M **do**
  Initialization of λ_m;
  Calculation of λ_{m+1} by Rayleigh quotient minimization:
  $\lambda_{m+1} = \mathcal{R}(\lambda_m) \rightarrow (5.8)$;
  Compute:
  $\mathbf{X}_{m+1} = \mathcal{F}(\lambda_{m+1}) \rightarrow (5.7)$;
  Update of $\mathbf{R}_{m+1} = \mathbf{R}_m - \mathbf{K}\mathbf{X}_m\lambda_m$;
  Convergency check;

This algorithm has the decisive advantage of compute directly equation (5.7) without passing through iterations. Of course some iteration are needed to find λ_{m+1} but only scalar products have to be made. On the other hand, thanks to the Rayleigh quotient contribution, the heavy computational matrix product has to be compute only one time for PGD couple's construction. This algorithm has some important advantages over Algorithm 1 and Algorithm 3. Nevertheless its convergency is strongly influenced by the bad condition number. For this reason the pre-conditioner presented in Section 1 is necessary to guarantee fast and smooth convergency. Another problem of this algorithm is the presence of a $\mathbf{K}^*\mathbf{K}$ in its formulation. As previously stated this product is heavy to compute and can introduce numerical pollution. The effect of numerical pollution is limited by the presence of a strong pre-conditioner but could appear again if very big matrices have to be processed. Moreover such a product is very expensive to calculate. For these reasons this algorithm should not be seen as a state of the art algorithm for PGD-VTCR. Its role has been to establish a new path of research and a basis for a new algorithm. This algorithm combining numerical advantages of the Rayleigh based algorithm and the numerical stability given by the absence on $\mathbf{K}^*\mathbf{K}$ (as in Petrov-Galerkin) is presented in the next Section.

3 Minimal residue direction algorithm: the state of the art for PGD-VTCR on frequency bands

From the previous section is clear that an alliance between the "Block SVD" pre-conditioner and a Rayleigh quotient based algorithm is a very promising path to built the most performant algorithm ever for PGD-VTCR on broad frequency band. The key point to solve, is the presence of $\mathbf{K}^*\mathbf{K}$ which strongly decreases robustness and performances. In this section an innovative strategy is proposed to overcome this limitation and provide a *state of the art* algorithm. Let us consider again a target PGD decomposition and the definition of residue:

$$\mathbf{X}(\omega) \simeq \mathbf{X}_M(\omega) = \sum_{m=1}^{M} \mathbf{X}_m\lambda_m(\omega) \tag{5.11}$$

$$\mathbf{R}_M(\omega) = \mathbf{F}(\omega) - \mathbf{K}(\omega)\mathbf{X}(\omega) = \mathbf{F}(\omega) - \mathbf{K}(\omega)\left(\sum_{i=m}^{M} \mathbf{X}_m(\theta)\lambda_m(\omega)\right) \tag{5.12}$$

This time residue at step $m+1$ is searched as:

$$\mathbf{R}_{m+1} = \mathbf{R}_m + \Delta\mathbf{R}_{m+1} = \mathbf{R}_m + \mathbf{K}\Delta\mathbf{X}_{m+1} \tag{5.13}$$

where $\Delta\mathbf{R}$ is the optimal minimization term of residue searched as $\mathbf{K}$ matrix multiplied for a minimization direction $\Delta\mathbf{X}$. This minimization direction is searched in PGD form:

$$\Delta\mathbf{X}^M = \sum_{m=1}^{M} \mathbf{X}_m\lambda_m(\omega) \tag{5.14}$$

If $\mathbf{R}_m$ is known it is also possible to write the subsequent decomposition [Ladevèze, 1999]:

$$\mathbf{R}_m = \mathbf{B}_\omega\Delta\mathbf{X}_m = \mathbf{B}_\omega \sum_{m=1}^{M} \mathbf{X}_m\lambda_m(\omega) \tag{5.15}$$

where $\mathbf{B}_\omega$ is a frequency dependent function arbitrary chosen. This kind of approximation is not yet a PGD one. Here the vector $\mathbf{R}_m$ is known. The equation (5.17) only approximates a known quantity in a suitable way for the following development. $\mathbf{B}_\omega$ is a complete arbitrary choice:

$$\mathbf{B}_\omega = \mathbf{b}(\omega)\mathbf{B} \tag{5.16}$$

where $\mathbf{b}(\omega)$ is a frequency dependent vector and $\mathbf{B}$ is a constant matrix. Injecting (5.16) in (5.17) we obtain:

$$\mathbf{R}_m = \mathbf{b}(\omega)\mathbf{B} \sum_{m=1}^{M} \mathbf{X}_m\lambda_m(\omega) \tag{5.17}$$

In order to find the approximation of $\mathbf{R}_m$ an error is to minimize:

$$\int_{\omega_0-\frac{\Delta\omega}{2}}^{\omega_0+\frac{\Delta\omega}{2}} \int_\Omega (\mathbf{R}_m(\omega) - \mathbf{B}_\omega\mathbf{X}_m(\theta)\lambda_m(\omega))^2 \mathrm{d}\omega\mathrm{d}\theta \tag{5.18}$$

Equation (5.18) is very close to PGD error minimization but, again, is to underline that no update process is made. From the minimization two equations can be drawn:

$$\lambda(\omega) = \frac{\int_\Omega \mathbf{R}_m\mathbf{X}(\theta)\mathrm{d}\theta}{\mathbf{X}^2(\theta)d\theta} \tag{5.19}$$

$$\mathbf{X}(\theta) = \int_{\frac{\Delta\omega}{2}}^{\frac{\Delta\omega}{2}} \mathbf{R}_m\lambda_m(\omega)\mathrm{d}\omega \tag{5.20}$$

Combining equation (5.20) and (5.19) the associated Rayleigh quotient can be drawn:

$$\mathcal{R}(\lambda) = \frac{\int_{\omega_0-\frac{\Delta\omega}{2}}^{\omega_0+\frac{\Delta\omega}{2}} d\omega(\int_\Omega \mathbf{R}_m\lambda_m\mathrm{d}\Omega)^2}{\int_\Omega \lambda_m^2\mathrm{d}\Omega} \tag{5.21}$$

λ_m is found by minimization of Rayleigh quotient in (5.21) and $\mathbf{X}_m$ by simple substitution in (5.20). Once $\mathbf{R}_m$ is so decomposed is possible to start searching for $\mathbf{R}_{m+1}$:

$$\mathbf{R}_{m+1} = \mathbf{R}_m + \Delta\mathbf{R}_{m+1} = \mathbf{R}_m + \mathbf{K}\Delta\mathbf{X}_{m+1} = \mathbf{R}_m + \mathbf{K}\mathbf{X}_m\lambda_{m+1}(\omega) \tag{5.22}$$

In equation (5.22) λ_{m+1} represents the updated frequency function. The presence of this term allows to update the residue to the step $m+1$ building a PDG form approximation. λ_{m+1} is computed minimizing the subsequent local error:

$$\int_{\omega_0-\frac{\Delta\omega}{2}}^{\omega_0+\frac{\Delta\omega}{2}} \int_{\Omega} (\mathbf{R}_m + \Delta\mathbf{R}_{m+1}) \mathrm{d}\omega \mathrm{d}\theta \tag{5.23}$$

from which is withdrawn the λ function update equation:

$$\lambda_{m+1}(\omega) = \frac{\int_{\Omega} \mathbf{R}_m \mathbf{X}_m(\theta) \mathrm{d}\theta}{\int_{\Omega} \mathbf{X}_m^2(\theta) \mathrm{d}\theta} \tag{5.24}$$

Once λ is updated by equation (5.24) updated $\mathbf{R}_{m+1}$ is solved. The process can be iterated to built PGD approximation as follow:

Algorithm 5: Minimal residue direction PGD algorithm for brad band problems

Initialization of $\mathbf{R}_0 = \mathbf{F}$;
for $m = 1$ *to* M **do**
  Calculation of λ_m by Rayleigh quotient minimization:
  $\lambda_m = \mathcal{R}(\lambda_m) \rightarrow (5.21)$;
  Compute:
  $\mathbf{X}_m = \mathcal{F}(\lambda_m) \rightarrow (5.20)$;
  Update of λ_m to λ_{m+1}:
  $\lambda_{m+1} = \mathcal{F}(\mathbf{X}_m) \rightarrow (5.24)$;
  Definition of $\Delta\mathbf{R}_{m+1}$;
  Update of $\mathbf{R}_{m+1} = \mathbf{R}_m + \Delta\mathbf{R}_{m+1}$;
  Convergency check;

This algorithm still needs a pre-conditioner but it solves the $\mathbf{K}^*\mathbf{K}$ problem without passing trough a Petrov-Galerkin approach. A numerical example will show its performances and why this algorithm should be considered the state of art for PGD-VTCR.

3.1 A numerical example

Let us consider the L-shaped acoustic cavity presented in Figure 5.4. Ω is filled with air ($\rho_0 = 1.25\ [kg/m]^3$, $c_0 = 340\ m/s$, $\eta = 0.01$) and is partitioned in 3 sub-cavities. Different boundary conditions are prescribed (pressure $P = 0\ [Pa]$, velocity $V = 1\ [m/s]$ and impedance $Z = 845 + i50\ [Pa.s/m]$). The considered frequency band is defined by

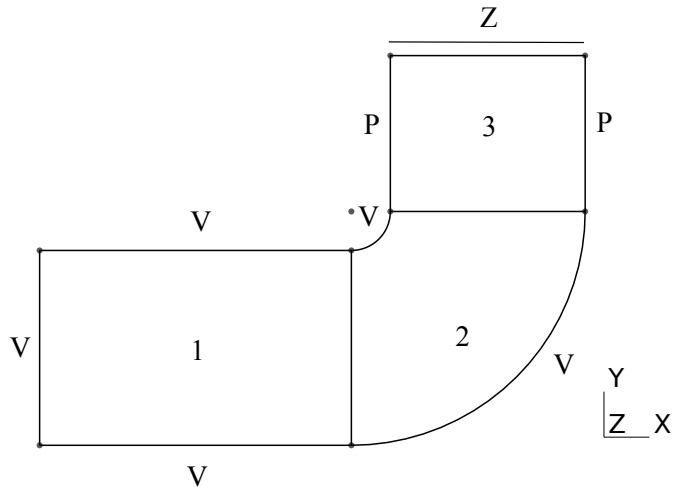

Figure 5.4: L-shaped acoustic cavity

$\omega_0 = 2.\pi.1300\ [Hz]$ and $\Delta\omega = 2.\pi.300\ [Hz]$. As usual, the solving Algorithm 6 consists in compute a frequency base with few test points and then built the PGD approximation. This time a pre-conditioner in applied.

Algorithm 6: Approximation building algorithm with pre-conditioner

for $j = 1$ *to "frequency test point number"* **do**
  Find $\mathbf{K}_j = \mathbf{K}(\omega)$;
  Find $\mathbf{F}_j = \mathbf{F}(\omega)$;
  Pre-condition of $\mathbf{K}_j \rightarrow \mathbf{K}_j^c$ and $\mathbf{F}_j^c$;

Apply algorithm 5 $\leftarrow (\{\mathbf{K}\}_j^c, \{\mathbf{F}\}_j^c)$;
  $\hookrightarrow$ PGD modes $\{(\mathbf{X}(\theta), \lambda(\omega))\}_m$

The PGD formulation in Section 3 allows an immediate introduction of a relative error criteria:

$$Error = \int_{\omega_0-\Delta\omega}^{\omega_0+\Delta\omega} \|\underline{R}_m(\omega)\|^2 d\omega / \int_{\omega_0-\Delta\omega}^{\omega_0+\Delta\omega} \|\underline{F}(\omega)\|^2 d\omega \tag{5.25}$$

In Figure 5.5 error convergency is shown if Algorithm 5 is applied without pre-conditioner. We can observe a slow and not smooth convergency. In Figure 5.6 the error convergency after pre-conditioning operation is plotted. The evidence shows that the pre-conditioned algorithm improve sensibly order and speed of convergency. Moreover a very smooth convergency is present. One can remark that pre-conditioned error plot exhibits a change of slope around PGD couple number 6. This change of slope means that PGD base starts to saturate and additional couples will not improve approximation in term of relative error. This is actually a very nice characteristic. Indeed we can exploit the change of slope to put an automatic stopping criteria in building PGD approximation. These excellent results in terms of convergency are confirmed over the frequency response functions in

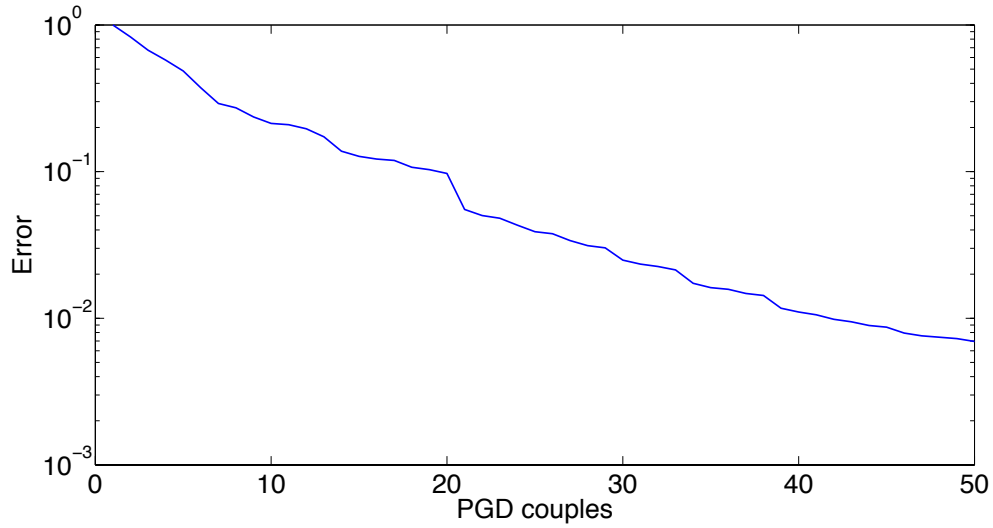

Figure 5.5: Convergence curve for an L-shaped cavity.

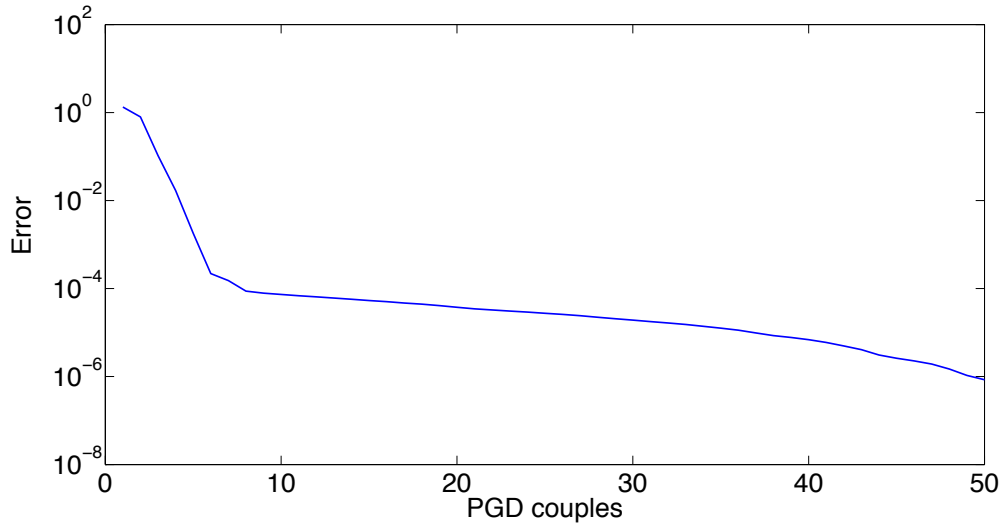

Figure 5.6: Convergence curve for an L-shaped cavity, with a preconditioned matrix system.

terms of global energy on the L-shaped cavity, which are plotted on Figure 5.7 for the first five PGD couples, and compared to a reference VTCR computation done frequency by frequency. It is clear from Figure 5.7 that five PGD couples are enough to give an extremely good approximation of the energy. Good results are of course confirmed in terms of pressure field as shown in Figure 5.8.

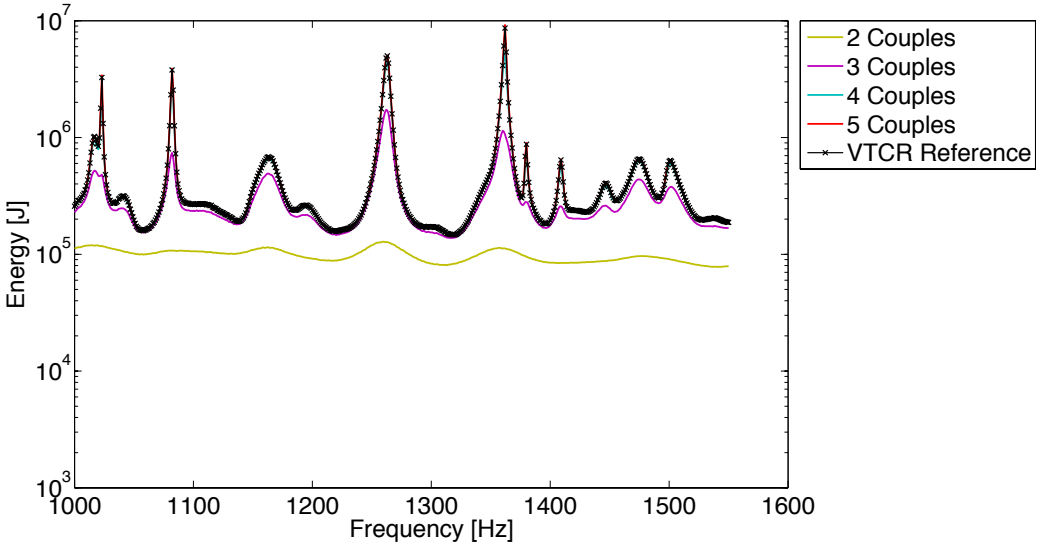

Figure 5.7: Global energy of the L-shaped acoustic cavity for 2, 3, 4 or 5 PGD couples. The reference solution is computed with the VTCR, frequency by frequency.

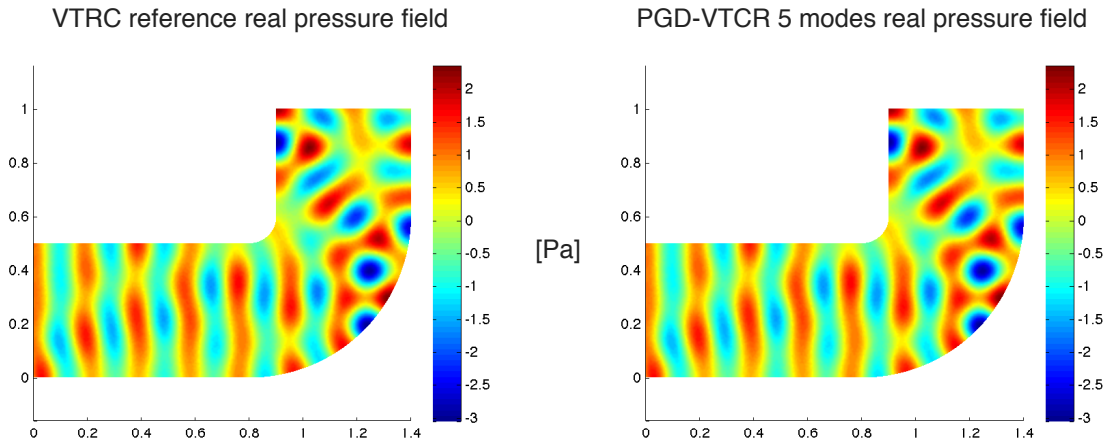

Figure 5.8: Compared real pressure field for $\omega = 2\pi 1500[Hz]$

4 Conclusion

In this Chapter some decisive improvements to PGD-VTCR technique have been provided. At the base of any possible new algorithm stands the introduction of a new pre-conditioner. A "block SVD" has been introduced in Section 1. This pre-conditioner seems, from a first analysis, the most adapted to VTCR. SVD pre-conditioner is known as a very powerful but expensive tool. The key point to contain its cost and still have most of the advantages is to apply SVD only to diagonal blocks. VTCR prefers few big sub-domains so the cost of this preconditioned is completely affordable. The introduction of this so called "block SVD pre-conditioner" allows an extreme effectiveness of PGD

iterative process and give more robustness to VTCR.

The consequence of this increased robustness has been the introduction of two new algorithms. The first one is based on a Rayleigh quotient minimization. Its introduction allowed a big step in terms of PGD understanding and open to a new path in PGD algorithms. Unluckily the presence of a $\mathbf{K}^*\mathbf{K}$ term deprives this approach of any numerical and practical interest. The second algorithm arise directly from the effort to remove $\mathbf{K}^*\mathbf{K}$ limitation from the Rayleigh quotient based PGD. The resulting technique, as shown by numerical results, establishes a new reference in PGD-VTCR applications. Its performances in terms of convergency, accuracy of energy approximation and pressure approximation are unreached by any other tested algorithm. Moreover these results are reached with only few PGD couples.

The minimal residue direction algorithm sets a standard for PGD-VTCR. Thanks to this new fields of application of the technique can be explored. A possibility to increase the potentiality of the method is to add to classical space-frequency decomposition other parameters. In the next chapter an uncertainty parameter will be added to extend the technique to uncertainty.

Chapter 6

PGD applied to acoustic with uncertainty parameters

In this Chapter uncertainties over a mid-frequency broad band will be introduced thanks to a PGD approximation. As a first step, a brief introduction about the necessity of uncertainty in mid-frequency will be provided. Than a dedicated PGD algorithm will introduce in VTCR formulation uncertainty over a wide frequency band. A simple numerical example will give an idea of the potentiality of the method dealing with this kind of problems.

Contents

1 Uncertainty in Mid-Frequency acoustic 112

2 A PGD technique to take account for uncertainty in VTCR for Mid-Frequency analysis 113

2.1 1D validation example 114

2.2 A low cost solution towards high-frequency 121

2.3 2D preliminary results 121

3 Conclusion 123

1 Uncertainty in Mid-Frequency acoustic

Different frequency bands show a different sensibility to uncertainty parameters. This affirmation lies on some experimental evidence. An example of this phenomena in shown in Figure 6.1. These experiments, published in [Kompella and Bernhard, 1993], are con-

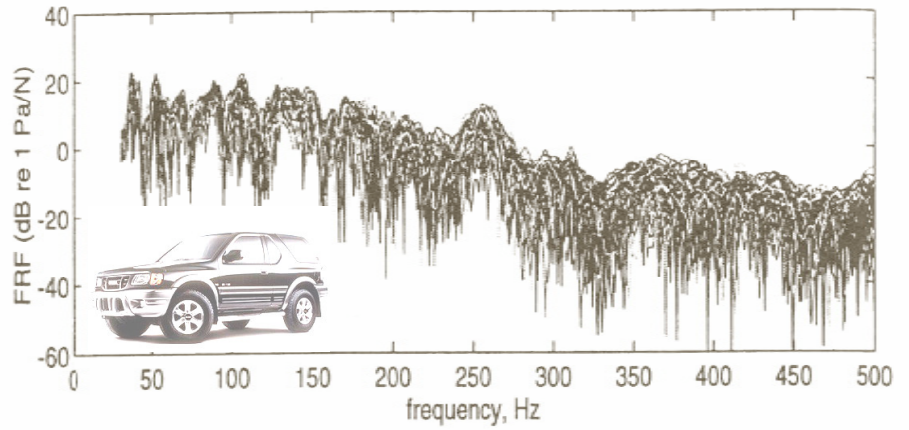

Figure 6.1: Frequency response of 98 "identical" cars from the same production line (courtesy of Toyota)

ducted on 98 nominally identical cars. The model and the production line is the same for every of the 98 cars. Experiments shows that low frequency dependency from the presence of little variation is little. This means that if a low frequency analysis is conducted deterministic models like FEM are effective and meaningful. The situation changes increasing frequency. Effect of uncertainties are very strong in mid-frequency band and decisive in high-frequency. From this experimental evidence borns the consideration that a mid-frequency method should keep in account uncertainty. This is particularly true if an extension of these methods to large-frequency is desired.

VTCR is for its nature a full deterministic method. Deterministic methods are vey effective and accurate when a deterministic problem is to solve but when is necessary to propagate a mid-frequency parametric uncertainty the question is not trivial. The most common way to do it is the well known Monte Carlo simulation [Metropolis, 1987]. Given a probability density function Monte Carlo simulation prescribes to effectuate a high number of deterministic calculations in order to get the mean value σ and the variance μ of the response. This method is simple, effective and non-invasive in the considered deterministic formulation. On the other hand many deterministic calculations are needed and this can be extremely expensive. This technique is particularly not warn for frequency dependent techniques. High computational cost due to frequency dependency combined to Monte Carlo's cost limits the application of such a combination.

Increasing frequency, uncertainty loses gradually dependance from a parametric distribution. In this case non-parametric approaches are more suited. In these technique no hypothesis is made on the nature nor on shape of the distribution. To this category

belongs the quantum chaos theory [Mortessagne et al., 1993] or the random matrix theory [Weaver, 1989]. This last methods has been widely used with great success in computational structural dynamics [Soize, 2000].

For mid-frequency the authors considers fundamental the introduction of parametric uncertainty. In order to overcome Monte Carlo simulation limitation in terms of computational cost a PGD approximation, is proposed. The value of this technique in dealing uncertainty has been proved in [Nouy, 2007] and a successful example in structural dynamic can be found in [Chevreuil and Nouy, 2011].

This section proposes an original application of PGD-VTCR over uncertainly parameter, space and frequency. In this way an effective manner to propagate uncertainty over a wide frequency band is introduced. The main idea is to combine the high reduction power over frequency found in previous chapters with the well know effectiveness (see [Nouy, 2007]) of PGD on stochastic.

2 A PGD technique to take account for uncertainty in VTCR for Mid-Frequency analysis

If considering a system response over a wave band and a stochastic parameter $s \in \mathcal{S}$ the final VTCR equation can be written as:

$$\mathbf{K}(\omega,s)\mathbf{X}(\omega,s) = \mathbf{F}(\omega,s) \tag{6.1}$$

the objective is to find an approximation of $\mathbf{X}$ such as:

$$\mathbf{X}(\omega,s) \approx \mathbf{X}^m(\omega;s) = \sum_{i=1}^{m} \mathbf{X}_i \lambda_i(\omega)\sigma_i(s) \tag{6.2}$$

where $\mathbf{X}_i$ is a space dependent vector, λ_i is a frequency dependent function and $\sigma_i(s)$ is a function representing the uncertainty contribution. In order to simplify the formulation new operators are defined:

$$\int_I \bullet \, \mathrm{d}\omega = (\bullet)_\omega \quad ; \quad \int_{\mathcal{S}} \bullet \, \mathrm{d}P(s) = (\bullet)_s \quad ; \quad \int_{\mathcal{S}} \int_I \bullet \, \mathrm{d}\omega \mathrm{d}P(s) = (\bullet)_{\omega,s} \tag{6.3}$$

with $\| \bullet \| = (\bullet \cdot \mathbf{I} \cdot \bullet^*)$ where $\bullet^*$ is the complex conjugate operator.

In order to find the required approximation the norm of the scalar product of the residue, respect the m order of the approximation, is to minimize:

$$\left(\|\mathbf{R}_{m+1}\|^2\right)_{\omega,s} = \left(\|\mathbf{R}_m - \mathbf{K}\mathbf{X}_{m+1}\lambda_{m+1}(\omega)\sigma_{m+1}(s)\|^2\right)_{\omega,s} \tag{6.4}$$

The scalar product is made considering $[\mathbf{K}^*\mathbf{K}]^{-1}$ matrix. Minimizing equation 6.4 over the three variables, a triplet of equation is obtained:

$$\sigma_{m+1} = \frac{\left(\Re(\lambda_{m+1}\, \mathbf{R}_m^* \mathbf{K}\mathbf{X}_{m+1})\right)_\omega}{\left(\lambda_{m+1}\mathbf{X}_{m+1}^*\, \mathbf{K}^*\, \mathbf{K}\mathbf{X}_{m+1}\lambda_{m+1}\right)_\omega} \tag{6.5a}$$

$$\lambda_{m+1} = \frac{\left(\Re(\sigma_{m+1}\,\mathbf{R}_m^*\,\mathbf{K}\mathbf{X}_{m+1})\right)_s}{\left(\sigma_{m+1}\mathbf{X}_{m+1}^*\,\mathbf{K}^*\,\mathbf{K}\mathbf{X}_{m+1}\sigma_{m+1}\right)_s} \tag{6.5b}$$

$$\mathbf{X}_{m+1} = \left(\lambda_{m+1}\sigma_{m+1}\,\mathbf{K}^*\,\mathbf{K}\sigma_{m+1}\lambda_{m+1}\right)_{\omega,s}^{-1}\left(\lambda_{m+1}\sigma_{m+1}\,\mathbf{K}^*\,\mathbf{R}_m\sigma_{m+1}\lambda_{m+1}\right)_{\omega,s} \tag{6.5c}$$

In order to perform the minimization a power type algorithm is required:

Algorithm 7: PGD for stochastic broad band problems

Initialization of $\mathbf{R}_0 = \mathbf{F}$;
for $i = 1$ *to* m **do**
  Initialization of $\mathbf{X}_i^0$;
  Initialization of λ_i^0;
  for $k = 1$ *to* k_{max} **do**
    Compute:
    $\sigma_i^k = (\mathbf{X}_i^{k-1}, \lambda_i^{k-1}) \rightarrow (6.5a)$;
    $\lambda_i^k = (\mathbf{X}_i^{k-1}, \sigma_i^k) \rightarrow (6.5b)$;
    $\mathbf{X}_i^k = (\lambda_i^k, \sigma_i^k) \rightarrow (6.5c)$;
    Stationarity check $(\mathbf{X}_i^k, \sigma_i^k, \lambda_i^k)$;
  Update of $\mathbf{R}_{i+1} = \mathbf{R}_i - \mathbf{K}\mathbf{X}_i\sigma_i\lambda_i^k$;
  Convergency check;

Is to remark that any initialization would leads to convergency but, an initialization choice somehow linked to the problem could leads to a sensible faster convergency. For the sake of simplicity, Algorithm 7 is a simple symmetrized Galerkin. Of course, if needed, more sophisticated Algorithms (as presented in this manuscript) can be used.

2.1 1D validation example

Being the first time VTCR is extended to uncertainty, the simple 1D problem defined in Figure 6.2 is considered.

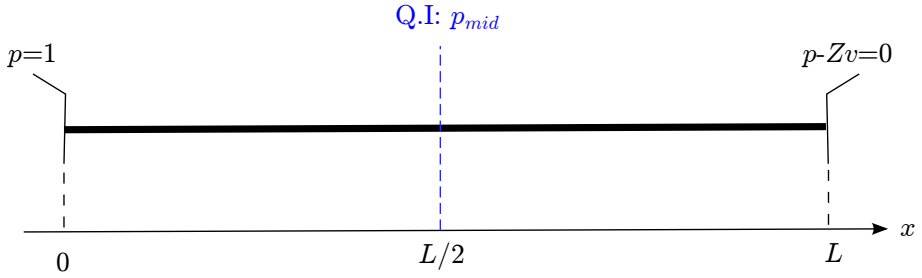

Figure 6.2: 1D problem to assest stochastic PGD-VTCR

The example consists in an "acoustic rod" of $L = 2$ $[m]$ where on $x = 0$ a unitary pressure is imposed and a variable Robin condition is applied on $x = L$. Considered fluid

is air (density is $\rho_0 = 1,125$ [kg.m^{-3}] and sound speed is $c = 320$m. [s^{-1}]). The problem is defined on a frequency band $f \in]1000,4500[$ Hz and the real part of impedance is considered uncertain between 100 and 500 ($s = \Re(Z)$) on an uniform distribution. This example is particularly useful in this explorative phase for two main reasons: there is a simple analytic reference to compare PGD approximation with and PDG results are of immediate and clear interpretation. For a 1D case the ensemble of admissible solution is found on the function family of $\{e^{ikx}, e^{-ikx}\}$ with $k = \omega/c$. For this reason unknown pressure is expressed in the form:

$$p(x) = X^+ e^{ikx} + X^- e^{-ikx} \tag{6.6}$$

and v is:

$$v(x) = -\frac{k}{\rho_0 \omega}(X^+ e^{ikx} - X^- e^{-ikx}) \tag{6.7}$$

The analytical solution is found solving:

$$\begin{cases} p(0) & = 1 \\ p(L) & -Zv(L) = h_{ed} \end{cases} \tag{6.8}$$

or in matrix form:

$$\begin{bmatrix} 1 & 1 \\ e^{ikL}\left(1 + \frac{Zk}{\rho_0 \omega}\right) & e^{-ikL}\left(1 - \frac{Zk}{\rho_0 \omega}\right) \end{bmatrix} \begin{pmatrix} X^+ \\ X^- \end{pmatrix} = \begin{pmatrix} 1 \\ h_{ed} \end{pmatrix} \tag{6.9}$$

In order to find a PGD-VTCR approximation a number of tests matrices K and vectors F is to find through a coarse discretization of the frequency and stochastic spaces. The variational formulation (2.8) can be easily particularized for 1D problems as:

$$\begin{aligned} &(X^+ + X^- - 1)\frac{k}{\rho_0 \omega}(\delta X^+ - \delta X^-) + \\ &\left(X^+ e^{ikL}\left(1 + \frac{Zk}{\rho_0 \omega}\right) + X^- e^{-ikL}\left(1 - \frac{Zk}{\rho_0 \omega}\right) - h_{ed}\right)\frac{k}{\rho_0 \omega}(-\delta X^+ e^{-ikL} + \delta X^- e^{ikL}) = 0 \end{aligned} \tag{6.10}$$

or in matrix form:

$$\begin{bmatrix} \frac{-Zk}{\rho_0} & \left(1-e^{-2ikL}\left(1-\frac{Zk}{\rho_0\omega}\right)\right) \\ \left(e^{2ikL}\left(1+\frac{Zk}{\rho_0\omega}\right)-1\right) & \frac{-Zk}{\rho_0} \end{bmatrix} \begin{pmatrix} X^+ \\ X^- \end{pmatrix} = \begin{pmatrix} \left(1-h_{ed}e^{-ikL}\right) \\ \left(h_{ed}e^{ikL}-1\right) \end{pmatrix} \tag{6.11}$$

which is exactly the synthetic formulation expressed in (6.1). Once the test matrices are found a PGD iterative algorithm is applied to find the desired approximation:

Algorithm 8: 1D stochastic PGD algorithm

for $i = 1$ *to "stochastic test point number"* **do**
  for $j = 1$ *to "frequency test point number"* **do**
    Find $\mathbf{K}_{i,j} = \mathbf{K}(\omega, s)$;
    Find $\mathbf{F}_{i,j} = \mathbf{F}(\omega, s)$;

Apply algorithm 7 $\leftarrow (\{\mathbf{K}\}_{i,j}, \{\mathbf{F}\}_{i,j})$;
  $\hookrightarrow$ PGD triplets $\{(\mathbf{X}(\theta), \lambda(\omega)\sigma(s))\}_m$

Post-processing

Let us take an uniform distribution on Z. A PGD approximation can be built with 30 discretization points on stochastic and 1500 on frequency band. PGD solution is built with 150 triplets.

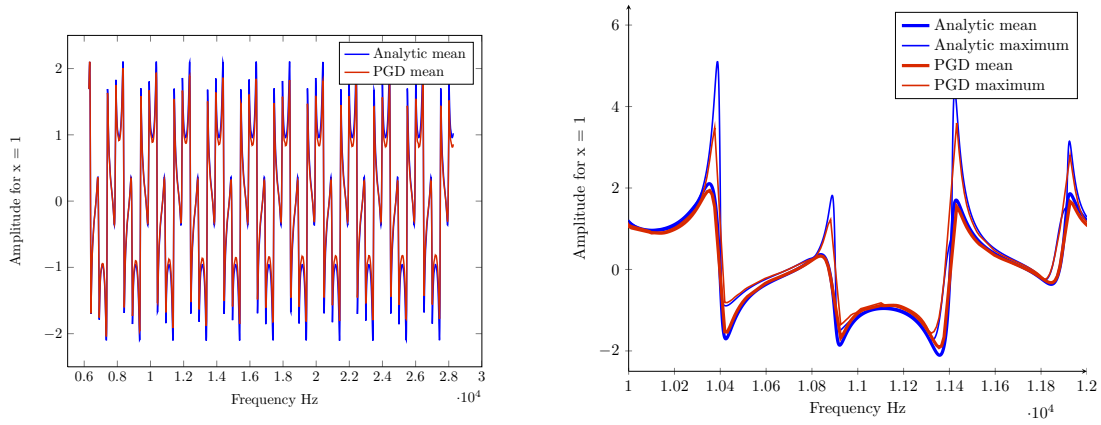

(a) FRF on frequency band

(b) Zoom on 1000 to 1200 Hz frequency band

Figure 6.3: PGD-VTCR mean pressure compared to mean reference

It is to remark the very good agreement between the PGD approximation and the reference both for the general FRF tendency and the peaks. Looking at convergency issues in Figure 6.4 we can see that a fast regular and smooth convergency is provided with a

modest number of algorithm sub-iterations (see Figure 6.5). As remarked in Chapter 4 Section 3.1 the suggested and most performing choice is to fix a small number of iteration (in this case 5 are enough) and go on with PGD triplets construction.

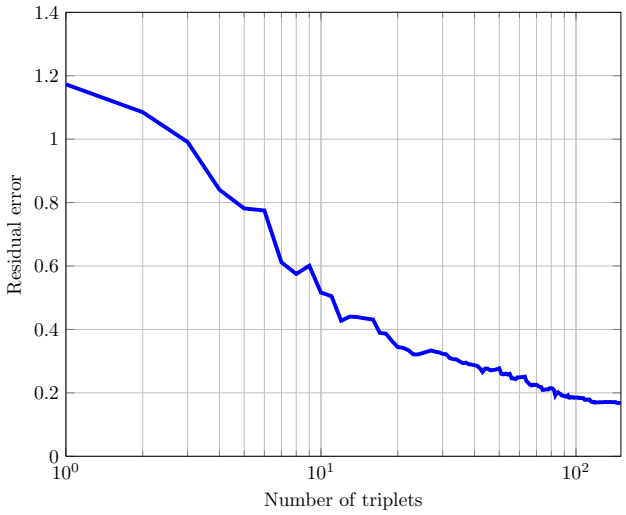

Figure 6.4: Residual error (5.23)

Looking in details how the approximation is is built during the minimization of the residue is useful to make some consideration on frequency functions evolution in Figure 6.6 and stochastic functions evolution in Figure 6.7.

From the analysis of Figures 6.6 and Figure 6.7 convergency properties are confirmed at a functional level. Moreover two other considerations can be drown:

- PGD approximation manage to find frequency periodic behavior from the first function without any *a priori* choice of basis.
- Stochastic functions are very regular so a very coarse discretization is possible in other to gain on calculation time.

Another interesting analysis is drawn from a ratio between real error and PGD residue as in Figure 6.8. A clear effect of saturation can be seen around 85^{th} triplets. Finally an evaluation of triplets contribution on the solution has been conducted in Figure 6.9.

All results showed are drown with the simplest choice of a uniform distribution as probability density function (PdF). In order to include a chosen distribution a simple post-processing is needed. In Figure 6.10 a post-process in made for a normal Gaussian with a mean of 250 and a variance of 25. As we can see the approximation of mean value, compared to analytic reference, is excellent (difference less than 10^{-6}) while the variance shows a little difference (less than 8%).

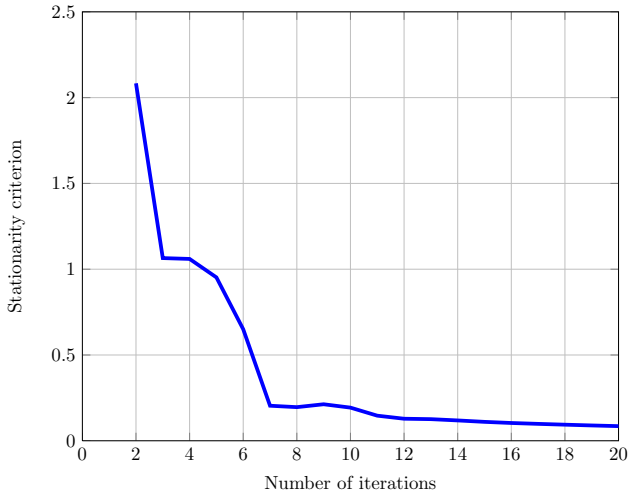

Figure 6.5: Evolution of sub-iteration number necessary to reach a stationarity criteria

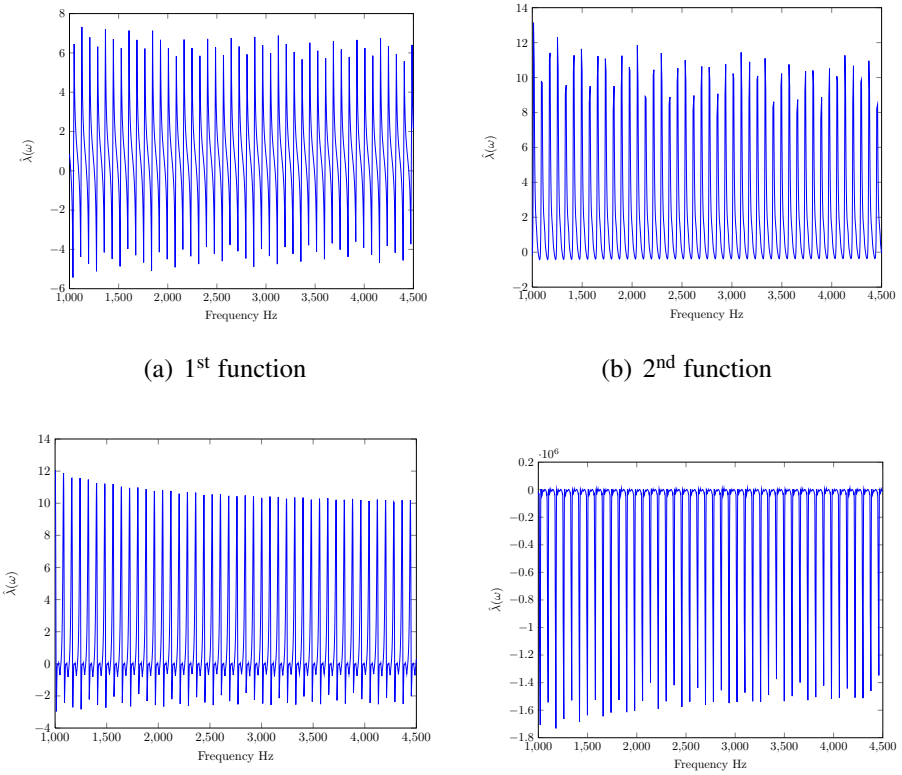

(a) 1st function

(b) 2nd function

(c) 4th function

(d) 50th function

Figure 6.6: Exemples of frequency functions on Example 6.2

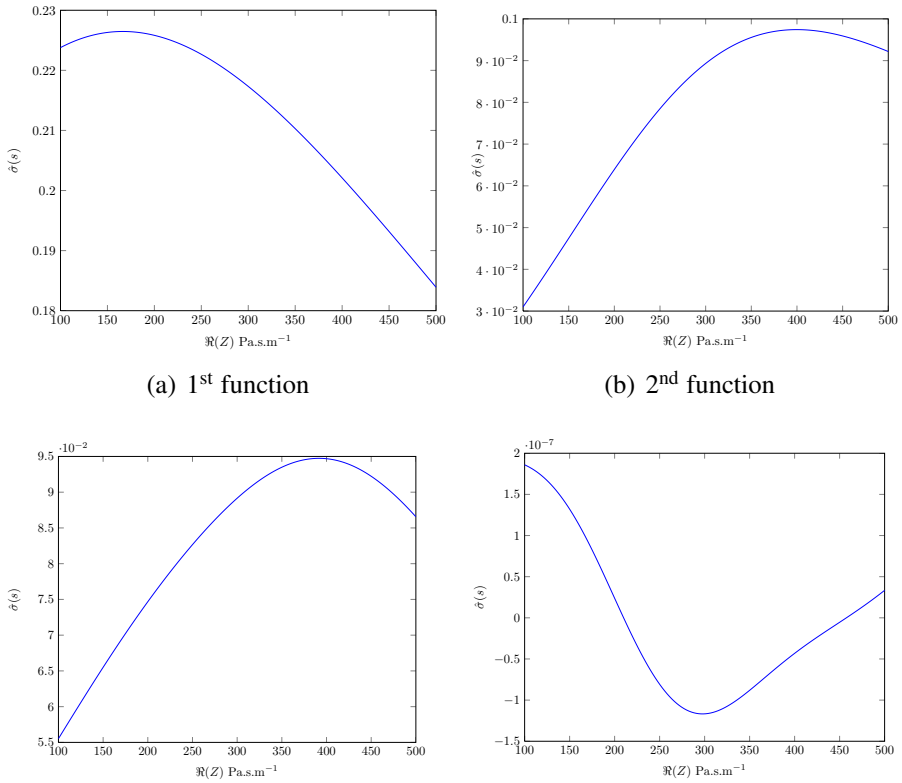

(a) 1st function (b) 2nd function

(c) 4th function (d) 50th function

Figure 6.7: Exemples of stochastic functions on Example 6.2

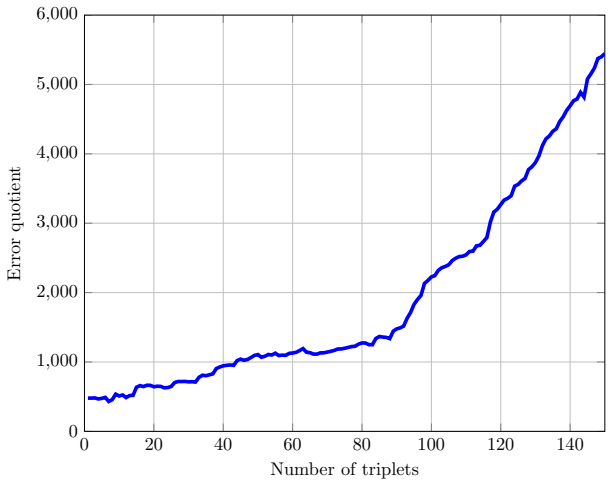

Figure 6.8: Ratio between real error and PGD residue

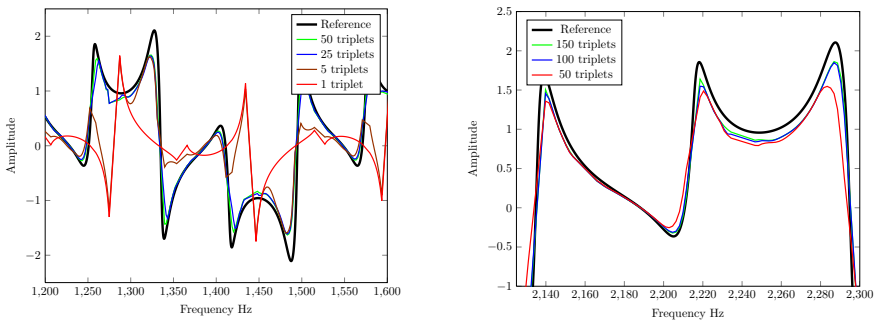

(a) Solution reconstruction for different PGD approximation orders

(b) Zoom on the peaks to show high order contributions

Figure 6.9: Real pressure evolution (middle point) with PGD approximation

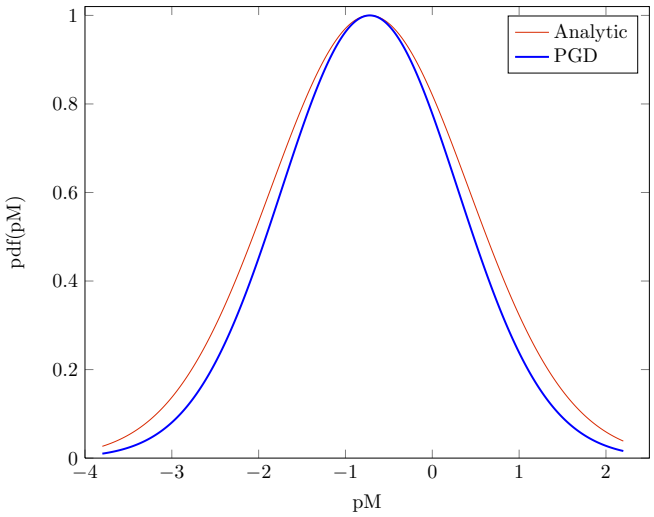

Figure 6.10: PDF of pressure on middle point for a normal gaussian distribution

2.2 A low cost solution towards high-frequency

A last consideration can be drawn considering the effectiveness of the technique. Previous results are calculated with a well studied discretization in terms of frequency and stochastic distribution in other to perfectly match the analytical results. On the other hand it is possible to built an hyper-reduced approximation in order to have fast solution of a desired problem. In Figure 6.11 is compared the analytical mean value of pressure with a mean pressure calculated with a very coarse PGD discretization. 5 stochastic test points, 120 frequency test points and 75 PGD triplets are taken into account to build the approximation. Even with such a strong approximation the quality of the solution is stills

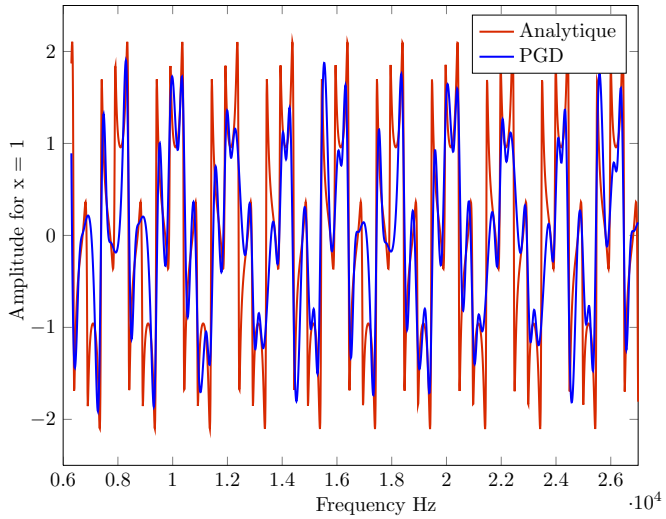

Figure 6.11: "Low-cost" PGD-VTCR mean pressure compared to mean reference

acceptable. This "Low-cost" approach can be used to approach high frequency where classical VTCR fails due to computational cost. Future extensive numerical tests will try to show the potentiality of this strategy.

2.3 2D preliminary results

The technique presented in Section 2 and previously successfully applied on a 1D example, is here applied on the 2D problem already presented in Chapter 5 Section 3.1. The considered frequency band is defined by $\omega_0 = 2.\pi.1300\ [Hz]$ and $\Delta\omega = 2.\pi.300\ [Hz]$. The considered variability on impedance $Z_0 = 845 + i50\ [Pa.s/m]$ is $\Delta Z = 400\ [Pa.s/m]$, where $Z \in [Z_0 - \Delta Z, Z_0 + \Delta Z]$ over an uniform distribution. Some preliminary results have been drawn using algorithm 7. In Figure 6.12 algorithm convergency is shown. The convergency is fast and smooth as for previous examples. In order to assets the coherency of the approximation two pressure field for a fixed frequency and impedance value are compared in Figure 6.13.

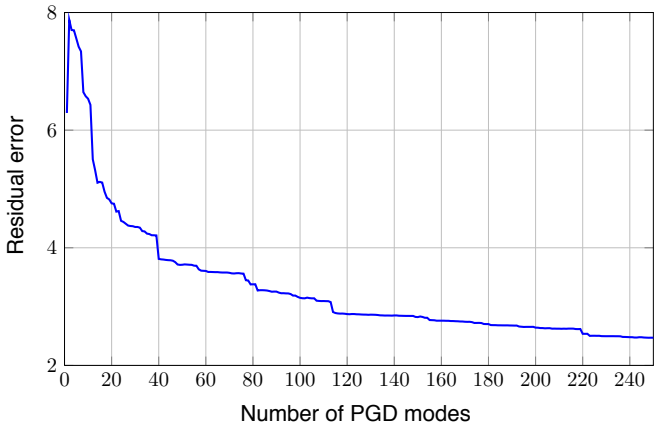

Figure 6.12: Convergency for 2D case

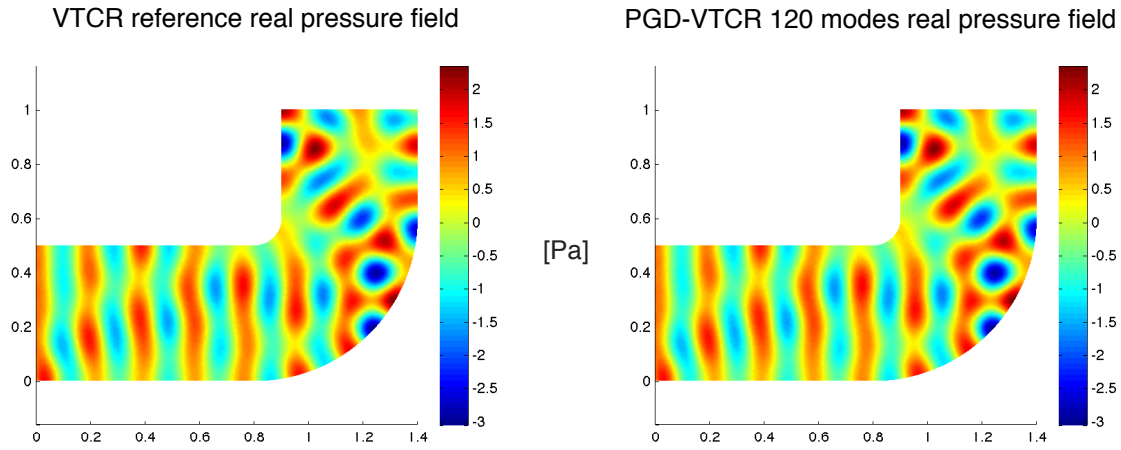

Figure 6.13: VTCR real pressure field compared to PGD-VTCR pressure field ($\omega = 2.\pi.1300$ and $Z = 845 + i50$)

These results shows potentiality of the method in 2D but can not be considered as a proof of its effectiveness. In the very next future the technique will be compared to a Monte Carlo based simulation and a SEA.

3 Conclusion

In this Section an extension of PGD-VTCR to stochastic problem has been proposed. After a brief introduction to the necessity of parametric uncertainty for mid-frequency problems, a PGD solution has been proposed. A new algorithm to take into account uncertainty has been proposed. Based on this algorithm a simple 1D example tested the performances of the approach. Some 2D test cases are on going. Preliminary results show huge potentiality of this approach and future research on VTRC will be strongly focused on this subject.

Conclusion

In order to predict the vibrational behavior of systems over frequency bands, standard numerical techniques usually involve many frequency-fixed computations, at many different frequencies. Although it is a straightforward and natural mean to answer to the posed problem when one has an efficient numerical tool at a fixed frequency, such a strategy can easily lead to huge computations, and the amount of data to store often increases significantly. This is particularly true in the context of medium frequency bands, where these responses have a strong sensitivity to the frequency. Indeed in such bands, a very fine frequency resolution of computation must be done, which accentuates the cited drawbacks. Then, for medium frequency vibrations, there is a clear need for improving the efficiency of prediction techniques on frequency bands.

This PhD work has been focused on the research of a numerical tool which would allow to compute mid-frequency over a wide frequency band at a limited computational cost. Moreover, an introduction of an uncertainty parameter was wished in order to keep in account mid-frequency sensibility to stochastic.

After an analysis of the literature survey in Chapter 1, the Variational Theory of Complex Rays was chosen as an effective mid-frequency tool. Despite its high efficiency and range of applicability (as shown in Chapter 2) VTCR had some major points to be improved:

- Its formulation is completely frequency dependent lowering its efficiency on a wide frequency band.
- Being a deterministic method, its extension to consider uncertainty parameters could be computationally inefficient if classical tools (like Monte Carlo simulations) are applied.

In order to extend its limits, an innovative Model Order Reduction (ROM) technique has been introduced. Model Order Reduction techniques are numerical tools which allows to solve complex problem with a little computational effort, as explained in Chapter 3. Among all possible reduction technique Proper Generalized Decomposition appeared as the perfect ally for VTCR. This ROM technique showed excellent performance on reduction of complex problem without any *a priori* knowledge of the solution.

In Chapter 4, for the first time in the history of the technique, a model reduction over frequency has been possible. This success lies on a deep analysis of VTCR characteristic and an intense research of the best performing algorithm.

In Chapter 5 a decisive improvement to the technique has been described. The introduction of a performant pre-conditioner based on a "Block SVD" allowed to introduce stability to the method. Due to these improved numerical characteristics, it was finally possible to introduce a state of the art PGD-VTCR algorithm based on a minimal residue direction research. Numerical evidences showed how this algorithm could be an answer to extension of VTCR to frequency band calculation.

As a consequence of this success and of PGD ability to deal with large number of parameters, an extension of the technique to stochastic was proposed in Chapter 6. The basic idea was to add to PGD decomposition in space and frequency an uncertainty parameter. The reduction is so performed over frequency and stochastic without performing any Monte Carlo simulation.

In this work a huge leap forward in VTCR application has been made. For the first time effective calculation over frequency bands were possible. Moreover, introduction of stochastic by PGD allows to combine deterministic model's accuracy with numerical efficiency.
Several are the perspective of this work:

- Application of the technique to real life 3D industrial cases
- Extension to structural dynamics
- Introduction of multi-parametric uncertainty
- On line - Off line calculation for real time simulation
- Low-cost solution to calculate high-frequency problems

Bibliography

[Allen and Berkley, 1979] Allen, J. and Berkley, D. (1979). Image method for efficiently simulating small-room acoustics. *J. Acoust. Soc. Am*, 65(4):943–950.

[Ammar et al., 2006] Ammar, A., Mokdad, B., Chinesta, F., and Keunings, R. (2006). A new family of solvers for some classes of multidimensional partial differential equations encountered in kinetic theory modeling of complex fluids. *Journal of Non-Newtonian Fluid Mechanics*, 139(3):153 – 176.

[Babuška et al., 1995] Babuška, I., Ihlenburg, F., Paik, E., and Sauter, S. (1995). A generalized finite element method for solving the helmholtz equation in two dimensions with minimal pollution. *Computer Methods in Applied Mechanics and Engineering*, 128:325–359.

[Banerjee, 1993] Banerjee, P. K. (1993). *The boundary element methods in engineering*. McGraw-Hill, London ;;New York, 2nd ed. edition.

[Barbarulo et al., 2012] Barbarulo, A., Ladevèze, P., Riou, H., and Kovalevsky, L. (2012). Proper generalized decomposition applied to linear acoustic: a new tool for broad band calculation. *Journal of Sound and Vibration*.

[Bayliss et al., 1983] Bayliss, A., Goldstein, C. I., and Turkel, E. (1983). An iterative method for the helmholtz equation. *Journal of Computational Physics*, 49(3):443 – 457.

[Belytschko et al., 1994] Belytschko, T., Lu, Y. Y., and Gu, L. (1994). Element-free galerkin methods. *International Journal for Numerical Methods in Engineering*, 37(2):229–256.

[Białecki et al., 2005] Białecki, R., Kassab, A., and Fic, A. (2005). Proper orthogonal decomposition and modal analysis for acceleration of transient fem thermal analysis. *International journal for numerical methods in engineering*, 62(6):774–797.

[Bonnet, 1999a] Bonnet, M. (1999a). Boundary integral equation methods for solids and fluids. *Meccanica*, 34(4):301–302.

[Bonnet, 1999b] Bonnet, M. (1999b). Boundary integral equation methods for solids and fluids. *Meccanica*, 34(4):301–302.

[Bonnet et al., 2008] Bonnet, M., Chaillat, S., and Semblat, J.-F. (2008). A multi-level fast multipole bem for 3-d elastodynamics in the frequency domain. *Computer Methods in Applied Mechanics and Engineering*, 197(49-50):4233–4249.

[Boucard and Ladeveze, 1999] Boucard, P. and Ladeveze, P. (1999). A multiple solution method for non-linear structural mechanics. *Mechanical Engineering*, 50(5):317–328.

[Bouillard and Suleau, 1998] Bouillard, P. and Suleau, S. (1998). Element-free galerkin solutions for helmholtz problems: formulation and numerical assessment of the pollution effect. *Computer Methods in Applied Mechanics and Engineering*, 162:317–335.

[Bouillard and Suleaub, 1998] Bouillard, P. and Suleaub, S. (1998). Element-free galerkin solutions for helmholtz problems: fomulation and numerical assessment of the pollution effect. *Computer Methods in Applied Mechanics and Engineering*, 162(14):317 – 335.

[Brezzi and Fortin, 1991] Brezzi, F. and Fortin, M. (1991). *Mixed and hybrid finite element methods*. Springer-Verlag New York, Inc.

[Carcaterra and Adamo, 1999] Carcaterra, A. and Adamo, L. (1999). Thermal analogy in wave energy transfer: Theoretical and experimental analysis. *Journal of Sound and Vibration*, 226(2):253 – 284.

[Cessenat and Despres, 1998] Cessenat, O. and Despres, B. (1998). Application of an ultra weak variational formulation of elliptic pdes to the two-dimensional helmholtz problem. *SIAM Journal on Numerical Analysis*, 35:255–299.

[Chae and Ih, 2001] Chae, K. and Ih, J. (2001). Prediction of vibrational energy distribution in the thin plate at high-frequency bands by using the ray tracing method. *Journal of sound and vibration*, 240(2):263–292.

[Chang and Liu, 2004] Chang, J. and Liu, R. (2004). An asymmetric indirect trefftz method for solving free-vibration problems. *Journal of sound and vibration*, 275(3):991–1008.

[Chevreuil et al., 2007] Chevreuil, M., Ladevèze, P., and Rouch, P. (2007). Transient analysis including the low- and the medium-frequency ranges of engineering structures. *Computers and Structures*, 85(17-18):1431 – 1444.

[Chevreuil and Nouy, 2011] Chevreuil, M. and Nouy, A. (2011). Model order reduction based on proper generalized decomposition for the propagation of uncertainties in structural dynamics. *International Journal for Numerical Methods in Engineering*, 89(2):241–268.

[Chinesta et al., 2010a] Chinesta, F., Ammar, A., and Cueto, E. (2010a). Recent advances and new challenges in the use of the proper generalized decomposition for

solving multidimensional models. *Archives of Computational Methods in Engineering*, 4(17):327–350.

[Chinesta et al., 2010b] Chinesta, F., Ammar, A., and Cueto, E. (2010b). Recent advances and new challenges in the use of the proper generalized decomposition for solving multidimensional models. *Archives of Computational methods in Engineering*, 17(4):327–350.

[Chinesta et al., 2011] Chinesta, F., Ladeveze, P., and Cueto, E. (2011). A short review on model order reduction based on proper generalized decomposition. *Archives of Computational Methods in Engineering*, (18):395–404.

[Cicirello and Langley, 2012] Cicirello, A. and Langley, R. (2012). The vibro-acoustic analysis of built-up systems using a hybrid method with parametric and non-parametric uncertainties. *Journal of Sound and Vibration*.

[Collins, 1993] Collins, M. (1993). A split-step padé solution for the parabolic equation method. *The Journal of the Acoustical Society of America*, 93:1736.

[Colton and Kress, 2001] Colton, D. and Kress, R. (2001). On the denseness of herglotz wave functions and electromagnetic herglotz pairs in sobolev spaces. *Mathematical Methods in the Applied Sciences*, 24:1289–1303.

[Cotoni et al., 2005] Cotoni, V., Langley, R., and Kidner, M. (2005). Numerical and experimental validation of variance prediction in the statistical energy analysis of built-up systems. *Journal of Sound and Vibration*, 288(3):701 – 728.

[De Rosa and Franco, 2008] De Rosa, S. and Franco, F. (2008). A scaling procedure for the response of an isolated system with high modal overlap factor. *Mechanical Systems and Signal Processing*, 22(7):1549–1565.

[De Rosa and Franco, 2010] De Rosa, S. and Franco, F. (2010). On the use of the asymptotic scaled modal analysis for time-harmonic structural analysis and for the prediction of coupling loss factors for similar systems. *Mechanical Systems and Signal Processing*, 24(2):455–480.

[Deckers et al., 2009] Deckers, E., Hörlin, N., Vandepitte, D., and Desmet, W. (2009). A novel wave based method for the efficient 2d dynamic modelling of the poro-elastic biot equations. *Comput Methods Appl Mech Eng*.

[Deckers et al., 2011] Deckers, E., Van Genechten, B., Vandepitte, D., and Desmet, W. (2011). Efficient treatment of stress singularities in poroelastic wave based models using special purpose enrichment functions. *Computers and Structures Structures*, 89(11):1117–1130.

[Deraemaeker et al., 1999] Deraemaeker, A., Babuška, I., and Bouillard, P. (1999). Dispersion and pollution of the fem solution for the helmholtz equation in one, two and three dimensions. *International Journal for Numerical Methods in Engineering*, (46):471–499.

[Desmet, 1998] Desmet, W. (1998). *A wave based prediciton technique for coupled vibro- acoustic analysis*. PhD thesis, Katholieke Universiteit Leuven, Belgium.

[Desmet et al., 2002a] Desmet, W., Hal, B. V., Sas, P., and Vandepitte, D. (2002a). A computationally efficient prediction technique for the steady-state dynamic analysis of coupled vibro-acoustic systems. *Advances in Engineering Software*, 33:527–540.

[Desmet et al., 2012] Desmet, W., Onur, A., and Pluymers, B. (2012). *"MID-FREQUENCY" CAE Methodologies for Mid-Frequency Analysis in Vibration and Acoustics*. Leuven University Press.

[Desmet et al., 2002b] Desmet, W., Van Hal, B., Sas, P., and Vandepitte, D. (2002b). A computationally efficient prediction technique for the steady-state dynamic analysis of coupled vibro-acoustic systems. *Advances in Engineering Software*, 33(7):527–540.

[Eckart and Young, 1936] Eckart, C. and Young, G. (1936). The approximation of one matrix by another of lower rank. *Psychometrika*, 1(3):211–218.

[Erlangga, 2008] Erlangga, Y. A. (2008). Advances in iterative methods and preconditioners for the helmholtz equation. *Archives of Computational Methods in Engineering*, 15(1):37–66.

[Erlangga et al., 2004] Erlangga, Y. A., Vuik, C., and Oosterlee, C. W. (2004). On a class of preconditioners for solving theâ helmholtz equation. *Applied Numerical Mathematics*, 50(3-4):409–425.

[Farhat et al., 2001] Farhat, C., Harari, I., and Franca, L. (2001). The discontinuous enrichment method. *Computer Methods in Applied Mechanics and Engineering*, 190:6455–6479.

[Farhat et al., 2003] Farhat, C., Harari, I., and Hetmaniuk, U. (2003). A discontinuous galerkin method with lagrange multipliers for the solution of helmholtz problems in the mid-frequency regime. *Computer Methods in Applied Mechanics and Engineering*, 192(11):1389–1419.

[Farhat et al., 2000] Farhat, C., Macedo, A., Lesoinne, M., Roux, F., Magoulés, F., and Bourdonnaie, A. (2000). Two-level domain decomposition methods with lagrange multipliers for the fast iterative solution of acoustic scattering problems. *Computer methods in applied mechanics and engineering*, 184(2):213–239.

[Farhat and Roux, 1991] Farhat, C. and Roux, F. (1991). A method of finite element tearing and interconnecting and its parallel solution algorithm. *International Journal for Numerical Methods in Engineering*, 32(6):1205–1227.

[Farhat et al., 2004a] Farhat, C., Tezaur, R., and Weidemann-Goiran, P. (2004a). Higher-order extensions of a discontinuous galerkin method for mid-frequency helmholtz problems. *International journal for numerical methods in engineering*, 61(11):1938–1956.

[Farhat et al., 2004b] Farhat, C., Wiedemann-Goiran, P., and Tezaur, R. (2004b). A discontinuous galerkin method with plane waves and lagrange multipliers for the solution of short wave exterior helmholtz problems on unstructured meshes. *Wave Motion*, 39(4):307–317.

[Fink and Rheinboldt, 1983] Fink, J. and Rheinboldt, W. (1983). On the error behavior of the reduced basis technique for nonlinear finite element approximations. *ZAMM-Journal of Applied Mathematics and Mechanics/Zeitschrift für Angewandte Mathematik und Mechanik*, 63(1):21–28.

[Franca et al., 1997] Franca, L., Farhat, C., Macedo, A., and Lesoinne, M. (1997). Residual-free bubbles for the helmholtz equation. *International journal for numerical methods in engineering*, 40(21):4003–4009.

[Franca and Carmo, 1989] Franca, L. P. and Carmo, E. G. D. D. (1989). The galerkin gradient least-squares method. *Computer Methods in Applied Mechanics and Engineering*, 74(1):41 – 54.

[Freitas, 1999] Freitas, J. (1999). Hybrid finite element formulations for elastodynamic analysis in the frequency domain. *International journal of solids and structures*, 36(13):1883–1923.

[Gabard, 2007] Gabard, G. (2007). Discontinuous galerkin methods with plane waves for time-harmonic problems. *Journal of Computational Physics*, 225(2):1961–1984.

[Genechten et al., 2010] Genechten, B., Bergen, B., Vandepitte, D., and Desmet, W. (2010). A trefftz-based numerical modelling framework for helmholtz problems with complex multiple-scatterer configurations. *Journal of Computational Physics*, 229(18):6623–6643.

[Gittelson et al., 2009] Gittelson, C., Hiptmair, R., and Perugia, I. (2009). Plane wave discontinuous galerkin methods: analysis of the h-version. *ESAIM: Mathematical Modelling and Numerical Analysis*, 43(02):297–331.

[Gosselet and Rey, 2006] Gosselet, P. and Rey, C. (2006). Non-overlapping domain decomposition methods in structural mechanics. *Archives of Computational Methods in Engineering*, 13(4):515–572.

[Grosu and Harari, 2008] Grosu, E. and Harari, I. (2008). Studies of the discontinuous enrichment method for two-dimensional acoustics. *Finite Elements in Analysis and Design*, 44(5):272–287.

[Guyader et al., 1988] Guyader, J., Boisson, C., and Lesueur, C. (1988). Méthode des coefficients d'influence énergétiques. *Rayonnement acoustique des structures*, page 317.

[Hackbusch and Nowak, 1989] Hackbusch, W. and Nowak, Z. (1989). On the fast matrix multiplication in the boundary element method by panel clustering. *Numerische Mathematik*, 54(4):463–491.

[Harari and Haham, 1998] Harari, I. and Haham, S. (1998). Improved finite element methods for elastic waves. *Computer Methods in Applied Mechanics and Engineering*, 166:143 – 164.

[Harari and Hughes, 1992] Harari, I. and Hughes, T. (1992). Galerkin/least-squares finite element methods for the reduced wave equation with non-reflecting boundary conditions in unbounded domains. *Computer Methods in Applied Mechanics and Engineering*, 98(2):411–454.

[Herrera, 1984] Herrera, I. (1984). *Boundary methods: an algebraic theory*. Pitman Advanced Pub. Program.

[Hughes, 1995] Hughes, T. (1995). Multiscale phenomena: Green's functions, the dirichlet-to-neumann formulation, subgrid scale models, bubbles and the origins of stabilized methods. *Computer methods in applied mechanics and engineering*, 127(1-4):387–401.

[Huttunen et al., 2006] Huttunen, T., Gamallo, P., and Astley, R. (2006). Comparison of two wave element methods for the helmholtz problem. Technical report, ISVR.

[Ichchou et al., 1997] Ichchou, M., Bot, A. L., and Jezequel, L. (1997). Energy models of one-dimensional, multi-propagative systems. *Journal of Sound and Vibration*, 201(5):535 – 554.

[Jirousek and Wroblewski, 1996] Jirousek, J. and Wroblewski, A. (1996). T-elements: state of the art and future trends. *Archives of Computational Methods in Engineering*, 3(4):323–434.

[Karhunen, 1946] Karhunen, K. (1946). *Zur spektraltheorie stochastischer prozesse*. Suomalainen tiedeakatemia.

[Kita and Kamiya, 1995] Kita, E. and Kamiya, N. (1995). Trefftz method: an overview. *Advances in Engineering Software*, 24(1):3–12.

[Kompella and Bernhard, 1993] Kompella, M. and Bernhard, R. (1993). Measurement of the statistical variation of structural-acoustic characteristics of automotive vehicles. In *SAE Noise and Vibration Conference*, volume 931272.

[Kovalevsky, 2011] Kovalevsky, L. (2011). *La theorie variationnelle des rayons complexes version Fourier*. PhD thesis, LMT ENS-Cachan.

[Kovalevsky et al., 2012a] Kovalevsky, L., Ladevèze, P., and Riou, H. (2012a). The fourier version of the variational theory of complex rays for medium-frequency acoustics. *Computer Methods in Applied Mechanics and Engineering*, 225–228(0):142–153.

[Kovalevsky et al., 2012b] Kovalevsky, L., Ladevèze, P., Riou, H., and Bonnet, M. (2012b). The variational theory of complex rays for three-dimensional helmholtz problems. *Journal of Computational Acoustics*.

[Krokstad et al., 1968] Krokstad, A., Strom, S., and Sørsdal, S. (1968). Calculating the acoustical room response by the use of a ray tracing technique. *Journal of Sound and Vibration*, 8(1):118–125.

[Krysl et al., 2001] Krysl, P., Lall, S., and Marsden, J. (2001). Dimensional model reduction in non-linear finite element dynamics of solids and structures. *International Journal for Numerical Methods in Engineering*, 51(4):479–504.

[Kunisch and Volkwein, 2001] Kunisch, K. and Volkwein, S. (2001). Galerkin proper orthogonal decomposition methods for parabolic problems. *Numerische Mathematik*, 90(1):117–148.

[Kurz et al., 2002] Kurz, S., Rain, O., and Rjasanow, S. (2002). The adaptive cross-approximation technique for the 3d boundary-element method. *Magnetics, IEEE Transactions on*, 38(2):421–424.

[Lacroix et al., 2003] Lacroix, V., Bouillard, P., and Villon, P. (2003). An iterative defect-correction type meshless method for acoustics. *International Journal for Numerical Methods in Engineering*, 57(15):2131–2146.

[Ladevèze, 1996] Ladevèze, P. (1996). A new computational approach for structure vibrations in the medium frequency range. *Comptes Rendus Académie des Sciences Paris*, 332(2b):849–856.

[Ladevèze, 1999] Ladevèze, P. (1999). *Nonlinear computationnal structural mechanics—new approaches and non-incremental methods of calculation*. Springer, Berlin.

[Ladevèze et al., 2001] Ladevèze, P., Arnaud, L., Rouch, P., and Blanzé, C. (2001). The variational theory of complex rays for the calculation of medium-frequency vibrations. *Engineering Computations*, (18):193–214.

[Ladevèze et al., 2003a] Ladevèze, P., Blanc, L., Rouch, P., and Blanzé, C. (2003a). A multiscale computational method for medium-frequency vibrations of assemblies of heterogeneous plates. *Computers and Structures*, 81:1267–1276.

[Ladevèze and Chamoin, 2011] Ladevèze, P. and Chamoin, L. (2011). On the verification of model reduction methods based on the proper generalized decomposition. *Computer Methods in Applied Mechanics and Engineering*, 200:2032–2047.

[Ladevèze et al., 2010] Ladevèze, P., Passieux, J.-C., and Néron, D. (2010). The LATIN multiscale computational method and the Proper Generalized Decomposition. *Computer Methods in Applied Mechanics and Engineering*, 199:1287–1296.

[Ladevèze and Riou, 2005] Ladevèze, P. and Riou, H. (2005). Calculation of medium-frequency vibrations over a wide frequency range. *Computer Methods in Applied Mechanics and Engineering*, 194:3167 – 3191.

[Ladevèze et al., 2003b] Ladevèze, P., Rouch, P., Riou, H., and Bohineust, X. (2003b). Analysis of medium-frequency vibrations in a frequency range. *Journal of Computational Acoustics*, (11):255–284.

[Lancaster and Salkauskas, 1981] Lancaster, P. and Salkauskas, K. (1981). Surfaces generated by moving least squares methods. *Mathematics of Computation*, 37(155):141–158.

[Langley, 1992] Langley, R. (1992). A wave intensity technique for the analysis of high frequency vibrations. *Journal of Sound and Vibration*, 159(3):483–502.

[Langley, 1995] Langley, R. (1995). On the vibrational conductivity approach to high frequency dynamics for two-dimensional structural components. *Journal of sound and vibration*, 182(4):637–657.

[Langley and Brown, 2004] Langley, R. and Brown, A. (2004). The ensemble statistics of the band-averaged energy of a random system. *Journal of Sound and Vibration*, 275(35):847 – 857.

[Langley and Cordioli, 2009] Langley, R. and Cordioli, J. (2009). Hybrid deterministic-statistical analysis of vibro-acoustic systems with domain couplings on statistical components. *Journal of Sound and Vibration*, 321(3):893–912.

[Langley and Cotoni, 2007] Langley, R. and Cotoni, V. (2007). Response variance prediction for uncertain vibro-acoustic systems using a hybrid deterministic-statistical method. *The Journal of the Acoustical Society of America*, 122:3445.

[Langley et al., 1997] Langley, R., Smith, J., and Fahy, F. (1997). Statistical energy analysis of periodically stiffened damped plate structures. *Journal of Sound and Vibration*, 208(3):407 – 426.

[Lase et al., 1996] Lase, Y., Ichchou, M., and Jezequel, L. (1996). Energy flow analysis of bars and beams: Theoretical formulations. *Journal of Sound and Vibration*, 192(1):281 – 305.

[Lieu et al., 2006] Lieu, T., Farhat, C., and Lesoinne, M. (2006). Reduced-order fluid/structure modeling of a complete aircraft configuration. *Computer Methods in Applied Mechanics and Engineering*, 195(41-43):5730–5742.

[Loeve, 1955] Loeve, M. (1955). *Probability Theory; Foundations, Random Sequences*. New York: D. Van Nostrand Company.

[Lyon and Maidanik, 1962] Lyon, R. H. and Maidanik, G. (1962). Power flow between linearly coupled oscillators. *Journal of Acoustical Society of America*, 34:640–647.

[Mace, 2003] Mace, B. (2003). Statistical energy analysis, energy distribution models and system modes. *Journal of Sound and Vibration*, 264(2):391 – 409.

[Machiels et al., 2000] Machiels, L., Maday, Y., Oliveira, I., Patera, A., and Rovas, D. (2000). Output bounds for reduced-basis approximations of symmetric positive definite eigenvalue problems. *Comptes Rendus de l'Academie des Sciences Series I Mathematics*, 331(2):153–158.

[MacNeal, 1971] MacNeal, R. (1971). A hybrid method of component mode synthesis. *Computers & Structures*, 1(4):581–601.

[Maday and Rønquist, 2002] Maday, Y. and Rønquist, E. (2002). A reduced-basis element method. *Journal of Scientific Computing*, 17(1):447–459.

[Magoules et al., 2000] Magoules, F., Meerbergen, K., and Coyette, J. (2000). Application of a domain decomposition method with lagrange multipliers to acoustic problems arising from the automotive industry. *Journal of Computational Acoustics*, 8(03):503–521.

[Mandel, 2002] Mandel, J. (2002). An iterative substructuring method for coupled fluid–solid acoustic problems. *Journal of Computational Physics*, 177(1):95–116.

[Massimi et al., 2008] Massimi, P., Tezaur, R., and Farhat, C. (2008). A discontinuous enrichment method for three-dimensional multiscale harmonic wave propagation problems in multi-fluid and fluid–solid media. *International Journal for Numerical Methods in Engineering*, 76(3):400–425.

[Maxit and Guyader, 2001a] Maxit, L. and Guyader, J. (2001a). Estimation of sea coupling loss factors using a dual formulation and fem modal information, part i: theory. *Journal of sound and vibration*, 239(5):907–930.

[Maxit and Guyader, 2001b] Maxit, L. and Guyader, J. (2001b). Estimation of sea coupling loss factors using a dual formulation and fem modal information, part ii: Numerical applications. *Journal of sound and vibration*, 239(5):931–948.

[Melenk and Babuška, 1996] Melenk, J. M. and Babuška, I. (1996). The partition of unity finite element method: Basic theory and applications. *Computer Methods in Applied Mechanics and Engineering*, 139:289–314.

[Metropolis, 1987] Metropolis, N. (1987). The beginning of the monte carlo method. *Los Alamos Science*, 15(584):125–130.

[Monk and Wang, 1999a] Monk, P. and Wang, D. (1999a). A least-squares method for the helmholtz equation. *Computer Methods in Applied Mechanics and Engineering*, 175:121–136.

[Monk and Wang, 1999b] Monk, P. and Wang, D. (1999b). A least-squares method for the helmholtz equation. *Computer Methods in Applied Mechanics and Engineering*, 175(1):121–136.

[Monserrat et al., 2001] Monserrat, C., Meier, U., Alcaniz, M., Chinesta, F., and Juan, M. (2001). A new approach for the real-time simulation of tissue deformations in surgery simulation. *Computer Methods and Programs in Biomedicine*, 64(2):77–85.

[Mortessagne et al., 1993] Mortessagne, F., Legrand, O., and Sornette, D. (1993). Transient chaos in room acoustics. *Chaos (Woodbury, NY)*, 3(4):529.

[Nayroles et al., 1992] Nayroles, B., Touzot, G., and Villon, P. (1992). Generalizing the finite element method: Diffuse approximation and diffuse elements. *Computational Mechanics*, 10(5):307–318.

[Néron and Ladevèze, 2010] Néron, D. and Ladevèze, P. (2010). Proper generalized decomposition for multiscale and multiphysics problems. *Archives of Computational Methods in Engineering*, 17(4):351–372.

[Nouy, 2007] Nouy, A. (2007). A generalized spectral decomposition technique to solve a class of linear stochastic partial differential equations. *Computer Methods in Applied Mechanics and Engineering*, 196(45-48):4521 – 4537.

[Nouy, 2010] Nouy, A. (2010). A priori model reduction through proper generalized decomposition for solving time-dependent partial differential equations. *Computer Methods in Applied Mechanics and Engineering*, 199(23-24):1603 – 1626.

[Ochs, 1989] Ochs, R. (1989). A version of runge's theorem for the helmoltz equation with applications to scattering theory. *Proceedings of the Edinburgh Mathematical Society*, (32):107–119.

[Patera and Rozza, 2007] Patera, A. and Rozza, G. (2007). Reduced basis approximation and a posteriori error estimation for parametrized partial differential equations.

[Pearson, 1901] Pearson, K. (1901). On lines and planes of closest fit to systems of points in space. *The London, Edinburgh, and Dublin Philosophical Magazine and Journal of Science*, 2(11):559–572.

[Perrey-Debain et al., 2003] Perrey-Debain, E., Trevelyan, J., and Bettess, P. (2003). Plane wave interpolation in direct collocation boundary element method for radiation and wave scattering: numerical aspects and applications. *Journal of sound and vibration*, 261(5):839–858.

[Perrey-Debain et al., 2004] Perrey-Debain, E., Trevelyan, J., and Bettess, P. (2004). Wave boundary elements: a theoretical overview presenting applications in scattering of short waves. *Engineering Analysis with Boundary Elements*, 28:131–141.

[Pluymers et al., 2007] Pluymers, B., Van Hal, B., Vandepitte, D., and Desmet, W. (2007). Trefftz-based methods for time-harmonic acoustics. *Archives of Computational Methods in Engineering*, 14(4):343–381.

[Riou et al., 2004] Riou, H., Ladevèze, P., and Rouch, P. (2004). Extension of the variational theory of complex rays to shells for medium-frequency vibrations. *Journal of Sound and Vibration*, 272(1-2):341–360.

[Riou et al., 2008] Riou, H., Ladevèze, P., and Sourcis, B. (2008). The multiscale vtcr approach applied to acoustics problems. *Journal of Computational Acoustics*, 16(4):487–505.

[Rouch and Ladevèze, 2003] Rouch, P. and Ladevèze, P. (2003). The variational theory of complex rays: a predictive tool for medium-frequency vibrations. *Computer Methods in Applied Mechanics and Engineering*, 192(28-30):3301–3315.

[Rumpler et al., 2011] Rumpler, R., Legay, A., and Deü, J. (2011). Performance of a restrained-interface substructuring fe model for reduction of structural-acoustic problems with poroelastic damping. *Computers & structures*, 89(23):2233–2248.

[Ryckelynck et al., 2006] Ryckelynck, D., Chinesta, F., Cueto, E., and Ammar, A. (2006). On the a priori model reduction: overview and recent developments. *Archives of Computational Methods in Engineering*, 13(1):91–128.

[Sandberg et al., 2001] Sandberg, G., Hansson, P., and Gustavsson, M. (2001). Domain decomposition in acoustic and structure-acoustic analysis. *Computer methods in applied mechanics and engineering*, 190(24-25):2979–2988.

[Shorter and Langley, 2005] Shorter, P. and Langley, R. (2005). Vibro-acoustic analysis of complex systems. *Journal of Sound and Vibration*, 288(3):669–699.

[Soize, 1998] Soize, C. (1998). Reduced models in the medium frequency range for the general dissipative structural dynamic systems. *European Journal of Mechanics - A/Solids*, 17:657–685.

[Soize, 2000] Soize, C. (2000). A nonparametric model of random uncertainties for reduced matrix models in structural dynamics. *Probabilistic Engineering Mechanics*, 15(3):277–294.

[Stewart and Hughes, 1996] Stewart, J. and Hughes, T. (1996). Explicit residual-based a posteriori error estimation for finite element discretizations of the helmholtz equation: Computation of the constant and new measures of error estimator quality. *Computer methods in applied mechanics and engineering*, 131(3-4):335–363.

[Stewart and Hughes, 1997] Stewart, J. and Hughes, T. (1997). h-adaptive finite element computation of time-harmonic exterior acoustics problems in two dimensions. *Computer methods in applied mechanics and engineering*, 146(1-2):65–89.

[Stojek, 1998] Stojek, M. (1998). Least-squares trefftz-type elements for the helmholtz equation. *International journal for numerical methods in engineering*, 41(5):831–849.

[Strouboulis et al., 2000] Strouboulis, T., Copps, K., and Babuška, I. (2000). The generalized finite element method: an example of its implementation and illustration of its performance. *International Journal for Numerical Methods in Engineering*, 47:1401–1417.

[Strouboulis and Hidajat, 2006] Strouboulis, T. and Hidajat, R. (2006). Partition of unity method for helmholtz equation: q-convergence for plane-wave and wave-band local bases. *Applications of Mathematics*, 51:181–204.

[Suleau et al., 2000] Suleau, S., Deraemaeker, A., and Bouillard, P. (2000). Dispersion and pollution of meshless solutions for the helmholtz equation. *Computer Methods in Applied Mechanics and Engineering*, 190(57):639 – 657.

[Tezaur and Farhat, 2006] Tezaur, R. and Farhat, C. (2006). Three-dimensional discontinuous galerkin elements with plane waves and lagrange multipliers for the solution of mid-frequency helmholtz problems. *International journal for numerical methods in engineering*, 66(5):796–815.

[Tezaur et al., 2001] Tezaur, R., Macedo, A., and Farhat, C. (2001). Iterative solution of large-scale acoustic scattering problems with multiple right hand-sides by a domain decomposition method with lagrange multipliers. *International Journal for Numerical Methods in Engineering*, 51(10):1175–1193.

[Thompson and Pinsky, 1995] Thompson, L. and Pinsky, P. (1995). A galerkin least-squares finite element method for the two-dimensional helmholtz equation. *International Journal for Numerical Methods in Engineering*, 38(3):371–397.

[Totaro et al., 2009] Totaro, N., Dodard, C., and Guyader, J. (2009). Sea coupling loss factors of complex vibro-acoustic systems. *Journal of Vibration and Acoustics*, 131:041009.

[Trefftz, 1926] Trefftz, E. (1926). Ein gegenstuck zum ritzschen verfahren. *Second International Congress on Applied Mechanics*, pages 131–137.

[Troclet, 1995] Troclet, B. (1995). Prediction of structure-borne noise in launch vehicles and aircrafts. In *EURO-NOISE 95*.

[Van Genechten et al., 2011] Van Genechten, B., Vandepitte, D., and Desmet, W. (2011). A direct hybrid finite element–wave based modelling technique for efficient coupled vibro-acoustic analysis. *Computer Methods in Applied Mechanics and Engineering*, 200(5):742–764.

[Van Hal et al., 2005] Van Hal, B., Desmet, W., and Vandepitte, D. (2005). Hybrid finite elementwave-based method for steady-state interior structural acoustic problems. *Computers and Structures*, 83(2):167–180.

[Vanmaele et al., 2007] Vanmaele, C., Vandepitte, D., and Desmet, W. (2007). An efficient wave based prediction technique for plate bending vibrations. *Computer methods in applied mechanics and engineering*, 196(33):3178–3189.

[Vanmaele et al., 2009] Vanmaele, C., Vandepitte, D., and Desmet, W. (2009). An efficient wave based prediction technique for dynamic plate bending problems with corner stress singularities. *Computer Methods in Applied Mechanics and Engineering*, 198(30):2227–2245.

[Weaver, 1989] Weaver, R. (1989). Spectral statistics in elastodynamics. *J. Acoust. Soc. Am*, 85(3):1005–1013.

[Weck, 2004] Weck, N. (2004). Approximation by herglotz wave functions. *Mathematical methods in the applied sciences*, 27(2):155–162.

[Yeih et al., 2006] Yeih, W., Liu, R., Chang, J., Kuo, S., et al. (2006). Numerical instability of the direct trefftz method for laplace problems for a 2d finite domain. *International Journal of Applied Mathematics and Mechanics*, 2(1):41–66.

[Zienkiewicz, 1997] Zienkiewicz, O. (1997). Trefftz type approximation and the generalized finite element method- history and development. *COMPUT ASSIS MECH ENG SCI*, 4(3):305–316.

[Zienkiewicz et al., 2005] Zienkiewicz, O., Taylor, R., and Taylor, R. (2005). *The finite element method for solid and structural mechanics*, volume 2. Butterworth-Heinemann.

[Zienkiewicz, 1977] Zienkiewicz, O. C. (1977). *The Finite Element Method*. McGraw-Hill.